République Algérienne Démocratique et Populaire
Ministère de l'Enseignement Supérieur et de la Recherche Scientifique

École Nationale Polytechnique

Département d'Automatique

Laboratoire de Commande des Processus

End of studies' project

In view of obtaining the State Engineering Diploma in Automatic Control

---

Modeling, Identification and Control Strategies for a Reverse Osmosis-Based Desalination System

---

Presented by : GUENDOUZ Khaled and BENSEDDIK Akram

Under the supervision of :

Pr. BOUCHERIT Mohamed Seghier and **Dr. BENKOUIDER Ouarda**

Publicly presented and defended on 23/06/2025 in front of the jury composed of :

President :	Dr. ACHOUR Hakim	ENP
Examinator :	Pr. BOUDANA Djamel	ENP
Promoters :	Pr. BOUCHERIT Mohamed Seghier	ENP
	Dr. BENKOUIDER Ouarda	ENP

ENP 2025

République Algérienne Démocratique et Populaire
Ministère de l'Enseignement Supérieur et de la Recherche Scientifique

École Nationale Polytechnique

Département d'Automatique

Laboratoire de Commande des Processus

End of studies' project

In view of obtaining the State Engineering Diploma in Automatic Control

---

Modeling, Identification and Control Strategies for a Reverse Osmosis-Based Desalination System

---

Presented by : GUENDOUZ Khaled and BENSEDDIK Akram

Under the supervision of :

Pr. BOUCHERIT Mohamed Seghier and **Dr. BENKOUIDER Ouarda**

Publicly presented and defended on 23/06/2025 in front of the jury composed of :

President :	Dr. ACHOUR Hakim	ENP
Examinator :	Pr. BOUDANA Djamel	ENP
Promoters :	Pr. BOUCHERIT Mohamed Seghier	ENP
	Dr. BENKOUIDER Ouarda	ENP

ENP 2025

République Algérienne Démocratique et Populaire
Ministère de l'Enseignement Supérieur et de la Recherche Scientifique

École Nationale Polytechnique

Département d'Automatique

Laboratoire de Commande des Processus

Mémoire de Projet de Fin d'Études

En vue de l'obtention du diplôme d'Ingénieur d'État en Automatique

---

Modélisation, Identification et Commande d'un Système de Dessalement par Osmose Inverse

---

Présenté par : GUENDOUZ Khaled et BENSEDDIK Akram

Sous la supervision de :
Pr. BOUCHERIT Mohamed Seghier et **Dr. BENKOUIDER Ouarda**

Présenté et soutenu publiquement le 23/06/2025 devant le jury composé de :

Président :	Dr. ACHOUR Hakim	ENP
Examinateur :	Pr. BOUDANA Djamel	ENP
Promoteurs :	Pr. BOUCHERIT Mohamed Seghier	ENP
	Dr. BENKOUIDER Ouarda	ENP

ENP 2025

ملخص:

يتناول هذا البحث مسألة النمذجة، والتعرف، والتحكم في نظام تحلية المياه باستخدام تقنية التناضح العكسي، كحل فعّال ومستدام لمشكلة ندرة الموارد المائية العذبة. في المرحلة الأولى، تم تطوير نموذج ديناميكي للعملية بالاعتماد على بيانات تجريبية، مما سمح بتمثيل دقيق للعلاقات بين المتغيرات الأساسية (الضغط، الرقم الهيدروجيني، تدفق الماء المنتج، والتوصيلية). تمت دراسة وتطبيق استراتيجيتين للتحكم: الأولى تتمثل في التحكم التنبؤي على نموذج وآخر متعدد المتغيرات، والثانية هي التحكم التقليدي، بالإضافة إلى نسخة محسنّة منه مبيّنة على تقنيات التحكم بالنموذج الداخلي. أظهرت نتائج المحاكاة فعالية واستقرار كل من الطريقتين، إلى جانب توضيح الحدود المرتبطة بالتقنيات تحت ظروف عدم اليقين في النمذجة.

الكلمات المفتاحية: تحلية المياه، التناضح العكسي، النمذجة، التحكم التنبؤي، المتحكم التناسبي-التكاملي-التفاضلي، المتحكم ذو البنية الداخلية، المتانة.

Résumé

Ce mémoire porte sur la modélisation, l'identification et la commande d'un système de dessalement par osmose inverse RO Reverse Osmosis Dans un contexte marqué par la raréfaction des ressources en eau douce, cette technologie s'impose comme une solution viable et durable Une première phase est consacrée à la modélisation dynamique du procédé à partir de données expérimentales, permettant de représenter avec précision les relations entre les variables clés telles que la pression, le pH, le débit du perméat et la conductivité Deux stratégies de commande ont été développées, à savoir la commande prédictive MPC appliquée à la fois sur un modèle découplé et sur un modèle multivariable, ainsi que la commande PID classique et sa variante améliorée IMC-PID L'analyse des résultats met en évidence les performances, la robustesse et les limites de chaque approche face aux incertitudes du système

Mots-clés : Dessalement, Osmose inverse, Modélisation, Commande prédictive, PID, IMC, Robustesse.

Abstract

This thesis focuses on the modeling, identification, and control of a reverse osmosis (RO) desalination system. In response to the growing scarcity of freshwater resources, RO technology offers a viable and sustainable solution. The first phase involves the development of a dynamic model based on experimental data, accurately capturing the interactions between key variables such as feed pressure, pH, permeate flow rate, and conductivity. Two control strategies are explored : Model Predictive Control (MPC), implemented on both decoupled and multivariable models, and classical PID control, including an improved IMC-PID version. The results obtained highlight the performance, robustness, and limitations of each control approach under model uncertainties.

Keywords : Desalination, Reverse Osmosis, Modeling, Predictive Control, PID, IMC, Robustness.

Acknowledgements

First and foremost, we extend our heartfelt gratitude to **GOD Almighty Allah** for granting us the strength, patience, and perseverance to carry out this humble work. Without His guidance and mercy, none of this would have been possible.

We would also like to express our profound appreciation to our **parents**, whose unwavering support, unconditional love, and constant encouragement have been the cornerstone of our academic journey. Their sacrifices and belief in us have been a continuous source of motivation.

Our sincere thanks go to our supervisors : Professor **BOUCHERIT Mohamed Seghir**, Professor **Mohamed TADJINE**, and Doctor **Messaoud CHAKIR**. Their expertise, insightful guidance, and generous mentorship have been instrumental in the development of this project. Their dedication and commitment to excellence have greatly influenced our learning and personal growth.

Lastly, we are grateful to all those who, in one way or another, contributed to the success of this work. Whether through direct involvement or silent support, their contributions have played a meaningful role in the realization of this project.

Dedication

To my dear father,

To my dear mother ,

To my brothers Larbi, Abdennour and Djaoued,

To my sister,

To all my family and friends,

To my partner in this work Khaled,

Akram

To all my family and friends,

To my partner in this work Akram,

Khaled

Contents

List of Tables

List of Figures

List of Abbreviations

RO	Reverse Osmosis
MPC	Model Predictive Control
PID	Proportional – Integral – Derivative
IMC	Internal Model Control
SISO	Single Input – Single Output
MIMO	Multiple Input – Multiple Output
RMSE	Root Mean Square Error
NRMSE	Normalized Root Mean Square Error
MAE	Mean Absolute Error
R^2	Coefficient of Determination
Ts	Sampling Time
Np	Prediction Horizon
Nc	Control Horizon

List of Symbols

$G_{ij}(s)$	Transfer function from input j to output i
u	Control variable (input)
y	Output variable (measured)
r	Reference signal (setpoint)
e	Control error, $e = r - y$
K_p	Proportional gain
T_i	Integral time constant
T_d	Derivative time constant
λ	Weight on control input variation
Q	Weighting matrix for output tracking in cost function
R	Weighting matrix for input effort in cost function
Δu	Change in control input
x_{op}	Operating point (reference state)
π	Osmotic pressure
T	Temperature (K)
R	Universal gas constant (J/K mol)
V_B	Volume of the solvent (m^3)
X_B	Mole fraction of the solvent
C_{A_i}	Solute concentration (mol/m^3)

General Introduction

"**We made from water every living thing**"

Approximate translation of verse 30, Surah Al-Anbya, the Quran

Freshwater is an essential resource for life, yet it is becoming increasingly scarce on a global scale.This scarcity is driven by several factors, including population growth, rapid urbanization, industrial development, and the effects of climate change. In certain arid regions or areas experiencing significant water stress, access to clean and safe drinking water is a major challenge. To address this issue, seawater desalination has emerged as a viable and sustainable solution to meet the growing demand for freshwater.

Among the available technologies, reverse osmosis (RO) is currently one of the most widely used methods. It enables the production of high-quality water from saline sources while offering a degree of operational flexibility. However, this technology remains complex and energy-intensive. Its efficiency strongly depends on the precise control of key variables such as feed pressure, permeate flow rate, and the conductivity of the produced water.

This work is organized into several chapters to provide a systematic and comprehensive exploration of the proposed problem of modeling and control of a reverse osmosis desalination system, with particular attention to membrane fouling prediction. The following outlines the organization of the thesis :

This chapter introduces the topic, providing an overview of the motivations, objectives, and contributions of this work. It also presents the scope of our work and outlines the organization of the subsequent chapters.

Chapter 1 presents reverse osmosis as a key desalination technology, outlining its fundamental operating principles, the underlying physical phenomena, and the main stages of a typical RO process. These stages include seawater intake, pretreatment, membrane separation using semi-permeable membranes, post-treatment, and final storage. The objective is to establish a comprehensive technological and operational framework for the system under investigation.

The chapter 2 is dedicated to the development of a dynamic model describing the behavior of a reverse osmosis (RO) desalination system. Based on physical principles and experimental data, the model captures the relationships between key variables such as feed pressure, pH, permeate flow rate, and conductivity. The mathematical formulation is linearized around an operating point and validated through experimental tests. The accuracy of the model is assessed using performance metrics including RMSE, NRMSE, and the coefficient of determination (R^2),

ensuring its reliability for control design purposes.

In chapter 3, focuses on the implementation of Model Predictive Control (MPC) strategies for the RO process. Two approaches are examined : the first applies MPC to a decoupled model representing separate control loops, while the second addresses the system in its full multivariable form. The MPC controllers are designed based on state-space representations, with constraints and cost functions defined to optimize tracking performance and system stability. Simulation results demonstrate the influence of prediction and control horizons on the system's responsiveness and robustness.

The chapter 4 explores classical PID control and its enhancement through the Internal Model Control (IMC) framework. Controllers are designed and applied to the two main control loops : permeate flow ($G_{11}(s)$) and conductivity ($G_{22}(s)$). A comparative analysis is conducted between the PID controllers obtained from literature and those designed using the IMC methodology. The results highlight the advantages of IMC-based PID tuning in terms of faster response, improved stability, and better disturbance rejection.

The final technical chapter 5 investigates the robustness of the proposed control strategies in the presence of modeling uncertainties, particularly multiplicative disturbances affecting the system dynamics. Frequency-domain analysis using singular value plots, along with time-domain closed-loop simulations, are used to evaluate the impact of these uncertainties. Conditions for robust stability are derived and tested on both control loops, providing insights into the system's capacity to maintain performance under imperfect model knowledge.

Finally, the general conclusion presents This work summarizes the complete set of tasks undertaken : rigorous modeling, development and comparison of various control strategies (MPC, PID, IMC-PID), and robustness analysis. The overarching objective is to enhance the performance, stability, and reliability of reverse osmosis desalination processes.

Chapitre 1

Reverse Osmosis Desalination

1.1 Introduction

At the beginning of the 20th century, inspired by the osmotic nature of cell membranes, researchers proposed the idea of using a membrane to separate salt from seawater. In the 1960s, American and Japanese scientists developed semi-permeable membranes for industrial purposes and quickly realized that these same membranes could be used for seawater desalination.[8].

In nature, osmosis is a vital mechanism for maintaining biological balance. However, in industrial applications, the process is referred to as reverse osmosis, as high pressure P (above the osmotic pressure, approximately 80 bars) is applied to force saltwater to flow from the highly concentrated compartment to the freshwater side through a semi-permeable membrane. In doing so, the freshwater compartment becomes enriched with clean water. If this pressure were not applied, osmosis would naturally cause the freshwater to migrate into the saltwater side, increasing its salinity.[8].

1.2 Fundamentals of Reverse Osmosis

1.2.1 Reverse Osmosis Phenomenon

Reverse osmosis is a membrane separation process that operates at the molecular scale in the liquid phase. Separation occurs by permeation through a permselective membrane under the action of a pressure gradient. It is based purely on physical principles and does not involve any chemical additives. The process typically operates at ambient temperature and is easily automated and scalable, with adaptable membrane surface areas.

Osmosis is a natural process in which species migrate from a dilute solution to a more concentrated one Figure 4.6 (a).When pressure is applied to the compartment containing the concentrated solution, the flow between the two compartments decreases until it reaches zero. The pressure at which the net flow stops is called the osmotic pressure Figure 4.6 (b). If the applied pressure - typically increased using a pump—exceeds the osmotic pressure, the flow is reversed : species move from the more concentrated side to the less concentrated side. This is known as the reverse osmosis phenomenon Figure 4.6 (c) [9].

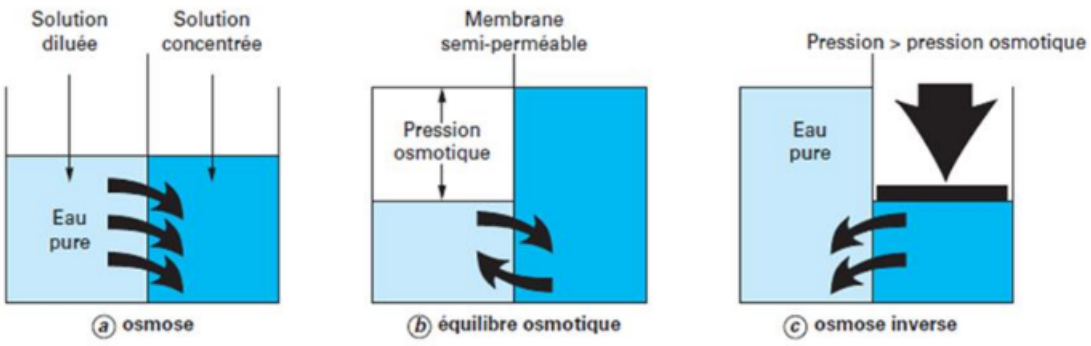

Fig. 1.1 : Schematic of (a) osmosis (b) osmotic equilibrium (c) RO

According to [4], the osmotic pressure (π_i) is a thermodynamic property of the solution, and it is related to the mole fraction of the solvent X_{B_i}, as follows :

$$\pi_i = -\left(\frac{RT}{V_B}\right) \ln X_{B_i} \tag{1.1}$$

where R is the universal gas constant (J/K mol), T is the temperature (K), and V_B is the volume of the solvent (m^3).
For dilute solutions, it has been shown that the previous equation can be simplified to the Van't Hoff equation, as follows :

$$\pi_i = C_{A_i} RT \tag{1.2}$$

where C_{A_i} is the solute concentration (mol/m^3).
Thus, the pressure difference across the membrane, $\Delta\pi$, is related to the concentration difference, $C_{A_2} - C_{A_3}$.
Osmotic pressure does not depend on the type of solute or the size of its molecules, but solely on its molar concentration, as shown in the Eq. 1.2[4]

1.3 Reverse Osmosis Process Stages

This work focuses on this type of desalination, as it is the most commonly employed method worldwide.

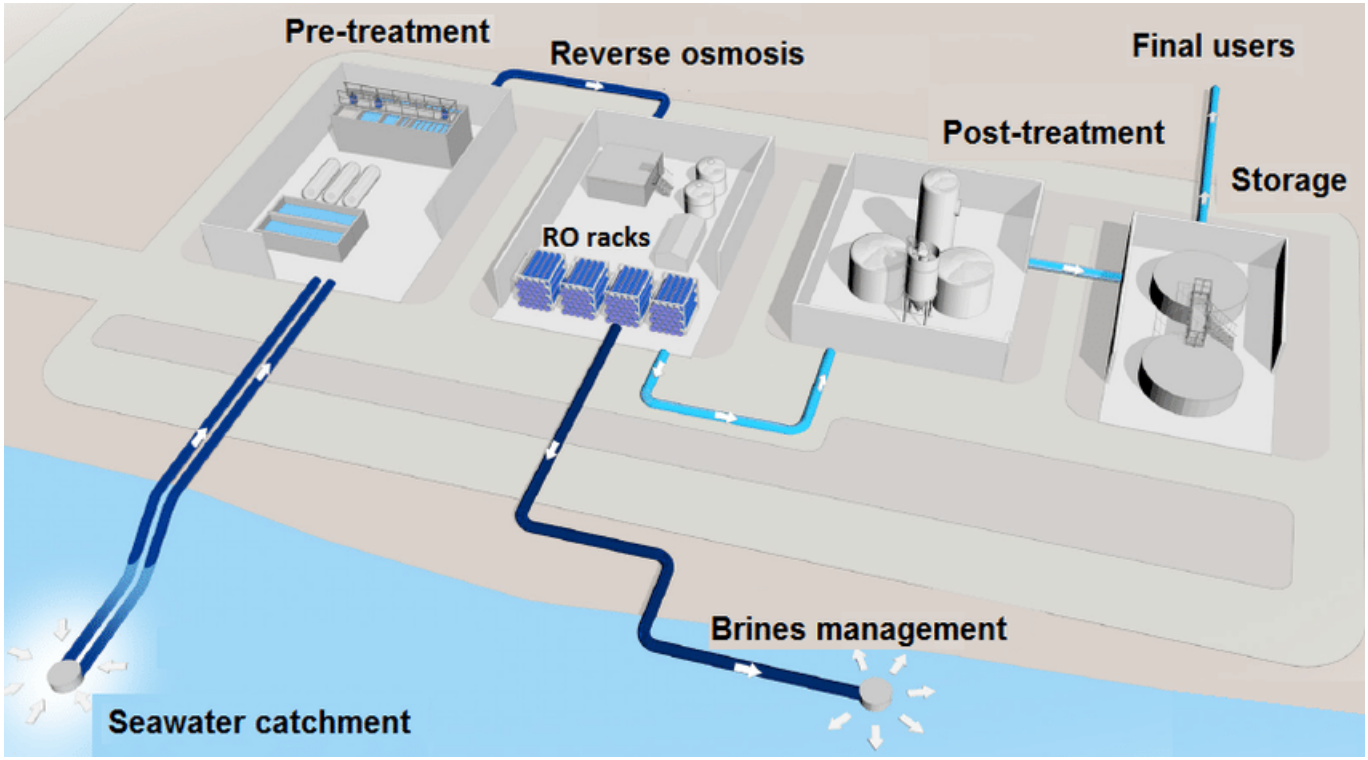

Fig. 1.2 : Membrane-Based Seawater Desalination via Reverse Osmosis

This process consists of five essential stages, which are :

1.3.1 Seawater Intake

The desalination process begins with the collection of seawater, primarily through open intakes or beach wells.

1.3.1.1 Open intakes

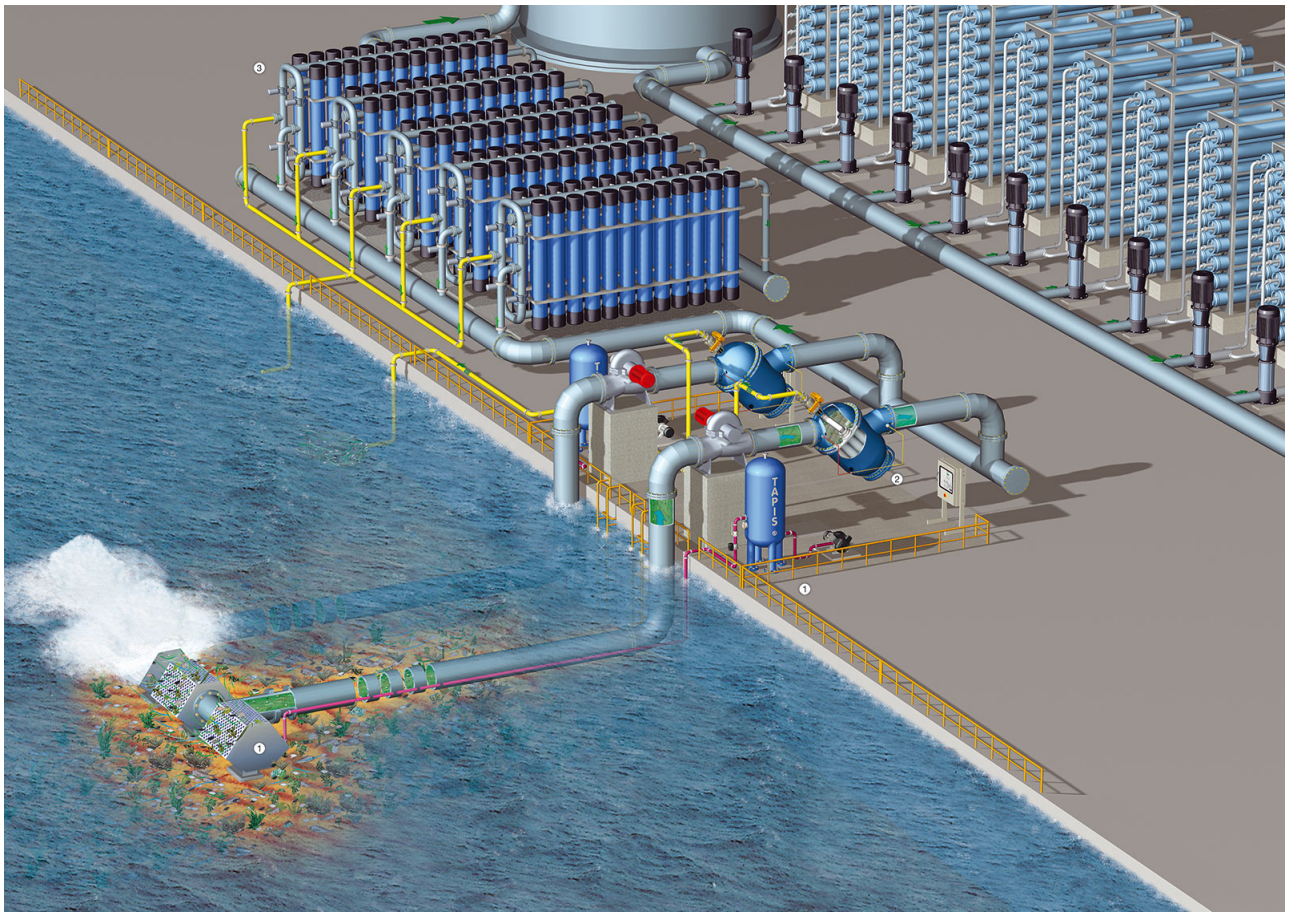

Fig. 1.3 : Seawater Collection through Open Intake Systems

Open seawater intakes allow for the collection of larger volumes of water and represent the most commonly used method in large-scale desalination plants.

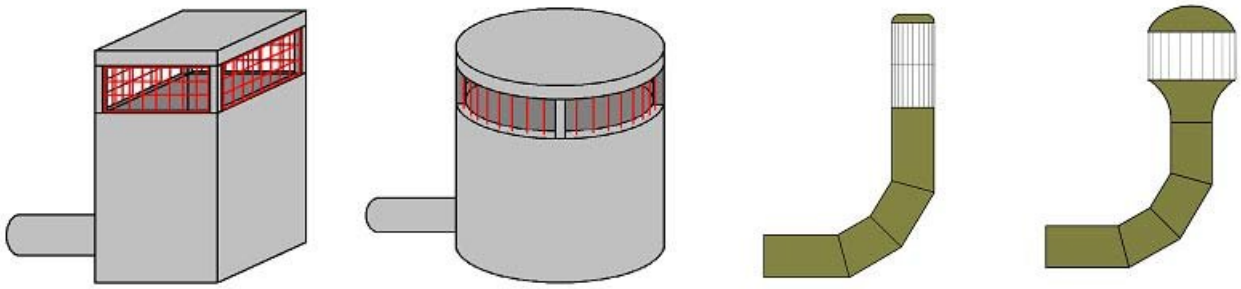

Fig. 1.4 : Water intakes [14]

However, the quality of the water provided is not consistently stable over time, as it is affected by turbidity, temperature fluctuations, marine discharges, and storm events.

1.3.1.2 Beach Wells

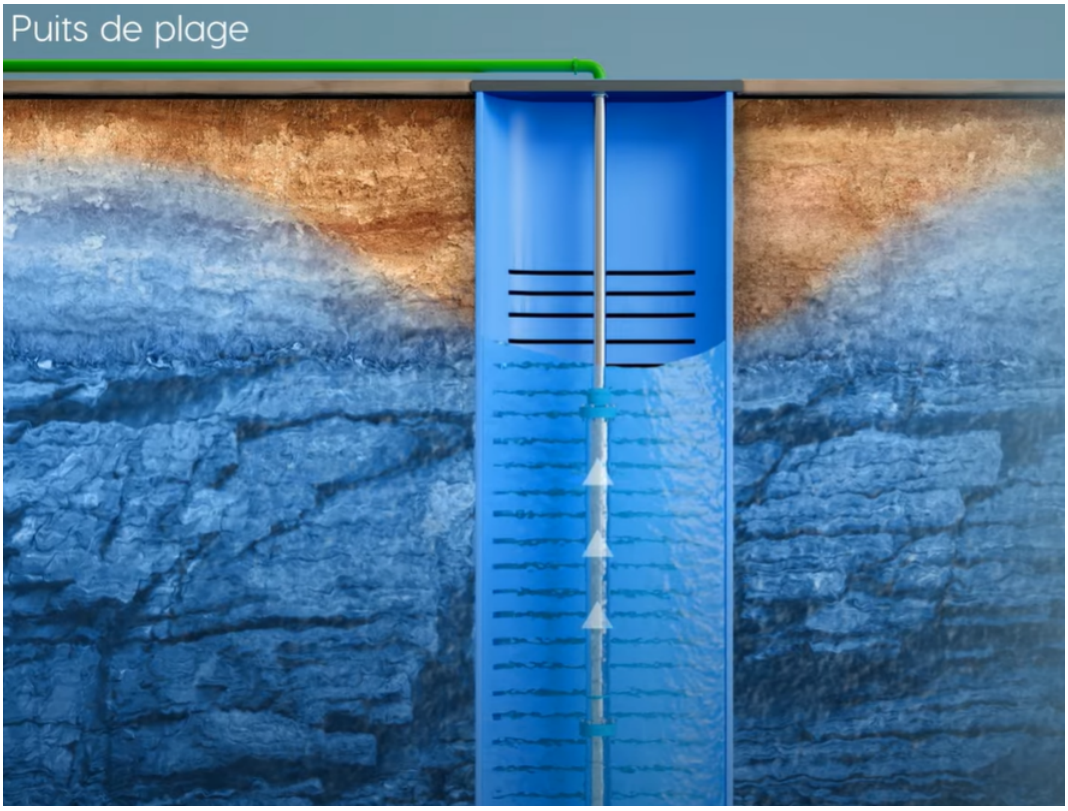

Fig. 1.5 : Seawater Wells

The well system provides higher and more stable water quality, thanks to the natural filtration process that occurs in the soil.

1.3.1.3 Seawater Intake Pumps

It is necessary to use pumps to transport the seawater to the plant, which are either installed on the surface (for water collected via open intakes) or submersible (for water drawn from seawater wells).

- **Submersible Pump :**

  As shown in Figure 1.6, **submersible pump** operates by being fully immersed in water, usually inside a seawater well. Unlike surface pumps, it pushes water to the surface rather than pulling it. This design minimizes the risk of cavitation and is suitable for deep water extraction with stable quality due to natural filtration through sediments.

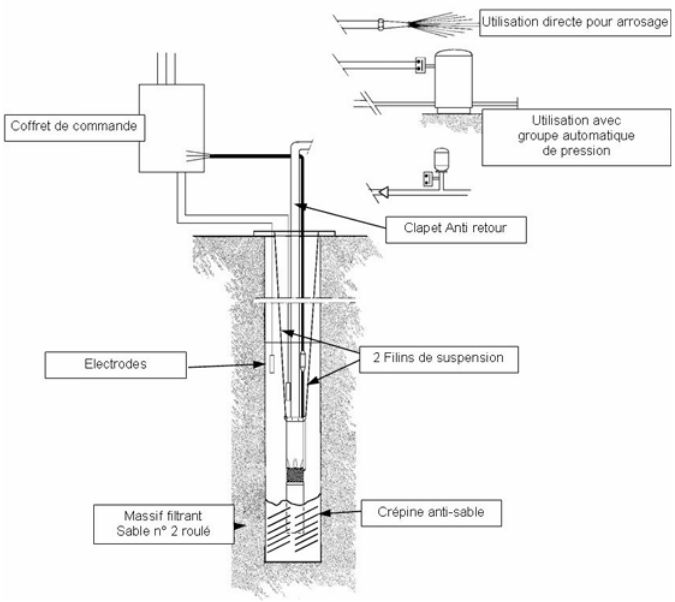

Fig. 1.6 : Diagram of the Submersible Pump Operation [23]

- **Pump installed on the surface :**

  A **surface pump** is a type of pump installed above the water level, typically on land. It is used to draw seawater through suction pipes and is commonly employed in open intake desalination systems. Surface pumps require careful installation to avoid issues like cavitation and must compensate for pressure losses due to suction height and friction in the pipes.

1.3.2 Pretreatment

Pretreatment is a critical stage in the reverse osmosis (RO) desalination process. Its main purpose is to protect the membranes by removing suspended solids, organic matter, and chemical components that can cause scaling, fouling, or damage to the RO system. The quality and stability of pretreatment directly affect the longevity and performance of the membranes.

1.3.2.1 Sand Filters (Raw Media Filter – RDMT)

Most suspended solids larger than 20 microns are retained at this stage.

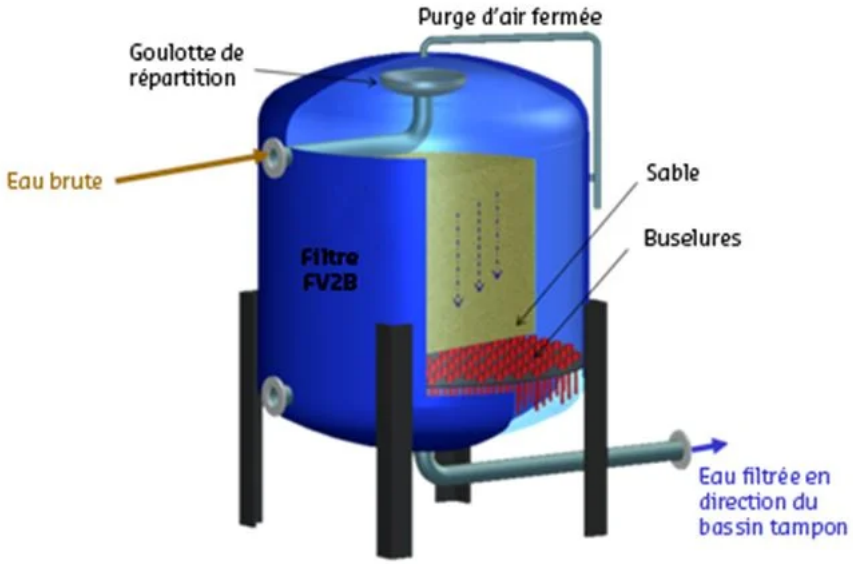

Fig. 1.7 : Filtration with Granular Media [12]

These filters must be cleaned regularly in order to be reused.

1.3.2.2 Additional Protection

- **Chemicals :** It is common practice to add an antiscalant along with various chemicals such as coagulants and sodium hypochlorite before starting the process, in order to prevent salt deposit buildup on the membranes.

	Produits	Exemple de concentrations relevées dans les eaux de rejet	Remarques
Produits antibactériens et antisalissure	Eau de javel (hypochlorite de sodium), chlore, sels de cuivre,	0,2 à 0,5 mg/L de chlore (libre + combiné) ont été reportés dans des effluents d'usines à procédé thermique (Dawoud, 2012)	
Produits anti-mousses	Polyglycols alkylés, acides gras, esters d'acides gras		Particulièrement utilisés dans les usines à osmose inverse
Floculants utlisés pour retirer les matières en suspension de l'eau	Chlorure ferrique ($FeCl_3$), chlorure d'aluminium ($AlCl_3$)		Non utilisé dans les usines à procédé thermique
Produits antitartre pour éviter la formation de tartre dans les tuyaux et membranes	Hexamétaphosphate de sodium ($NaPO_3$), polymères de l'acide maléique	La concentration habituelle d'acide maléique dans les eaux de rejets est proche de 0,5 mg/L (Morton, 1996)	
Solutions acides ou basiques pour ajuster le pH de l'eau	Acide sulfurique (H_2SO_4), acide chloridrique (HCl), chaux	Entre 1 500 et 4 800 mg/L de SO_4 dans les effluents d'usines de pays du Golf (Dawoud, 2012)	
Produits issus de la corrosion	Métaux lourds dont cuivre, fer et nickel	Entre 0,015 et 0,1 mg/L de cuivre dans les effluents rejetés par les usines à osmose inverse (Dawoud, 2012)	Cette corrosion et les rejets induits sont plus élevés dans les usines à procédé thermique

Fig. 1.8 : A list of some chemicals that need to be added

- **Cartridge Filters :** Cartridge filters are an additional safety system installed upstream of the high-pressure pumps and reverse osmosis membranes. Their purpose is to protect

the equipment by capturing microparticles that may have passed through the previous pretreatment stages.

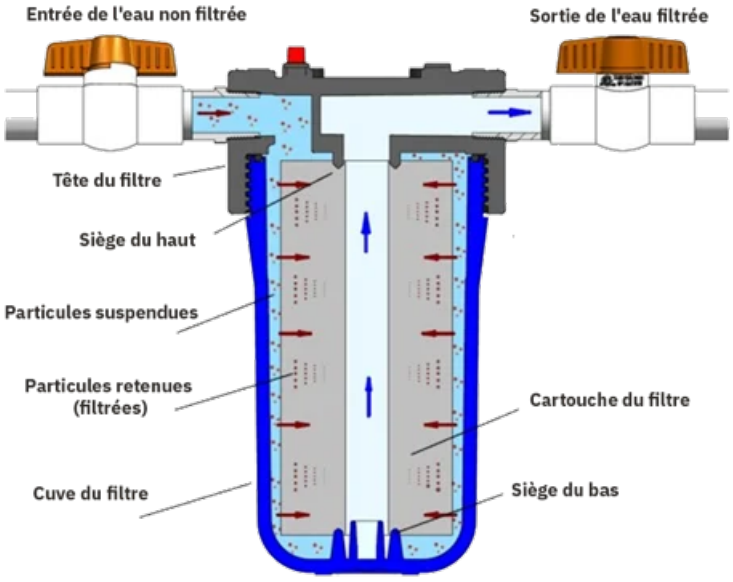

Fig. 1.9 : An Explanatory Diagram of Cartridge Filters [11]

The filtration size of cartridge filters generally ranges between 1 and 5 nominal microns. These filters are used to remove even finer particles and to further improve the quality of the water.

- **Disc Filters :** These filters, composed of stacked discs, are used to achieve an optimal level of purity before the water reaches the reverse osmosis module.

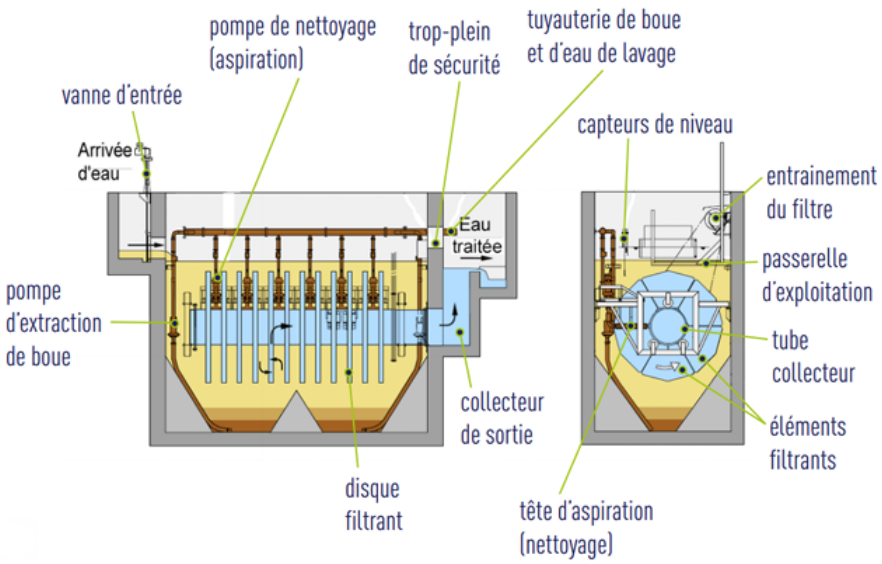

Fig. 1.10 : An Explanatory Diagram of Cartridge Filters

- **Equalization Tank :** The equalization tank serves to mix the pretreated water in order to smooth out fluctuations in flow rate and quality that may result from irregular raw water

intake.
It helps ensure a continuous and consistent supply to the system.

- **Pressurized Treatment :** Once the water has been pretreated, it must be subjected to sufficient pressure—typically between 50 and 60 bars—before being pumped into the pressure vessels containing the membranes. This is achieved using a high-pressure pump.

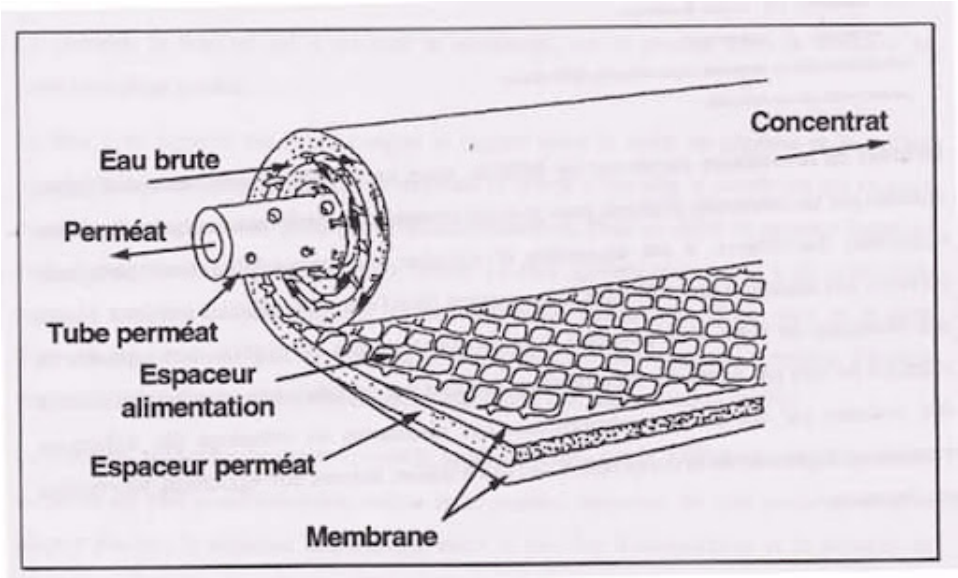

Fig. 1.11 : Explanatory Diagram of Water Flow Through RO Membranes [10]

1.3.3 RO Membranes (Reverse Osmosis Membranes)

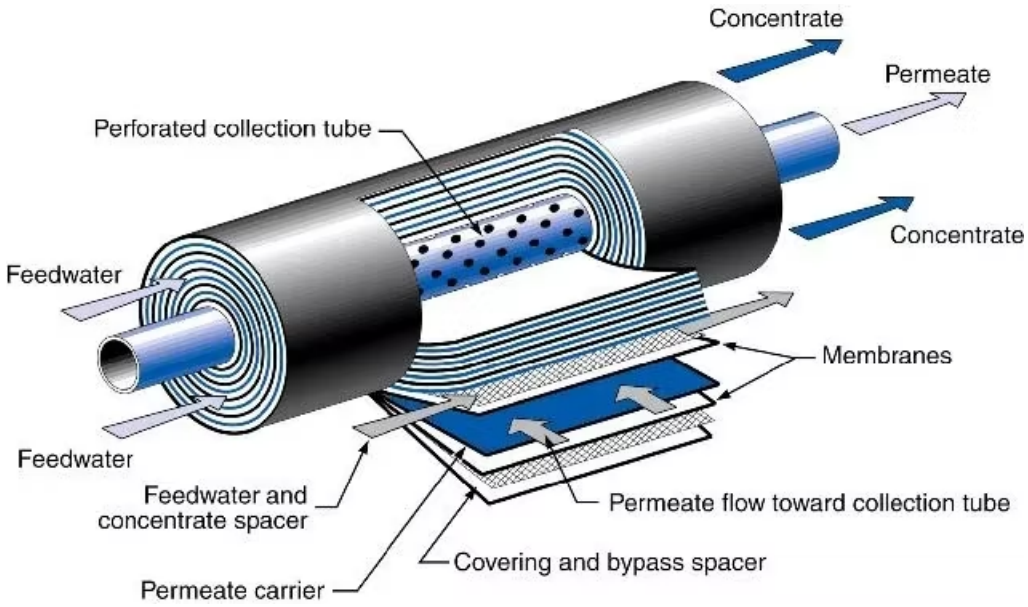

Fig. 1.12 : Explanatory Diagram of RO Membranes [13]

The system includes a series of pressure vessels, each containing several membranes (typically seven membranes arranged in series per vessel).
The flow of seawater molecules through the membranes occurs in a tangential manner.

1.3.4 Post-Treatment

After passing through the reverse osmosis membranes, the water is essentially free from dissolved salts, particles, and organic contaminants. However, the produced water (permeate) is not yet suitable for direct human consumption or industrial use. A post-treatment process is therefore required to adjust its chemical composition, ensure its stability, and meet quality standards. This process generally includes the following steps :

1. **Remineralization :** Since reverse osmosis water is highly demineralized, it is aggressive to pipelines and lacks essential minerals. Minerals (typically calcium and magnesium) are added to increase hardness and stabilize the pH. This is done through :
    - Filtration through a limestone bed ($CaCO_3$)
    - Injection of lime ($Ca(OH)_2$) or caustic soda (NaOH)
2. **pH Adjustment :** The pH is adjusted to prevent pipe corrosion and to comply with drinking water standards. This step is often combined with remineralization.
3. **Disinfection :** A final disinfection step is applied to eliminate any potential microbial contamination. This may include :
    - Chlorine injection (Cl_2)
    - Ozonation (O_3)
    - UV sterilization
4. **Quality Control :** Analyses are carried out to ensure that the treated water meets quality standards (e.g., WHO, EPA), particularly with respect to residual salts, pH, hardness, and absence of pathogens.

1.3.5 Storage and Distribution

Once the water has been remineralized, and if it is intended for human consumption, chlorination is carried out in the distribution tanks in order to comply with current public health regulations.

1.4 Conclusion

This chapter presented the main components and stages of a reverse osmosis (RO) desalination system. It highlighted the importance of each phase, from seawater intake and pretreatment to membrane separation, post-treatment, and storage. These stages are essential to ensure high-quality potable water production and to protect the membranes from fouling or damage. This overview lays the technical foundation necessary for the modeling and control strategies addressed in the following chapters.

Chapitre 2

Modeling and Validation of a Reverse Osmosis (RO) System

2.1 Introduction

Reverse osmosis (RO) desalination is a vital technology for addressing water scarcity. However, its efficiency depends on the precise control of key parameters : permeate flow rate (productivity) and conductivity (quality). These variables, influenced by feed pressure and pH, require rigorous dynamic modeling to optimize control systems.

2.2 Objective

The prototype was developed to study and optimize the control of critical parameters in a reverse osmosis (RO) desalination system, namely :

- Permeate flow rate (an indicator of productivity).
- Permeate conductivity (an indicator of quality, related to salinity).

The main objective was to design a robust closed-loop control system for efficient and sustainable operation.

2.3 Prototype Description

The system under study is a pilot-scale reverse osmosis (RO) desalination unit installed in the R&D laboratory of a water treatment facility in Kuwait [26].

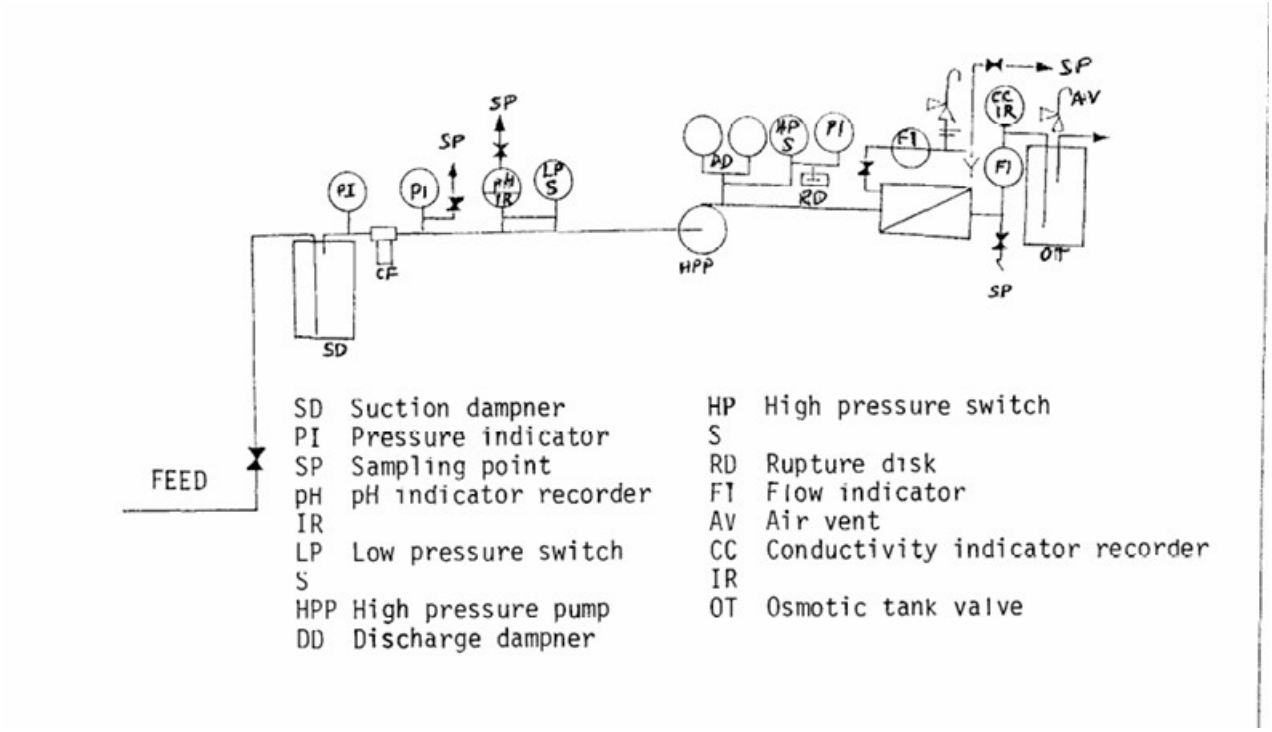

Fig. 2.1 : P$ID Diagram of the RO Prototype [26]

Process Components :
The prototype consists of the following elements :

- **High-Pressure Pump :** Capacity up to 80 bar (1,160 psi).
- **Permeator :**
  - **Model :** B-10 Permasep (DuPont)
  - **Configuration :** Hollow aramid fibers
  - **Nominal capacity :** 1,400 GPD (5.30 m^3/day)
  - **Operating pressure :** 800–1,200 psig (5,515–8,274 kPa)
- **Pretreatment :**
  - Dual media pressure filters (20 μm)
  - Dosing of Fe^{3+} (coagulation) and H_2SO_4 (pH adjustment)
- **Instrumentation :**
  - Pressure, pH, conductivity, and flow sensors
  - Data acquisition systems for real-time monitoring

2.4 Modeling of the Reverse Osmosis Desalination Process (in GPM, psi, µS/cm)

The reverse osmosis process is based on the separation of solutes from a solution using a semi-permeable membrane under the effect of a pressure gradient.
In the following, we present a symbolic model of the permeate flux and the permeate conductivity as functions of the system's physical parameters.

2.4.1 Permeate Flux Expression

The permeate flux F (expressed in gallons per minute – GPM) can be modeled using a modified form of the generalized Darcy's law :

$$F = A_w \cdot (\Delta P - \Delta\pi) \tag{2.1}$$

where :

- A_w : hydraulic permeability of the membrane (GPM/psi),
- $\Delta P = P_f - P_p$: total pressure difference (in psi),
- $\Delta\pi = \pi_f - \pi_p$: osmotic pressure difference (in psi).

2.4.2 Simplifying Assumptions

In most systems, the permeate pressure as well as its osmotic pressure can be neglected. The previous equation can then be simplified as follows :

$$F = A_w \cdot (P_f - \pi_f) \tag{2.2}$$

2.4.3 Solute Concentration Relationship

The feed osmotic pressure can be modeled using Van't Hoff's law :

$$\pi_f = \phi \cdot C_f \tag{2.3}$$

where :

- ϕ : osmotic coefficient (psi·m³/mol),
- C_f : solute concentration in the feed (mol/m³).

This leads to the final expression for the flux :

$$F = A_w \cdot (P_f - \phi C_f) \tag{2.4}$$

2.4.4 Modeling of Permeate Conductivity

The permeate conductivity Cond (expressed in microsiemens per centimeter – µS/cm) depends on the concentration of residual ions in the permeate.
It can be approximated by the sum of ionic contributions :

$$\text{Cond} = \sum_i \lambda_i \cdot [C_i] \approx \lambda_{\text{eff}} \cdot C_p \tag{2.5}$$

where :

- λ_{eff} : average effective molar conductivity (µS·cm²/mol),
- C_p : ion concentration in the permeate (mol/m³).

2.4.5 Relationship Between Permeate Concentration and Rejection Rate

The concentration C_p depends on the membrane rejection rate R :

$$C_p = C_f \cdot (1 - R) \tag{2.6}$$

This rejection rate can be empirically modeled as a function of pressure :

$$R(P_f) = 1 - \exp(-\beta \cdot P_f) \tag{2.7}$$

Thus :

$$C_p = C_f \cdot \exp(-\beta \cdot P_f) \tag{2.8}$$

And consequently, the conductivity becomes :

$$\text{Cond} = \lambda_{\text{eff}} \cdot C_f \cdot \exp(-\beta \cdot P_f) \tag{2.9}$$

where :

- β : empirical rejection coefficient (1/psi).

2.4.6 Effect of pH on Conductivity

Under acidic or basic conditions, the ions H^+ and OH^- can significantly contribute to the overall conductivity :

$$\text{Cond} \approx \lambda_{\text{eff}} \cdot C_p + \lambda_{H^+} \cdot [H^+] + \lambda_{OH^-} \cdot [OH^-] \tag{2.10}$$

As a function of pH :

$$[H^+] = 10^{-pH}, \quad [OH^-] = 10^{-(14-pH)} \tag{2.11}$$

The complete form of the conductivity model becomes :

$$\text{Cond}(P_f, pH) = \lambda_{\text{eff}} \cdot C_f \cdot \exp(-\beta \cdot P_f) + \lambda_{H^+} \cdot 10^{-pH} + \lambda_{OH^-} \cdot 10^{-(14-pH)} \tag{2.12}$$

- F : permeate flux (GPM),
- P_f : feed pressure (psi),
- ϕ : osmotic coefficient (psi·m³/mol),
- A_w : hydraulic permeability (GPM/psi),
- C_f : feed solute concentration (mol/m³),

- Cond : permeate conductivity (µS/cm),
- λ_{eff} : effective molar conductivity (µS·cm²/mol),
- β : rejection coefficient (1/psi),
- PH : hydrogen ion concentration (−log scale),
- λ_{H^+}, λ_{OH^-} : molar conductivities of H^+ and OH^- (µS·cm²/mol).

The final relationships obtained for permeate flux and conductivity, taking into account the effects of both pressure and pH, are given by :

$$F = A_w \cdot (P_f - \phi \cdot C_f) \tag{2.13}$$

$$\text{Cond}(P_f, pH) = \lambda_{\text{eff}} \cdot C_f \cdot \exp(-\beta \cdot P_f) + \lambda_{H^+} \cdot 10^{-pH} + \lambda_{OH^-} \cdot 10^{-(14-pH)} \tag{2.14}$$

2.5 Mathematical Model

This linearized model is derived from the fundamental equations previously presented (permeate flux $F = A_w \cdot (P_f - \phi C_f)$ and conductivity $\text{Cond}(P_f, pH)$), and simplified under linearity assumptions that were experimentally validated by *Alatiqi et al. (1989)* [26] within the typical operating ranges of the system.

The model, linearized around the following nominal operating point :

Nominal Operating Point[26]

- **Feed Pressure : 900 psi** (reference pressure during step tests),
- **Permeate Flux : 1.05 gpm** (initial value before disturbances),
- **Permeate Conductivity : 430–440 µS/cm** (stable range before testing),
- **pH : 6.45** (nominal value prior to step variations)

is described by the following transfer function matrix :

$$\begin{bmatrix} F(s) \\ C(s) \end{bmatrix} = \begin{bmatrix} \dfrac{0.002\,(0.056s+1)}{0.003s^2+0.1s+1} & 0 \\ \dfrac{-0.51\,(0.35s+1)}{0.213s^2+0.7s+1} & \dfrac{-57\,(0.32s+1)}{0.6s^2+1.8s+1} \end{bmatrix} \begin{bmatrix} P(s) \\ \text{pH}(s) \end{bmatrix} \tag{2.15}$$

where :

$$\mathbf{Y}(s) = \begin{bmatrix} F(s) \\ C(s) \end{bmatrix}, \quad \mathbf{U}(s) = \begin{bmatrix} P(s) \\ \mathrm{pH}(s) \end{bmatrix}$$

- P : Feed pressure (psi),
- pH : Input fluid pH,
- F : Permeate flux (gpm),
- C : Permeate conductivity (μS/cm).

Interaction Analysis

Effect of P :

- **On F :** Static gain $+0.002$ gpm/psi, fast dynamics (dominant poles at $s = -33.33\,\mathrm{min}^{-1}$).
- **On C :** Static gain -0.51 μS/cm/psi, slower dynamics (pole at $s = -1.43\,\mathrm{min}^{-1}$).

Effect of PH :

- **On C :** Static gain -57 μS/cm per pH unit, second-order response.
- **On F :** No effect ($G_{p12} = 0$).

2.6 Experimental Validation and Performance Analysis

2.6.1 Data Preparation

The data used in the study [26] (Table 22 and Table 3) are experimental and were collected from a pilot-scale reverse osmosis (RO) unit at the R&D laboratory in Doha (Kuwait). These data include precise measurements of permeate flux and conductivity during step response testing.

Variables	**Approximate Ranges**
Flux (gpm)	0.85–1.25
Pressure (psig)	800–1000
Conductivity (μS/cm)	400–450
PH	6–7

Tab. 2.1 : Approximate operating ranges of system variables

2.6.2 Model Definition

In this study, the three transfer functions analyzed are based on a standard mathematical model of the following form :

$$G(s) = \frac{K_i\,(T_a s + 1)}{T^2 s^2 + 2\xi T s + 1} \tag{2.16}$$

2.6.2.1 Model Simulation

This step is central to the validation process. It enables the prediction of the model's behavior in response to real variations in the inputs (experimental data), and allows comparison between the model's predictions and the actual measured conductivity values.

2.6.3 Model vs. Experimental Comparison

2.6.3.1 Graphical Visualization

The following figures present the experimental data (actual measurements) alongside the model predictions for $G_{11}, G_{21},$ **and** G_{22}.

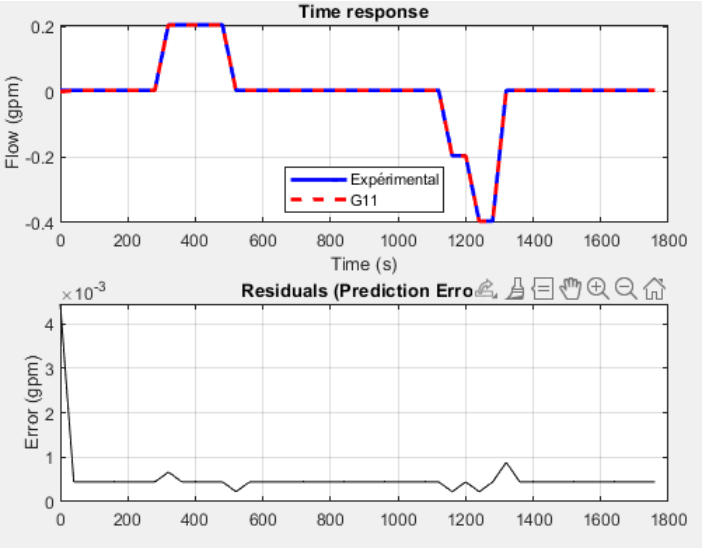

Fig. 2.2 : Time Response of Permeate Flux to Feed Pressure Disturbances and Prediction Errors G_{11}

Observations :

- The model predictions closely match the experimental data, validating the fast and linear pressure–flux dynamics described by G_{11}.
- The residuals (prediction errors) are extremely low.

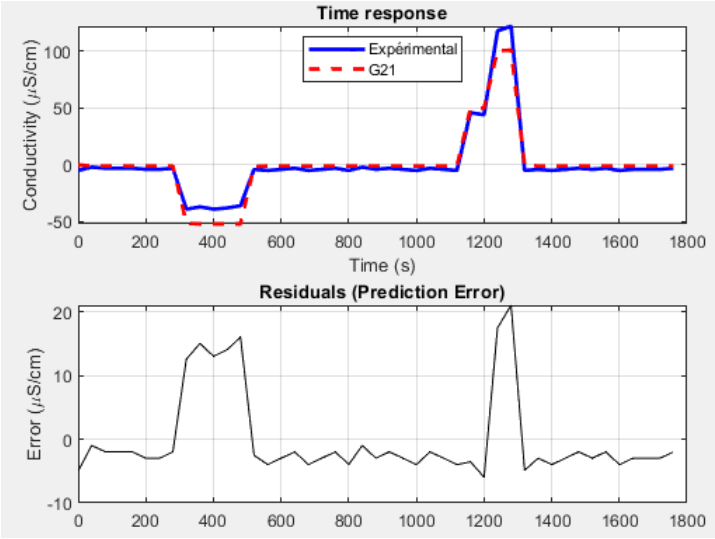

Fig. 2.3 : Time response of permeate conductivity to feed pressure disturbances and prediction errors (G_{21})

Observations :

- The model captures the general trend well, although minor deviations appear during rapid transitions (conductivity peaks).

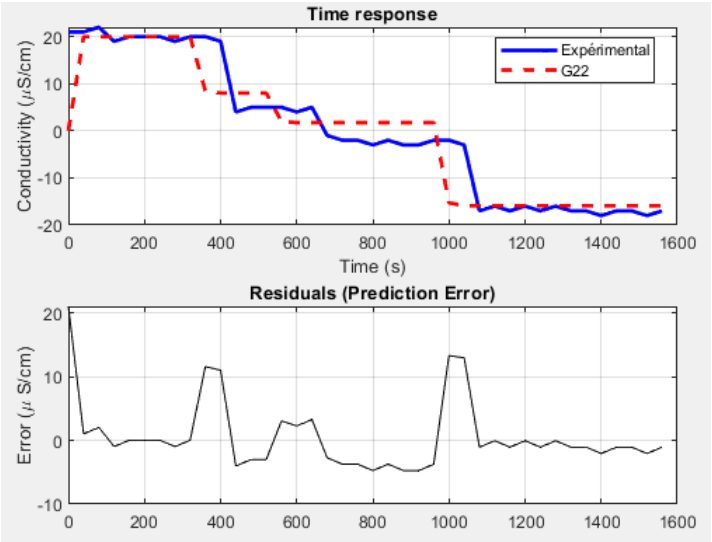

Fig. 2.4 : Time response of permeate conductivity to pH disturbances and prediction errors (G_{22})

Observations :

- The predictions follow the experimental trend, but with more noticeable errors, particularly during transient phases.

2.6.3.2 Residual Calculation

Residuals, defined as the difference between experimental values and model predictions, are computed at each time point t_i using the following expression :

$$\text{Residual}_i = \underbrace{y_{\text{exp},i}}_{\substack{\text{Experimental} \\ \text{value}}} - \underbrace{y_{\text{model},i}}_{\substack{\text{Predicted} \\ \text{value}}} \tag{2.17}$$

- $y_{\text{exp},i}$: Experimental output value at point i,
- $y_{\text{model},i}$: Model-predicted output at point i,
- $R_{\text{residual},i} = y_{\text{exp},i} - y_{\text{model},i}$: Deviation between measurement and prediction (modeling error).

Residual Visualization

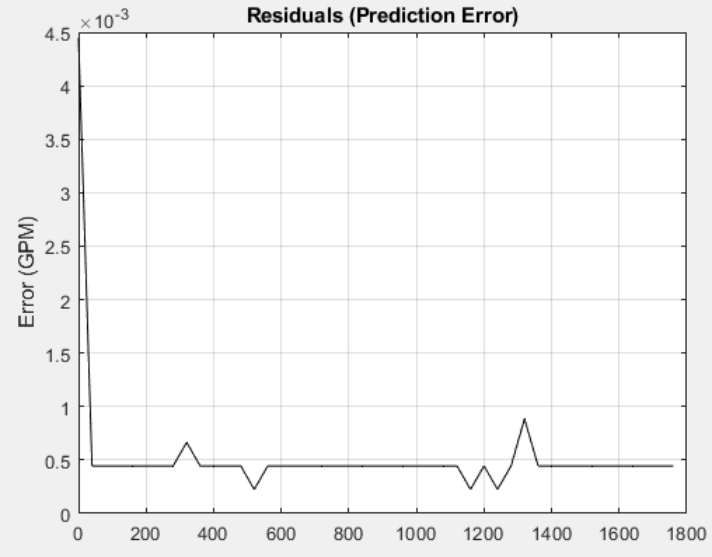

Fig. 2.5 : Prediction residuals for model G_{11}

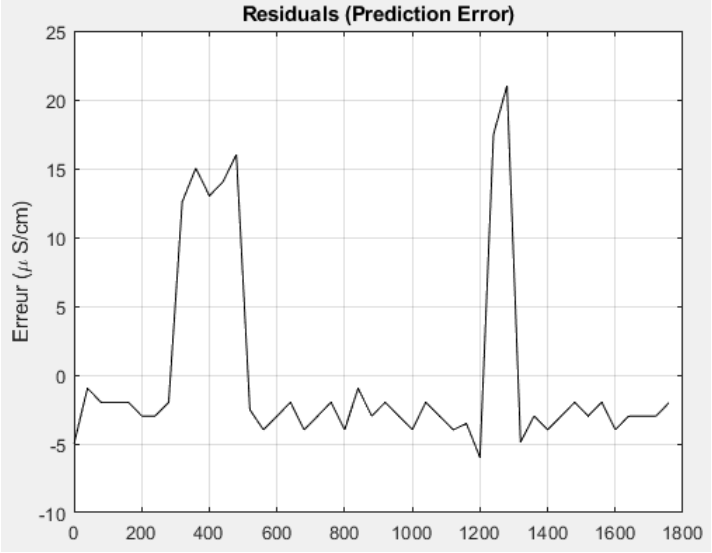

Fig. 2.6 : Prediction residuals for model G_{21}

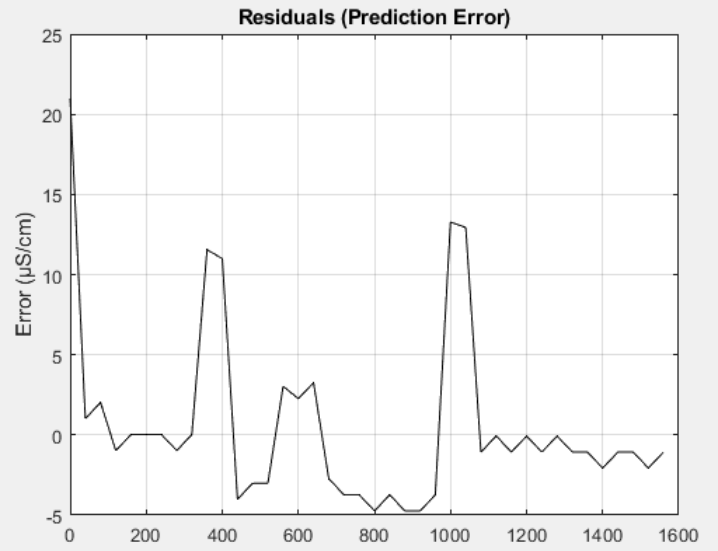

Fig. 2.7 : Prediction residuals for model G_{22}

Observations :

- **G_{11} :** Residuals are extremely small and random, confirming the model's reliability for real-time control.
- **G_{21} :** Residuals are small but exhibit a few localized peaks, likely due to unmodeled disturbances.
- **G_{22} :** Residuals are more significant and structured, highlighting the influence of pH nonlinearities on conductivity.

2.6.4 Performance Metrics (RMSE, NRMSE, R^2, MAE)

This section presents the metrics used to evaluate the accuracy of the identified dynamic model.

2.6.4.1 RMSE (Root Mean Square Error)

RMSE measures the average deviation between model predictions and experimental data :

$$\text{RMSE} = \sqrt{\frac{1}{N}\sum_{i=1}^{N}\left(y_{\text{exp},i} - y_{\text{model},i}\right)^2} \tag{2.18}$$

- N : Total number of experimental samples
- $y_{\text{exp},i}$: Measured output at time i
- $y_{\text{model},i}$: Model-predicted output at time i

2.6.4.2 NRMSE (Normalized Root Mean Square Error)

NRMSE normalizes RMSE by the dynamic range of the data :

$$\text{NRMSE} = \frac{\text{RMSE}}{y_{\text{max}} - y_{\text{min}}} \times 100\% \tag{2.19}$$

- y_{max} : Maximum value in the experimental dataset
- y_{min} : Minimum value in the experimental dataset

2.6.4.3 R^2 (Coefficient of Determination)

The R^2 coefficient quantifies the proportion of variance explained by the model :

$$R^2 = 1 - \frac{\sum_{i=1}^{N} \left(y_{\text{exp},i} - y_{\text{model},i}\right)^2}{\sum_{i=1}^{N} \left(y_{\text{exp},i} - \bar{y}_{\text{exp}}\right)^2} \tag{2.20}$$

- $\bar{y}_{\text{exp}}$: Mean of the experimental values :

$$\bar{y}_{\text{exp}} = \frac{1}{N} \sum_{i=1}^{N} y_{\text{exp},i}$$

2.6.4.5 MAE (Mean Absolute Error)

MAE provides the average absolute error :

$$\text{MAE} = \frac{1}{N} \sum_{i=1}^{N} |y_{\text{exp},i} - y_{\text{model},i}| \tag{2.21}$$

- N, $y_{\text{exp},i}$, $y_{\text{model},i}$: Defined as for RMSE

2.6.4.5 Computation Results :

Model	RMSE	NRMSE (%)	R^2	MAE
G11 (Pressure → Flux)	0.0008 gpm	0.0014	0.99995	0.0005 gpm
G21 (Pressure → Conductivity)	6.8787 µS/cm	0.0427	0.9475	4.9200 µS/cm
G22 (PH → Conductivity)	5.5976 µS/cm	0.1399	0.8502	3.4553 µS/cm

Tab. 2.2 : Performance metrics of the identified transfer functions

2.6.5 Results Analysis

G_{11} : An NRMSE of 0.0014% and an R^2 value close to 1 indicate that the model captures the pressure–flux relationship almost perfectly. Furthermore, the fast and linear dynamics between

pressure and flux justify this high level of performance. This model is sufficiently reliable to be used in real-time control loops.

G_{21} : An $R^2 > 0.94$ and a low NRMSE ($< 0.05\%$) confirm the model's ability to predict conductivity under pressure variations. The remaining 5.25% of unexplained variance may be attributed to external disturbances such as temperature or salinity fluctuations.

G_{22} : An $R^2 = 0.85$ and an NRMSE $< 0.2\%$ show that the model is usable, though less accurate than G_{11} and G_{21}. Nonlinear effects of PH—such as salt precipitation thresholds—are not captured by this linear model.

2.6.6 Open-Loop Simulation

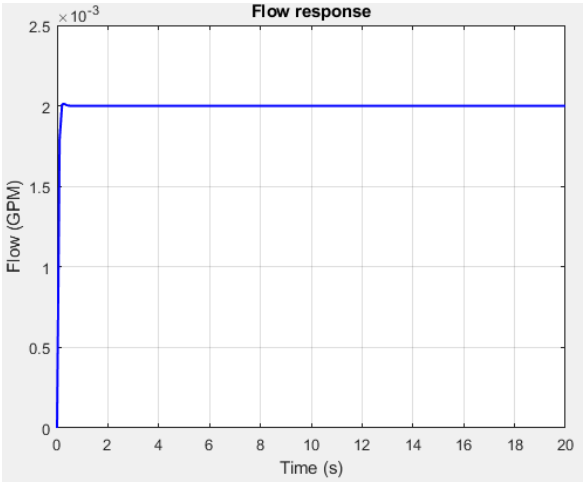

Fig. 2.8 : Open-loop step response – Permeate flux

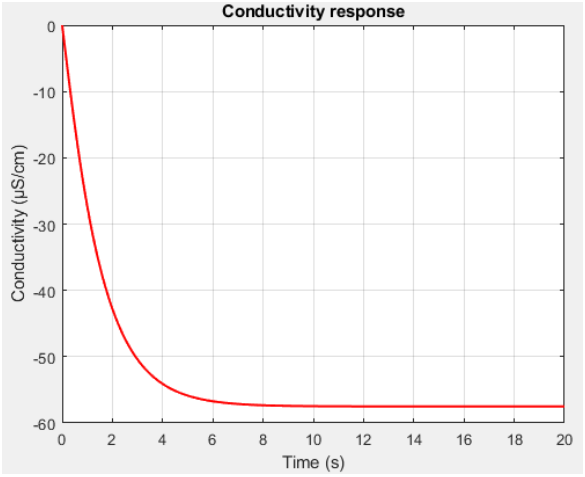

Fig. 2.9 : Open-loop step response – Conductivity

- The step response of the **flux** is comparable to that of a *first-order system*. Although G_{11} contains complex poles, the presence of a zero in the numerator acts as a derivative effect that damps oscillations.
- For **conductivity**, its step response also resembles that of a *first-order system*. The presence of a zero in the transfer functions G_{21} and G_{22} reduces oscillatory behavior, giving a response similar to that of a first-order system. However, the response evolves in the *opposite direction*, due to the *negative gain* of both transfer functions.
- **The flux response is faster than the conductivity response**, which is consistent with the inherent dynamics of each channel in the system, given the respective time constants ($T_{\text{Flux}} = 0.0959\,\text{s}$, $T_{\text{Cond}} = 3.1086\,\text{s}$).

2.7 Conclusion

Although the effect of PH on conductivity is inherently nonlinear (due in particular to salt precipitation and dissociation phenomena), a linear model was chosen for G_{22} in order to :

- Ensure the validity of a local approximation around the nominal operating point (the considered PH perturbations remain small) ;
- Reduce computational complexity with a view to real-time embedded implementation.

The good performance results (NRMSE $< 0.2\%$, $R^2 = 0.85$) demonstrate that, for the tested pH variations, this linearization is an acceptable compromise between accuracy and simplicity.

Linear relationships (pressure–flux) are easier to model than nonlinear ones (PH–conductivity).

The models G_{11}, G_{21}, and G_{22} are accurate enough to be used for control applications.

Chapitre 3

Model Predictive Control Strategies for Reverse Osmosis Systems

3.1 Introduction

Model Predictive Control (MPC) is an advanced control method based on a dynamic model of the system, enabling prediction of future behavior and optimization of control actions while respecting system constraints.
It is particularly well-suited for complex systems such as reverse osmosis (RO) in desalination processes. The objective is to ensure potable water quality, optimize system performance, and protect the membranes.
More specifically, the control aims to limit feed pressure to 900 psi, reduce permeate conductivity below 440 µS/cm, and stabilize the permeate flow around 1.25 GPM.

3.2 Objective

Controlling an RO system is intended to ensure compliance with water quality standards, maximize efficiency, and protect the equipment.
The main control objective is to maintain feed pressure below the maximum limit of 1000 psi to protect the membranes, to reduce permeate conductivity below 440 µS/cm to ensure water potability and prevent membrane fouling, and to keep the permeate flow rate close to 1.05 GPM, which corresponds to the system's nominal capacity [24].

Parameter	**Control Objective**
Permeate Conductivity	Maintain < 440 µS/cm to ensure potability
Permeate Flow Rate	Maintain near 1.05 GPM (nominal capacity)

Tab. 3.1 : Control objectives of the reverse osmosis system [24]

Remark :
The selection of the predictive controller parameters (whether for the decoupled model or the global model), namely the prediction horizon, the control horizon, and the weighting matrices Q , R and λ, was carried out empirically through a series of tests and trials.
The objective was to identify the combination of parameters that provides the best overall system performance in terms of **stability**, **response speed**, **tracking quality**, and **robustness** to disturbances.
The final tuning corresponds to the configuration that offers the **best trade-off** between these criteria.

3.3 The Linear RO System

3.3.1 Control Model

The linear model of the reverse osmosis (RO) system used in this chapter is based on experimentally identified transfer functions that describe the dynamic relationships between the inputs (pressure, pH) and outputs (permeate flow rate, conductivity). This model was established and validated in the previous chapter, confirming its relevance for the development of the control laws investigated in this work. It is based on the structure presented in the work of Alatiqi et al. (1989) [26].

The model is represented by the following transfer function matrix :

$$\begin{bmatrix} F(s) \\ \\ C(s) \end{bmatrix} = \begin{bmatrix} \dfrac{0.002\,(0.056s+1)}{0.003s^2+0.1s+1} & 0 \\ \\ \dfrac{-0.51\,(0.35s+1)}{0.213s^2+0.7s+1} & \dfrac{-57\,(0.32s+1)}{0.6s^2+1.8s+1} \end{bmatrix} \begin{bmatrix} P(s) \\ \\ \mathrm{pH}(s) \end{bmatrix} \tag{3.1}$$

where :

$$\mathbf{Y}(s) = \begin{bmatrix} F(s) \\ \\ C(s) \end{bmatrix}, \quad \mathbf{U}(s) = \begin{bmatrix} P(s) \\ \\ \mathrm{pH}(s) \end{bmatrix}$$

- P : Feed pressure (psi),
- pH : Input fluid pH,
- F : Permeate flow rate (gpm),
- C : Permeate conductivity (μS/cm).

3.3.2 System Decoupling

In multivariable systems, interactions between control loops can complicate controller design and degrade system performance, especially when coupling is strong.
In our case, analysis of the dynamic model shows that the system has an **upper triangular structure**, meaning that one of the two inputs affects both outputs :

- Feed pressure (P) affects both the permeate flow rate (F) **and** conductivity (C),
- Feed pH affects only the conductivity (C), with no significant influence on the flow rate (F).

Thus, the dynamic system matrix takes the form :

$$G(s) = \begin{bmatrix} G_{11}(s) & 0 \\ G_{21}(s) & G_{22}(s) \end{bmatrix} \tag{3.2}$$

This structure suggests the possibility of treating each loop independently. A structural analysis of the system is essential to select the most appropriate input–output pairings.
A common method for guiding this selection is the **Relative Gain Array (RGA)** analysis, which assesses cross-variable influence and helps select optimal input–output pairings.

The RGA matrix is defined from the static gain matrix $G(0)$ by :

$$\Lambda = G(0) \circ \left(G(0)^{-1}\right)^{\top} \tag{3.3}$$

where $\circ$ denotes the Hadamard (element-wise) product, and $G(0)$ is the matrix of static gains (i.e., transfer function values at $s = 0$).

The inverse of $G(0)$ is computed as :

$$G(0)^{-1} = \frac{1}{\det(G(0))} \begin{bmatrix} -57 & 0 \\ 0.51 & 0.002 \end{bmatrix} = \frac{1}{-0.114} \begin{bmatrix} -57 & 0 \\ 0.51 & 0.002 \end{bmatrix} \tag{3.4}$$

Which gives :

$$G(0)^{-1} = \begin{bmatrix} 500 & 0 \\ -4.47 & -0.0175 \end{bmatrix} \tag{3.5}$$

Therefore, the RGA matrix is calculated as :

$$\Lambda = G(0) \circ \left(G(0)^{-1}\right)^{\top} = \begin{bmatrix} 0.002 \cdot 500 & 0 \cdot (-4.47) \\ -0.51 \cdot 0 & -57 \cdot (-0.0175) \end{bmatrix} = \begin{bmatrix} 1 & 0 \\ 0 & 1 \end{bmatrix} \tag{3.6}$$

We now compute the decoupling matrix $D(s)$, with the goal of transforming the coupled transfer function matrix into a diagonal form :

$$G_D(s) = G(s) \cdot D(s) = \begin{pmatrix} G_{11} & G_{12} \\ G_{21} & G_{22} \end{pmatrix} \cdot \begin{pmatrix} 1 & d_1(s) \\ d_2(s) & 1 \end{pmatrix}$$

$$G_D(s) = \begin{pmatrix} G_{11} + G_{12}d_2(s) & G_{11}d_1(s) + G_{12} \\ G_{21} + G_{22}d_2(s) & G_{21}d_1(s) + G_{22} \end{pmatrix}$$

To obtain a diagonal matrix, we cancel the off-diagonal terms by solving :

$$\begin{cases} G_{11}d_1(s) + G_{12} = 0 \\ G_{21} + G_{22}d_2(s) = 0 \end{cases} \tag{3.7}$$

Solving these equations gives :

$$d_1(s) = -\frac{G_{12}}{G_{11}} = -\frac{0}{G_{11}} = 0$$

$$d_2(s) = -\frac{G_{21}}{G_{22}} = -\frac{0.1071s^3 + 0.6273s^2 + 1.097s + 0.51}{3.885s^3 + 24.91s^2 + 58.14s + 57}$$

Thus, the decoupler matrix is :

$$D(s) = \begin{bmatrix} 1 & 0 \\ -\frac{0.1071s^3+0.6273s^2+1.097s+0.51}{3.885s^3+24.91s^2+58.14s+57} & 1 \end{bmatrix}$$

The decoupled transfer function matrix becomes :

$$G_D(s) = \begin{bmatrix} G_{11} & 0 \\ 0 & G_{22} \end{bmatrix} = \begin{bmatrix} \frac{0.002(0.056s+1)}{0.003s^2+0.1s+1} & 0 \\ 0 & \frac{-57(0.32s+1)}{0.6s^2+1.8s+1} \end{bmatrix}$$

After decoupling, each output is predominantly influenced by its corresponding input :

- **Pressure** P primarily influences flow rate F,
- **pH** primarily influences conductivity C.

This decoupling greatly simplifies control, allowing each loop to be treated as a Single Input Single Output (SISO) system and enabling the use of classical controllers such as PID, without the need for complex cross-compensation strategies.

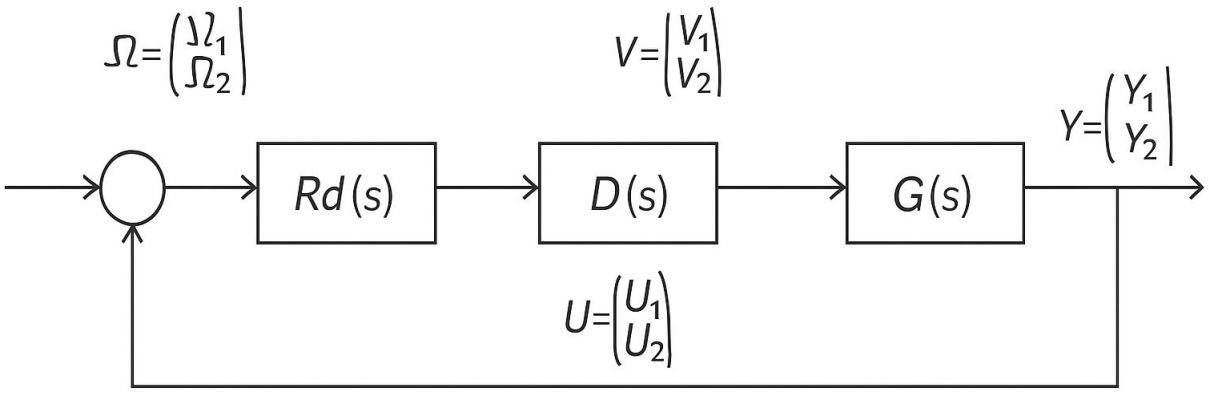

Fig. 3.1 : Final closed-loop structure of the multivariable system

The Figure 3.1 above shows the functional diagram of a multivariable system with implemented decoupling in Simulink. The structure includes three main blocks :

- $R_D(s)$: A diagonal matrix of PID controllers providing independent control of each loop :

$$R_D(s) = \begin{bmatrix} R_{11}(s) & 0 \\ 0 & R_{22}(s) \end{bmatrix}$$

  Each element controls one output independently : $R_{11}(s)$ regulates Y_1, and $R_{22}(s)$ regulates Y_2.

- $D(s)$: The decoupling block, used to eliminate dynamic interactions between system variables. It can be obtained from the inverse of $G(s)$ or by approximate methods.

- $G(s)$: The real two-input two-output multivariable system. Initially coupled, each input affects both outputs.

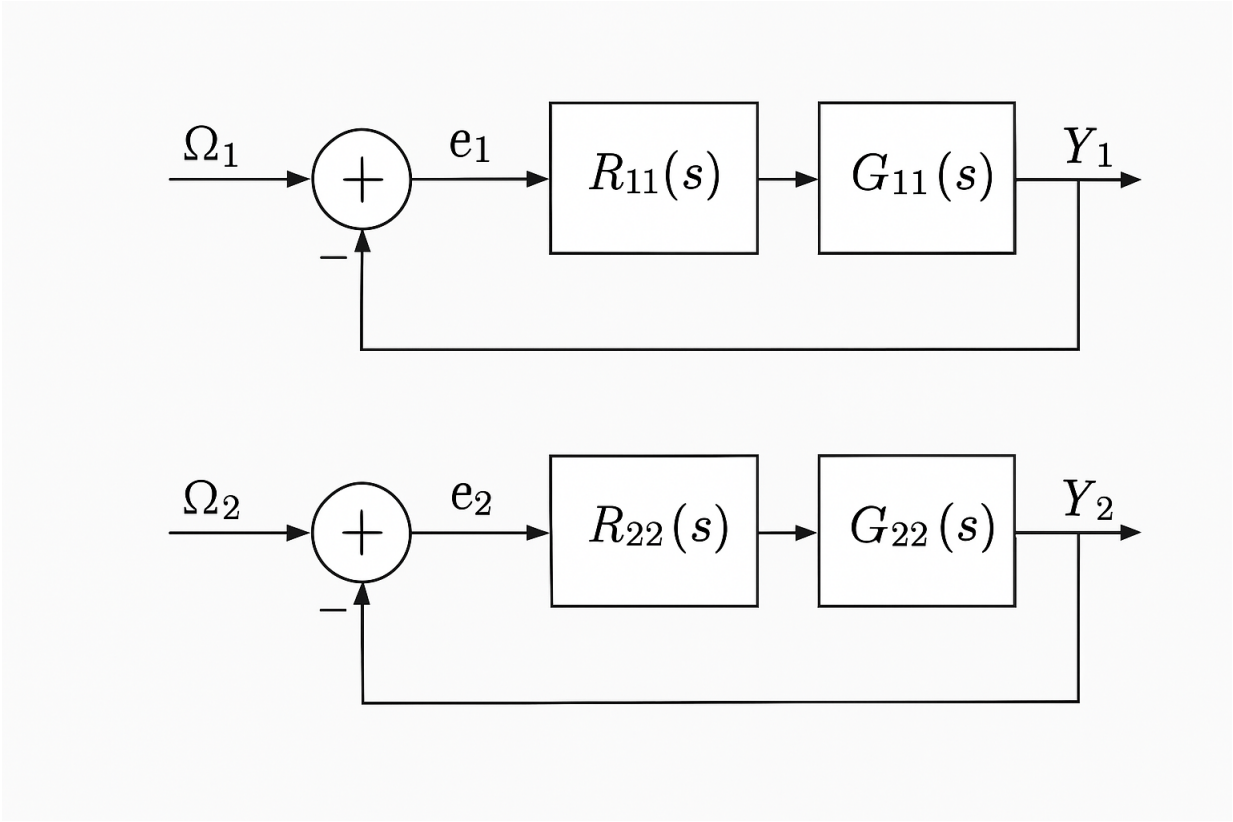

Fig. 3.2 : Functional diagram of the multivariable system with decoupler implemented in Simulink

The Figure 3.2 illustrates the **final closed-loop structure** of the multivariable system after dynamic decoupling. It clearly shows two **independent control loops**, each treated as a **SISO system** (Single Input Single Output).

This approach is particularly effective for complex industrial systems, where multivariable interactions often make direct regulation more difficult.

3.4 Predictive Control on Decoupled Model

In this section, we apply Model Predictive Control (MPC) to the two SISO systems resulting from the decoupling of the multivariable RO system. Each subsystem is treated independently. The objective is to implement and evaluate the performance of the MPC controller under various parameters and operating conditions.

3.4.0.1 Principle of the Approach

The decoupling was validated using the RGA matrix, indicating that the following pairings are optimal :

- The feed pressure P with the permeate flow rate F (loop G_{D11}).

- The feed pH with the conductivity C (loop G_{D22}).

Each loop is then considered as an independent SISO system, with an MPC controller implemented for each loop.

Models Used

The transfer functions used for the decoupled control are as follows :

- $G_{D11}(s) = \dfrac{0.002(0.056s + 1)}{0.003s^2 + 0.1s + 1}$.
- $G_{D22}(s) = \dfrac{-57(0.32s + 1)}{0.6s^2 + 1.8s + 1}$.

3.4.0.2 Model Discretization

In order to implement a predictive controller based on a discrete model, it is necessary to convert the continuous-time system into a discrete-time representation.

We employed the Zero-Order Hold (ZOH) method, which assumes that the control input remains constant between two sampling instants. The sampling time was chosen as follows :

$$T_s = 0.1 \text{ s}$$

The discretization was carried out in MATLAB using the `c2d` function. After converting the continuous-time models to their discrete-time counterparts, we obtained the following transfer functions :

$$G_{D22}(z) = \frac{-6.084\, z + 3.242}{z^2 - 1.499\, z + 0.5488}$$

$$G_{D11}(z) = \frac{0.002013\, z - 2.225 \times 10^{-5}}{z^2 - 0.005708\, z + 0.001273}$$

3.4.0.3 State-Space Transformation

Once the discrete transfer functions are obtained, it is essential to convert them into a state-space representation. Model Predictive Control (MPC) relies on this formulation to predict the future behavior of the system and optimize the control input. The discrete models $G_{11}(z)$ and $G_{22}(z)$ were thus transformed into state-space form according to the following structure :

$$x_{k+1} = Ax_k + Bu_k \quad ; \quad y_k = Cx_k + Du_k \tag{3.8}$$

where :

- x_k : state vector at time k,
- u_k : control input,
- y_k : measured output,
- A, B, C, D : matrices derived from the discretization of the continuous model.

The following matrices were obtained for the two systems :

3.4.0.3.1 Discrete State-Space Model of $G_{D11}(z)$

$$A_{11} = \begin{bmatrix} 0.0057 & -0.0407 \\ 0.0313 & 0 \end{bmatrix}, \quad B_{11} = \begin{bmatrix} 0.0625 \\ 0 \end{bmatrix} \tag{3.9}$$

$$C_{11} = \begin{bmatrix} 0.0322 & -0.0114 \end{bmatrix}, \quad D_{11} = 0 \tag{3.10}$$

$$x(t) = \begin{bmatrix} x_1(t) \\ x_2(t) \end{bmatrix} \tag{3.11}$$

then we got :

$$\dot{x}(t) = \begin{bmatrix} 0.0057 & -0.0407 \\ 0.0313 & 0 \end{bmatrix} x(t) + \begin{bmatrix} 0.0625 \\ 0 \end{bmatrix} u(t) \tag{3.12}$$

$$y(t) = \begin{bmatrix} 0.0322 & -0.0114 \end{bmatrix} x(t) \tag{3.13}$$

3.4.0.3.2 Discrete State-Space Model of $G_{D22}(z)$

$$A_{22} = \begin{bmatrix} 1.499 & -0.5488 \\ 1 & 0 \end{bmatrix}, \quad B_{22} = \begin{bmatrix} 4 \\ 0 \end{bmatrix} \tag{3.14}$$

$$C_{22} = \begin{bmatrix} -1.521 & 0.8106 \end{bmatrix}, \quad D_{22} = 0 \tag{3.15}$$

$$x(t) = \begin{bmatrix} x_1(t) \\ x_2(t) \end{bmatrix} \tag{3.16}$$

then we got :

$$\dot{x}(t) = \begin{bmatrix} 1.499 & -0.5488 \\ 1 & 0 \end{bmatrix} x(t) + \begin{bmatrix} 4 \\ 0 \end{bmatrix} u(t) \tag{3.17}$$

$$y(t) = \begin{bmatrix} -1.521 & 0.8106 \end{bmatrix} x(t) \tag{3.18}$$

3.4.0.3.2 Deviation Variables and Operating Point

In this work, predictive control is applied using *deviation variables*, i.e., the differences between system variables and their values at the nominal operating point. Formally, we define :

$$x_{\text{dev}} = x - x_{\text{op}} \tag{3.19}$$

where x represents an input or output variable, and x_{op} is its value at the operating point.

This formulation allows us to :

- Operate around a stable point x_{op}.
- Linearize the system dynamics.
- Express constraints in terms of deviations :

$$u_{\text{min}} - u_{\text{op}} \leq u_{\text{dev}} \leq u_{\text{max}} - u_{\text{op}} \tag{3.20}$$

$$y_{\text{min}} - y_{\text{op}} \leq y_{\text{dev}} \leq y_{\text{max}} - y_{\text{op}} \tag{3.21}$$

  It is often preferable not to penalize the absolute value of the control input, especially when the objective is to minimize variations and avoid abrupt changes.

- Formulate the cost function using deviation variables :

$$J = \sum_{k=0}^{N_p} (y_{\text{dev},k} - r_{\text{dev},k})^T Q (y_{\text{dev},k} - r_{\text{dev},k}) + \Delta u_{\text{dev},k}^T R \Delta u_{\text{dev},k} \tag{3.22}$$

This approach ensures effective regulation of deviations around the operating point.

3.4.1 Optimization Problem Formulation

Model Predictive Control (MPC) is a control strategy used to manage dynamic systems.
It relies on a mathematical model of the system to predict its future behavior over a given

prediction horizon.
Based on these predictions, the control input is calculated so as to achieve a predefined objective, such as minimizing tracking error or improving system performance.
This process involves solving an optimization problem at each time step, while accounting for the system's constraints.

In our case, for the reverse osmosis system, the objective is to maintain the outputs (permeate flow and conductivity) close to a reference value, reflecting an optimal operating point for the system and the desalination plant.

3.4.1.0.1 Objective Function At each time step k, an optimal control sequence is determined by solving an optimization problem that minimizes a performance criterion subject to system constraints.
The cost function (or objective function) to be minimized over the prediction horizon N_p is defined as :

$$J = \sum_{i=1}^{N_p} (y_{dev,k+i|k} - r_{dev,k+i})^2 + \lambda \sum_{i=0}^{N_c-1} (\Delta u_{dev,k+i})^2 \tag{3.23}$$

where :

- $r_{dev,k+i}$ is the reference trajectory to follow,
- $\Delta u_{dev,k+i} = u_{dev,k+i} - u_{dev,k+i-1}$ is the control input variation,
- N_p : prediction horizon,
- N_c : control horizon,
- λ : weighting factor on control effort variation.

In our application, the two objective functions associated with the models G_{D11} and G_{D22} are respectively :

- **For** G_{D11} (Flow control) :

$$J_{11} = \sum_{i=1}^{N_{p11}} (Flux_{k+i|k} - Flux_{ref})^2 + \lambda_{11} \sum_{i=0}^{N_{c11}-1} (\Delta p_{k+i})^2 \tag{3.24}$$

- **For** G_{D22} (Conductivity control) :

$$J_{22} = \sum_{i=1}^{N_{p22}} (cond_{k+i|k} - cond_{ref})^2 + \lambda_{22} \sum_{i=0}^{N_{c22}-1} (\Delta pH_{k+i})^2 \tag{3.25}$$

3.4.1.0.2 Horizon Selection Various combinations of N_p and N_c will be tested in the following sections to analyze their impact on the controllers' performance.
This analysis aims to evaluate how the prediction horizon (N_p) and control horizon (N_c) affect system stability, response time, and reference tracking quality.

3.4.1.0.3 Constraints MPC allows for the explicit inclusion of system constraints :

$$\begin{cases} x(k+1) = f(x(k), u(k)) & \textit{(system dynamics)} \\ P_{\text{min}} \leq P(k) \leq P_{\text{max}} \\ P_{dev,\text{min}} \leq P_{dev}(k) \leq P_{dev,\text{max}} \\ \text{Flux}_{\text{min}} \leq \text{Flux}(k) \leq \text{Flux}_{\text{max}} \\ \text{Flux}_{dev,\text{min}} \leq \text{Flux}_{dev}(k) \leq \text{Flux}_{dev,\text{max}} & \textit{(constraints)} \\ \text{pH}_{\text{min}} \leq \text{pH}(k) \leq \text{pH}_{\text{max}} \\ \text{pH}_{dev,\text{min}} \leq \text{pH}_{dev}(k) \leq \text{pH}_{dev,\text{max}} \\ C_{\text{min}} \leq C(k) \leq C_{\text{max}} \\ C_{dev,\text{min}} \leq C_{dev}(k) \leq C_{dev,\text{max}} \end{cases} \tag{3.26}$$

In our case, each subsystem is subject to constraints related to its input and output variables.

- **For the first system**, where the input is pressure and the output is permeate flow, the constraints are :
  - **Operating point (OP)** :

$$\text{Pressure}_{\text{op}} = 900 \text{ psi} \tag{3.27}$$

$$\text{Flow}_{\text{op}} = 1.05 \text{ GPM} \tag{3.28}$$

  - **Absolute constraints** :

$$\begin{cases} 700 \leq P \leq 1000 \\ 0.65 \leq \text{Flux} \leq 1.25 \end{cases} \tag{3.29}$$

  - **Relative constraints (around the operating point)** :

$$\begin{cases} -200 \leq P_{\text{dev}} \leq 100 \\ -0.40 \leq \text{Flux}_{\text{dev}} \leq 0.20 \end{cases} \tag{3.30}$$

- **For the second system**, where the input is pH and the output is conductivity, the considered constraints are :

– **Operating point (OP)** :

$$\mathrm{pH}_{\mathrm{op}} = 6.75 \tag{3.31}$$

$$\mathrm{Cond}_{\mathrm{op}} = 423\ \mu\mathrm{S/cm} \tag{3.32}$$

– **Absolute constraints** :

$$\begin{cases} 6.45 \leq \mathrm{pH} \leq 7.05 \\ 401 \leq C \leq 562 \end{cases} \tag{3.33}$$

– **Relative constraints (around the operating point)** :

$$\begin{cases} -0.30 \leq \mathrm{pH}_{\mathrm{dev}} \leq 0.30 \\ -20 \leq C_{\mathrm{dev}} \leq 20 \end{cases} \tag{3.34}$$

These constraints ensure compliance with the physical limits of the system and help maintain stable and efficient operation under the desired working conditions.

The control law

The predictive control law for a system without constraints

The predictive control law (without constraints) is given by :

$$u_k = -K_{\mathrm{mpc}} x_k \tag{3.35}$$

with :

$$K_{\mathrm{mpc}} = \left(\Phi^T \Phi + \bar{R}\right)^{-1} \Phi^T \Gamma \tag{3.36}$$

This gain is computed based on the prediction model :

$$x_{k+1} = Ax_k + Bu_k$$

and the cost function to minimize :

$$J = \sum_{i=0}^{N_p-1} \left[(x_{k+i|k} - x_{\mathrm{ref}})^T Q (x_{k+i|k} - x_{\mathrm{ref}}) + (u_{k+i|k} - u_{\mathrm{ref}})^T R (u_{k+i|k} - u_{\mathrm{ref}})\right] \tag{3.37}$$

The predictive control law for a system with constraints

At each time step k, the constrained MPC control input is computed by solving the following quadratic program :

$$\begin{aligned} \min_{\mathbf{U}} \quad & \frac{1}{2}\mathbf{U}^T H\mathbf{U} + f(x_k)^T\mathbf{U} \\ \text{subject to :} \quad & G\mathbf{U} \leq W + Ex_k \end{aligned} \tag{3.38}$$

where :

- $\mathbf{U} = \begin{bmatrix} u_{k|k} \\ u_{k+1|k} \\ \vdots \\ u_{k+N_c-1|k} \end{bmatrix}$ is the control sequence,
- $H = \Gamma^T Q_p \Gamma + R_p$ is the Hessian matrix,
- $f(x_k) = \Gamma^T Q_p(\Phi x_k - X_{\text{ref}})$ is the gradient vector,
- G, W, E encode state, input, and rate constraints.

3.4.2 Optimization Problem Solving

The control problem is formulated as a Quadratic Programming (QP) problem of the form :

$$\min_{\Delta U} \frac{1}{2}\Delta U^T H \Delta U + f^T \Delta U \tag{3.39}$$

subject to equality and inequality constraints. The solution to this problem yields the optimal sequence of control variations, but only the first element is applied :

$$u_k = u_{k-1} + \Delta u_k^{\text{opt}} \tag{3.40}$$

Then, the system is updated with the new state, and the procedure is repeated at the next time step.
Only the first control action of the computed optimal sequence is implemented on the actual system, according to the ”receding horizon” principle.
This optimization loop is executed at each time step, with the system state being updated based on new measurements.

3.4.2.1 Implementation in MATLAB

The implementation was carried out in MATLAB using the `mpc` object provided by the Model Predictive Control Toolbox. At each time step k :

- the model predicts the output evolution over 100 steps for the Flow–Pressure system and 10 steps for the Conductivity–pH system,

- a QP problem is solved to optimize the cost function J,
- only the first control input $\hat{u}_k$ is applied.

3.4.2.2 Using MATLAB MPC Toolbox as Optimization Solver

To solve the optimization problem related to model predictive control, we used the built-in solver available in MATLAB's MPC Toolbox. This solver automatically formulates and solves, at each time step, a quadratic programming (QP) problem while accounting for the constraints defined on inputs, outputs, and their variations.
The user does not need to manually implement the QP matrices : it is sufficient to specify high-level parameters using dedicated functions provided by the toolbox.

3.4.2.2.1 Creating the MPC Controller The main function to create a predictive controller is :

```
mpc_controller = mpc(sys_d, Ts, Np, Nc);
```

with the following parameters :

- `sys_d` : Discrete model of the system (obtained via `c2d`)
- `Ts` : Sampling period
- `Np` : Prediction horizon
- `Nc` : Control horizon

3.4.2.2.2 Defining the Cost Function Weights The cost function weights are specified directly in the MPC object using three key parameters :

```
mpc_controller.Weights.MV = 0.0001;
mpc_controller.Weights.MVRate = 0.1;
mpc_controller.Weights.OV = 2.5;
```

These parameters correspond to the following components of the quadratic cost function :

$$J = \sum_{i=1}^{N_p} \underbrace{Q}_{\texttt{OV}} \cdot \|y(k+i|k) - r(k+i)\|^2 + \sum_{i=0}^{N_c-1} \underbrace{R}_{\texttt{MVRate}} \cdot \|\Delta u(k+i)\|^2 + \sum_{i=0}^{N_c-1} \underbrace{\lambda}_{\texttt{MV}} \cdot \|u(k+i)\|^2$$

where :

- `Weights.OV` ($Q = 2.5$) : Weight on the output tracking error. A higher value favors fast reference tracking.

- `Weights.MVRate` ($R = 0.1$) : Weight on the control input variation Δu. This penalizes abrupt control changes to protect the actuators.
- `Weights.MV` ($\lambda = 0.0001$) : Weight on the control input amplitude u. This limits control effort and keeps inputs close to the operating point.

In our case, two systems were modeled and controlled :

For the pressure–flow system (G_{D11}) :

```
G11_d = c2d(G11, Ts, 'zoh');
Np = 100;
Nc = 20;
mpc_G11 = mpc(G11_d, Ts, Np, Nc);
```

For the pH–conductivity system (G_{D22}) :

```
G22_d = c2d(G22, Ts, 'zoh');
Np = 10;
Nc = 3;
mpc_G22 = mpc(G22_d, Ts, Np, Nc);
```

3.4.2.2.2.1 Managing Initial Conditions By default, the MPC toolbox assumes a zero initial state. To start the simulation from a different value (`flow_initial = 0.65`), the following steps are required :

1. Compute the constant input u_0 that maintains the output y_0 :

```
y0 = flow_initial - flow_op;
u0 = y0 / dcgain(G11_d);
```

2. Deduce the initial state x_0 :

```
x0 = (eye(size(Ad)) - Ad) \ (Bd * u0);
```

3. Use it in the simulation :

```
simOptions = mpcsimopt;
simOptions.PlantInitialState = x0;
```

3.4.2.2.3 Defining Constraints on Variables Once the controller is created, constraints on the manipulated variables (MV) and output variables (OV) can be specified. These constraints are defined as deviations from the operating point :

```
pressure_op = 900;
flow_op = 1.05;
mpc_controller.MV.Min = 700 - pressure_op;
```

```
mpc_controller.MV.Max = 1000 - pressure_op;
mpc_controller.OV.Min = 0.65 - flow_op;
mpc_controller.OV.Max = 1.25 - flow_op;
```

In this case :

- The control input (pressure) is constrained between 700 and 1000 psi
- The output (flow rate) is constrained between 0.65 and 1.25 GPM

By working in deviation mode, the controller optimizes values relative to the operating point, which simplifies system linearization and analysis.

3.4.2.2.4 Defining the Cost Function Weights The cost function minimized by the solver is a quadratic function of the form :

$$J = \sum_{i=1}^{N_p} Q \cdot \|y(k+i|k) - r(k+i)\|^2 + \sum_{i=0}^{N_c-1} R \cdot \|\Delta u(k+i)\|^2 + \sum_{i=0}^{N_c-1} \lambda \cdot \|u(k+i)\|^2$$

The associated weights are defined directly in the MPC object :

```
mpc_controller.Weights.MV = 0.0001;
mpc_controller.Weights.MVRate = 0.1;
mpc_controller.Weights.OV = 2.5;
```

- `Weights.MV` : corresponds to the weight λ applied to the absolute magnitude of the control input u. It limits the control effort.
- `Weights.MVRate` : represents the weight R on the control input variation Δu. It penalizes abrupt control changes.
- `Weights.OV` : refers to the weight Q on the output error, i.e., the deviation between predicted output and the reference. It directly influences tracking performance.

3.4.2.2.5 Automatic Solution at Each Time Step After configuration, the toolbox's solver automatically solves the QP problem at each time step via :

```
[Ysim, ~, Usim] = sim(mpc_controller, Nsim, RefSignal, []);
```

This function simulates the closed-loop system behavior over N_{sim} sampling steps, applying the optimal control at each time step. The arguments and outputs of the function are :

- `mpc_controller` : an `mpc` object containing the model, constraints, weights, prediction and control horizons.

- `Nsim` : total number of simulation steps. It is typically defined as the total simulation time $T_{\text{sim}} = 20s$ divided by the sampling time $T_s = 0.1s$.
- `RefSignal` : column vector representing the output reference trajectory. It can be constant, time-varying, or scenario-based.
- `[]` : fourth optional argument, used to specify initial conditions. If empty, default conditions (zero initial state) are assumed.

The outputs of the function are :

- `Ysim` : matrix containing simulated output values over time.
- `Usim` : matrix containing the optimal control inputs applied at each time step. Only the first control input from the optimized sequence is applied at each iteration, following the *receding horizon* principle.

This function automatically performs the following steps :

1. Predict future outputs over the horizon N_p
2. Formulate and solve the QP problem while considering constraints
3. Apply only the first optimal control input (receding horizon principle)
4. Repeat the process at each simulation step

3.4.3 Results – Influence of Prediction and Control Horizons

In these simulations, a step reference is applied from $t = 0$ seconds, representing a setpoint tracking scenario where the output variable is targeted.
Simulations are performed for different sets of parameters.

3.4.3.0.1 Parameters Used for the Pressure–Flow System (G_{D11})

- **Prediction horizon** : $N_p = 1, 10, 100, 1000, 10\,000$
- **Control horizon** : $N_c = 2, 5, 10, 20$
- **Weight on output error** : $Q = 2.5$
- **Weight on control variation** : $R = 0.1$
- **Weight on control magnitude** : $\lambda = 0.0001$
- **Operating point** : $P_{op} = 900$ psi, $F_{op} = 1.05$ GPM

- **Initial value** : $F_{initial} = 0.65$ GPM
- **Pressure constraints (in deviation)** : $-200 \leq P_{dev} \leq +100$
- **Flow constraints (in deviation)** : $-0.40 \leq F_{dev} \leq +0.20$

3.4.3.0.2 Parameters Used for the pH–Conductivity System (G_{D22})

- **Prediction horizon** : $N_p = 3, 10, 100, 1000$
- **Control horizon** : $N_c = 1, 3, 7$
- **Weight on output error** : $Q = 1$
- **Weight on control variation** : $R = 0.1$
- **Weight on control magnitude** : $\lambda = 0$
- **Operating point** : $\text{pH}_{op} = 6.75$, $\text{Conductivity}_{op} = 423$ μS/cm
- **Initial value** : $Cond_{initial} = 562$ μS/cm
- **pH constraints (in deviation)** : $-0.30 \leq \text{pH}_{dev} \leq +0.30$
- **Conductivity constraints (in deviation)** : $-20 \leq C_{dev} \leq +20$

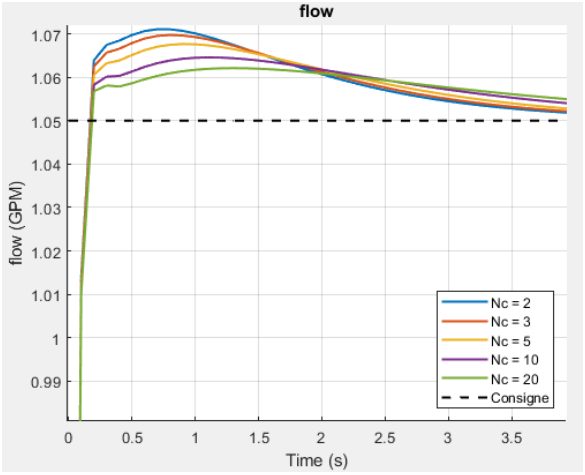

Fig. 3.3 : Flow–Pressure system response for various N_c values with fixed $N_p = 100$

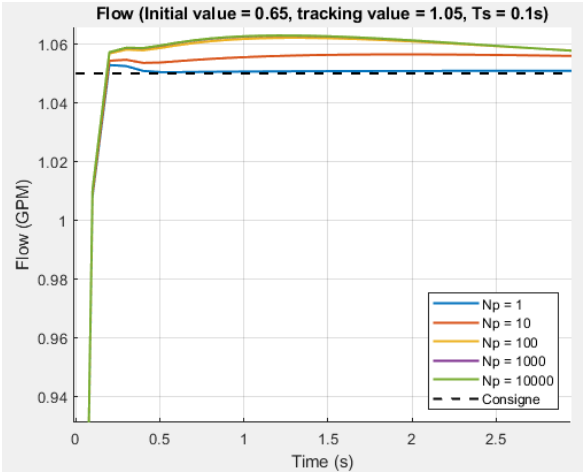

Fig. 3.4 : Flow–Pressure system response for various N_p values with fixed $N_c = 20$

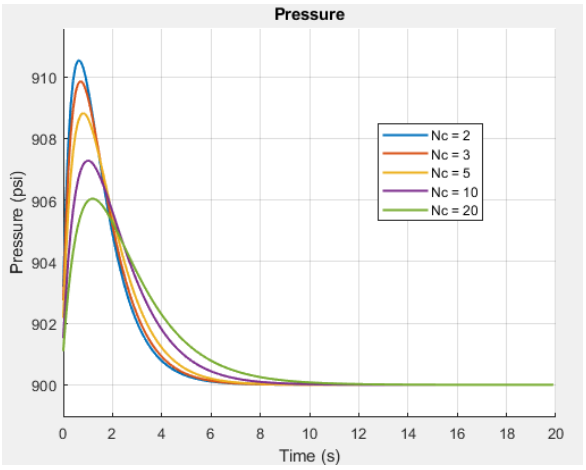

Fig. 3.5 : Pressure for various N_c values with fixed $N_p = 100$

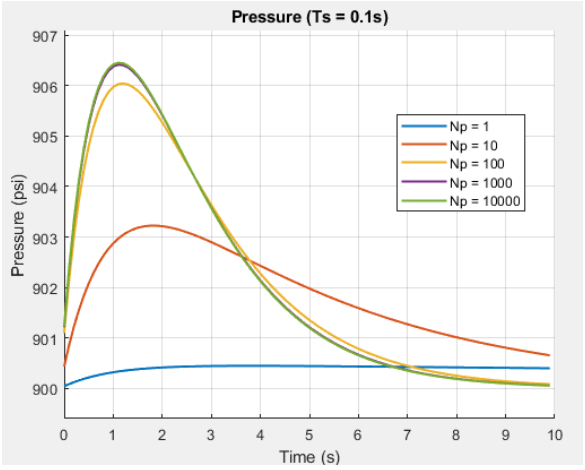

Fig. 3.6 : Pressure for various N_p values with fixed $N_c = 20$

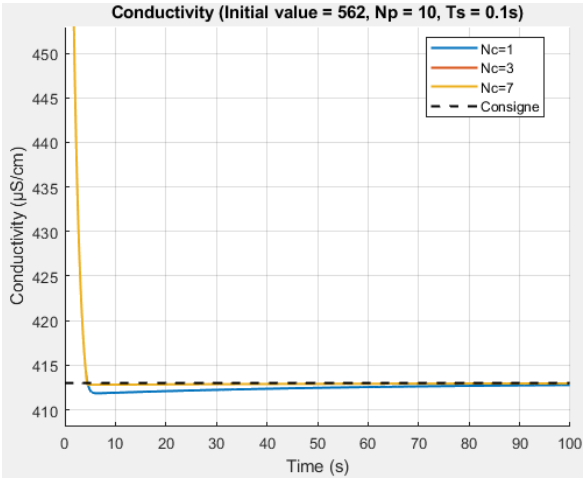

Fig. 3.7 : Conductivity–pH system response for various N_c values with fixed $N_p = 10$

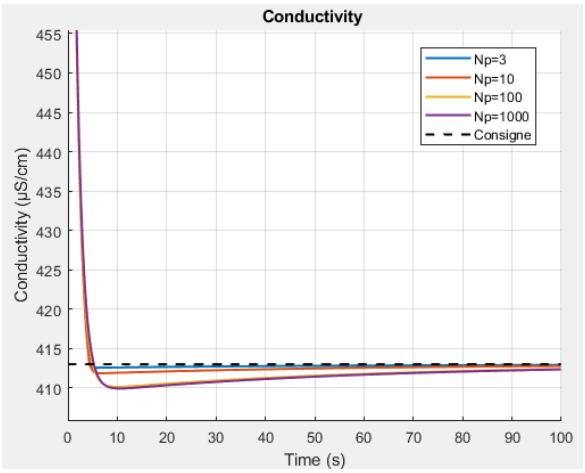

Fig. 3.8 : Conductivity–pH system response for various N_p values with fixed $N_c = 1$

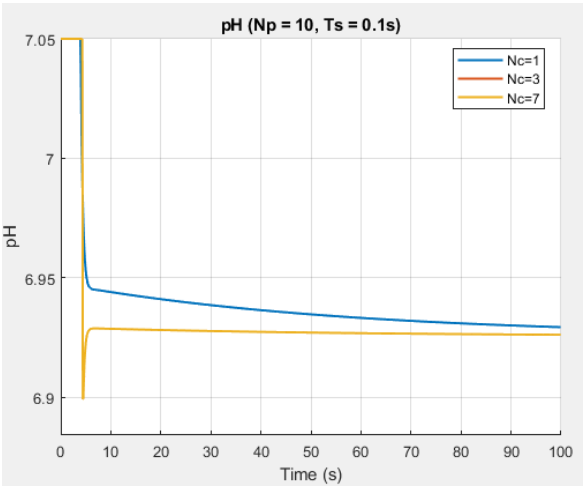

Fig. 3.9 : pH response for various N_c values with fixed $N_p = 10$

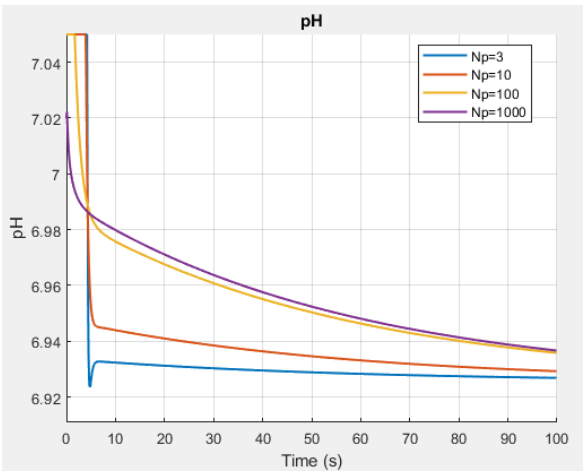

Fig. 3.10 : pH response for various N_p values with fixed $N_c = 1$

3.4.3.1 Flux/Pressure System Analysis

This first case study focuses on the regulation of the permeate flow rate (output, unit : GPM) to a setpoint value of 1.05 GPM, starting from an initial condition of 0.65 GPM. The manipulated variable is the pressure (input, unit : psi). The sampling time used for the simulations is $T_s = 0.1$ s. The relevant figures for this section show the evolution of the flow and pressure over time for various configurations of N_p and N_c.

3.4.3.1.1 Influence of the Prediction Horizon (N_p) with Fixed N_c In this set of simulations, the control horizon N_c is kept constant (assumed to be $N_c = 20$, consistent with other simulations), while the prediction horizon N_p takes the values : 1, 10, 100, 1000, and 10000.

3.4.3.1.2 Flow Response Analysis (Controlled Output) (see corresponding figure)

- $N_p = 1$ **:** The response is very slow. The controller, predicting only one step ahead, lacks anticipation and fails to reach the setpoint within the simulated time interval (20 seconds). This highlights the inefficiency of a very short prediction horizon.
- $N_p = 10$ **:** Increasing the prediction horizon significantly improves performance. The flow reaches the setpoint in about 4 seconds, with a slight overshoot before settling.
- $N_p = 100$ **:** The response is similar to that with $N_p = 10$, but the overshoot appears slightly more pronounced, indicating a slightly more aggressive initial strategy by the controller.
- $N_p = 1000$ **and** $N_p = 10000$ **:** The response curves are nearly identical to that for $N_p = 100$, indicating that increasing the prediction horizon beyond $N_p = 100$ brings no significant benefit for this particular system. The relevant future behavior for control is already well captured at $N_p = 100$.

3.4.3.1.3 Pressure Response Analysis (Manipulated Variable) (see corresponding figure)

- $N_p = 1$ **:** The pressure increases very slowly and stabilizes at a low value, consistent with the poor performance observed in the flow. The control action is very limited.
- $N_p = 10$ **:** The pressure rises rapidly, reaching a peak around 903.5 psi at approximately 1.5 s, then decreases toward the steady-state value (about 900 psi). This initial peak corresponds to the control effort required to accelerate the flow response.
- $N_p = 100$ **:** The pressure peak is higher (around 906 psi) and occurs earlier (around 1 s), confirming the more aggressive initial control action observed in the flow response.
- $N_p = 1000$ **and** $N_p = 10000$ **:** The pressure profiles are very close to that of $N_p = 100$, confirming that increasing N_p further has little impact on the overall control strategy in this scenario.

3.4.3.1.4 Influence of the Control Horizon (N_c) with $N_p = 100$ Here, the prediction horizon is fixed at $N_p = 100$ (considered sufficient based on the previous analysis), and the control horizon N_c varies : 2, 5, 10, and 20.

3.4.3.1.5 Flow Response Analysis (Controlled Output) (see corresponding figure)

- All tested values of N_c result in satisfactory tracking of the 1.05 GPM setpoint.
- A slight trend is observed : increasing N_c (from 2 to 20) marginally reduces the initial overshoot and slightly slows down the response.
- This suggests that for this system and with $N_p = 100$, the performance of the controlled output (flow) is relatively insensitive to the value of N_c within the range [2, 20].

3.4.3.1.6 Pressure Response Analysis (Manipulated Variable)

- The influence of N_c is more noticeable on the manipulated variable (pressure).
- $N_c = 2$ **:** The controller computes only a short sequence of two future control actions, resulting in a more aggressive control effort characterized by the highest and fastest initial pressure peak (around 906 psi).
- $N_c = 5$**, 10, 20:** As N_c increases, the controller optimizes over a longer control sequence, enabling it to plan a smoother trajectory for the pressure. The initial peak is gradually reduced (down to about 904.5 psi for $N_c = 20$), and convergence to the steady-state value is slower and more damped.
- Increasing N_c therefore leads to a less aggressive and smoother control action, which may be preferable for actuator longevity (e.g., pump), at the cost of slightly slower dynamics in the manipulated variable.

3.4.3.2 Analysis of the Conductivity/pH System

The second case study focuses on regulating the water conductivity (output, unit : µS/cm) to a target setpoint of 413 µS/cm, starting from a high initial condition of 562 µS/cm. The manipulated variable is pH (input, unitless). Operational constraints are defined : conductivity must remain within [403, 562] µS/cm, and pH within [6.45, 7.05]. The sampling time, based on figure captions, is $T_s = 0.1$ s.

3.4.3.2.1 Influence of the Prediction Horizon (N_p) with $N_c = 1$ In this configuration, the control horizon is fixed at its minimum value $N_c = 1$ (the controller optimizes only the next control move), while the prediction horizon N_p takes the values : 3, 10, 100, and 1000.

3.4.3.2.2 Conductivity Response Analysis (Controlled Output)

- $N_p = 3$ **:** With a very short prediction horizon and $N_c = 1$, the performance is poor. Conductivity decreases very slowly and does not reach the target value of $413\,\mu S/cm$ within the 100-second simulation window.
- $N_p = 10$ **:** Increasing N_p significantly improves performance. Conductivity reaches the target within about 10 seconds, with a fast and smooth response and no significant overshoot.
- $N_p = 100$ **and** $N_p = 1000$ **:** The responses are very similar to that with $N_p = 10$. There may be a slight acceleration in response, but the effect is marginal. This confirms that beyond a certain point ($N_p \approx 10$ in this case with $N_c = 1$), increasing N_p brings little additional benefit.

3.4.3.2.3 PH Response Analysis (Manipulated Variable)

- To reduce conductivity from 562 to 413, the controller must adjust the pH. An initial drop in pH is observed in all simulations.
- $N_p = 3$ **:** The pH decrease is minimal and stabilizes very slowly.
- $N_p = 10$**, 100, 1000**: **The control action is much more aggressive. A strong initial undershoot in pH increases (minimum around pH** 6.925 **for** $N_p = 1000$**). This rapid pH drop accelerates the conductivity response.**
- **After this undershoot, pH gradually returns to its steady-state value (about** 6.93**). Stabilization is faster for larger** N_p **values.**
- **It is noted that the upper pH constraint (7.05) is reached at the beginning of the simulation (**$t = 0$**) for high** N_p**, indicating the controller immediately applies the maximum allowable control to initiate conductivity reduction.**

3.4.3.2.4 Influence of the Control Horizon (N_c) with $N_p = 10$ Here, the prediction horizon is fixed at $N_p = 10$ (considered sufficient based on earlier analysis with $N_c = 1$), while the control horizon N_c varies : 1, 3, and 7.

3.4.3.2.5 Conductivity Response Analysis (Controlled Output) (see corresponding figure)

- The influence of N_c is visible in the dynamics of the conductivity.
- $N_c = 1$ **:** The fastest response, reaching the target in about 10 seconds.
- $N_c = 3$ **and** $N_c = 7$ **:** Increasing N_c slows the response. Both reach the target in about 15–20 seconds, with very similar curves.

3.4.3.2.6 PH Response Analysis (Manipulated Variable)

- The impact of N_c on the manipulated variable (pH) is significant.
- $N_c = 1$ **:** As previously observed, the control action is aggressive, with a sharp initial undershoot (pH down to around 6.9).
- $N_c = 3$ **and** $N_c = 7$ **:** Higher N_c values yield much smoother, less aggressive control. The undershoot is greatly reduced (pH drops only to about 6.925), and the response is more gradual.
- The upper constraint (pH = 7.05) is reached at the beginning and lasts slightly longer for $N_c = 3$ and $N_c = 7$, reflecting a milder initial control action.
- Thus, N_c provides a key tuning parameter to adjust the aggressiveness of pH control, with direct impact on conductivity response speed.

3.4.3.2.7 General Discussion and Summary This comparative analysis of the influence of the horizons N_p and N_c on both systems reveals general insights into their roles in MPC tuning.

Role of the Prediction Horizon (N_p) : The prediction horizon is fundamental to controller performance. Simulations clearly show that a very short N_p (e.g., 1 or 3) leads to poor performance—extremely slow or inadequate regulation—due to the controller's lack of foresight into system behavior and long-term effects of control actions. Increasing N_p allows better anticipation of system dynamics and constraints, yielding faster responses and improved setpoint tracking. However, beyond a certain threshold ($N_p \approx 100$ for Flow/Pressure and $N_p \approx 10$ for Conductivity/pH with $N_c = 1$), further increase does not improve performance significantly and only increases computational burden. The optimal N_p should be large enough to capture key dynamics and constraints, but not unnecessarily long.

Role of the Control Horizon (N_c) : The control horizon primarily affects the aggressiveness of the control action. A small N_c (typically $N_c = 1$) leads to fast but often aggressive control—characterized by sharp peaks or abrupt changes in the manipulated variable (e.g., pressure or pH). Increasing N_c allows the controller to plan a longer sequence of future control moves, providing more degrees of freedom for shaping smoother control trajectories. This results in less aggressive, more gradual actions—desirable for actuator protection and system stability—at the expense of slightly slower response in the controlled output. Thus, N_c provides a direct trade-off between fast/aggressive and smooth/gradual control. It is important to note that N_c must always be less than or equal to N_p.

3.4.3.3 Conclusion

This study has analyzed the critical influence of prediction (N_p) and control (N_c) horizons on the performance of MPC controllers applied to two distinct systems (Flow/Pressure and Conductivity/pH). Simulation results confirm the expected roles of these parameters.

The prediction horizon N_p must be large enough to allow the controller to anticipate system behavior and constraints, which is necessary for good performance. A very small N_p leads to poor results, while a very large N_p brings minimal benefit and increases computational complexity.

The control horizon N_c mainly governs the aggressiveness of the manipulated variable. A small N_c enables fast, but potentially harsh, control actions, while a larger N_c produces smoother control, at the cost of slower output response. The choice of N_c provides flexibility in balancing performance and actuator limitations.

In conclusion, proper tuning of N_p and N_c is essential to fully exploit the potential of MPC. It requires an understanding of system dynamics and clear performance objectives, to achieve the best compromise between responsiveness, accuracy, constraint handling, control smoothness, and computational efficiency. The presented analyses provide a concrete illustration of these principles and emphasize the value of simulation-based tuning for these fundamental parameters.

3.5 Predictive Control on the Global (Non-Decoupled) Model

3.5.1 Integrated Multivariable Approach

3.5.1.1 Residual Coupling Modeling

The global model considers the complete interactions between variables, represented in matrix form as follows :

$$\begin{bmatrix} F(z) \\ C(z) \end{bmatrix} = \begin{bmatrix} G_{11}(z) & G_{12}(z) \\ G_{21}(z) & G_{22}(z) \end{bmatrix} \begin{bmatrix} P(z) \\ \mathrm{pH}(z) \end{bmatrix} \tag{3.41}$$

where $G_{21}(z)$ represents the residual coupling from pressure to conductivity. This interaction, neglected in the decoupled approach, introduces additional dynamics described by :

$$G_{21}(z) = \frac{-0.037z + 0.032}{z^2 - 1.213z + 0.548} \tag{3.42}$$

3.5.1.1 Multivariable Discretization

Zero-order hold (ZOH) discretization with a sampling time $T_s = 0.2\,\mathrm{s}$ yields the following discrete-time transfer matrix :

$$G_{\mathrm{MIMO}}(z) = \begin{bmatrix} \frac{0.002z-0.0002}{z^2-0.005z+0.001} & 0 \\ \frac{-0.037z+0.032}{z^2-1.213z+0.548} & \frac{-6.084z+3.242}{z^2-1.499z+0.548} \end{bmatrix} \tag{3.43}$$

3.5.2 Formulation of the Multivariable MPC Controller

3.5.2.1 Augmented State Model

The discrete-time state-space representation includes the four system states :

$$\mathbf{x}_{k+1} = \begin{bmatrix} 0.005 & -0.041 & 0 & 0 \\ 0.031 & 0 & 0 & 0 \\ 0 & 0 & 1.499 & -0.549 \\ 0 & 0 & 1 & 0 \end{bmatrix} \mathbf{x}_k + \begin{bmatrix} 0.062 & 0 \\ 0 & 0 \\ 0 & 4 \\ 0 & 0 \end{bmatrix} \mathbf{u}_k \tag{3.44}$$

with :

$$\mathbf{x}_k = \begin{bmatrix} x_1(k) \\ x_2(k) \\ x_3(k) \\ x_4(k) \end{bmatrix}, \quad \mathbf{u}_k = \begin{bmatrix} u_1(k) \\ u_2(k) \end{bmatrix} \tag{3.45}$$

$$A = \begin{bmatrix} 0.005 & -0.041 & 0 & 0 \\ 0.031 & 0 & 0 & 0 \\ 0 & 0 & 1.499 & -0.549 \\ 0 & 0 & 1 & 0 \end{bmatrix} \tag{3.46}$$

$$B = \begin{bmatrix} 0.062 & 0 \\ 0 & 0 \\ 0 & 4 \\ 0 & 0 \end{bmatrix} \tag{3.47}$$

$$C = \begin{bmatrix} c_1 & c_2 & c_3 & c_4 \end{bmatrix}, \quad D = \begin{bmatrix} 0 & 0 \end{bmatrix} \tag{3.48}$$

3.5.2.2 Multi-Criteria Cost Function

The objective function integrates the tracking errors of both outputs and the control effort variations :

$$J = \sum_{k=1}^{N_p} \left(|F_k - F_{\text{ref}}| Q_F + |C_k - C_{\text{ref}}| Q_C \right) + \sum_{k=0}^{N_c - 1} \left(|\Delta P_k| R_P + |\Delta \text{pH}_k| R_{\text{pH}} \right) \tag{3.49}$$

With the following optimal weights :

- $Q_F = 1, Q_C = 1$ (equal priority on both outputs)
- $R_P = 0.1, R_{\text{pH}} = 0.1$ (moderate penalization on control inputs)

3.5.3 Implementation of Coupled Constraints

3.5.3.1 Absolute Constraints

$$700 \text{ psi} \leq P \leq 1000 \text{ psi} \tag{3.50}$$

$$6.45 \leq \text{pH} \leq 7.05 \tag{3.51}$$

$$0.65 \text{ GPM} \leq F \leq 1.25 \text{ GPM} \tag{3.52}$$

$$401\ \mu S/\text{cm} \leq C \leq 562\ \mu S/\text{cm} \tag{3.53}$$

3.5.3.2 Operational Limits

- Max pressure variation : $\Delta P_{\text{max}} = 50$ psi/step
- Max pH variation : $\Delta\text{pH}_{\text{max}} = 0.1$/step
- Conductivity response time : $< 30\ s$

3.5.4 Results – Influence of Input Conditions

To evaluate the RO unit's behavior under different pressure values, the system is simulated with $N_p = 10$, $N_c = 3$.
This study focuses on pressure as a key parameter in reverse osmosis (RO) systems :

- $P_{op} = 500, 900, 1500$

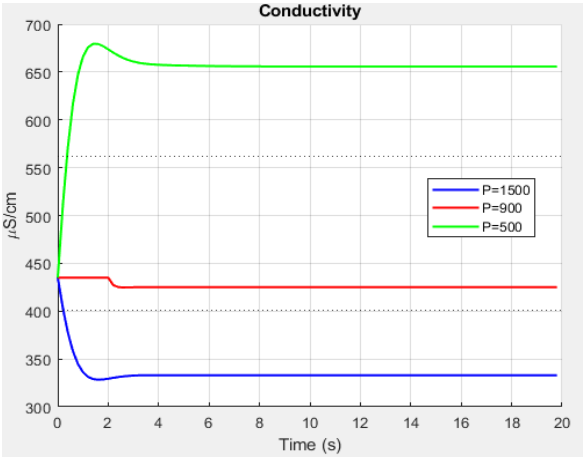

Fig. 3.11 : Conductivity response for various P_{op} with $pH_{op} = 6.45$

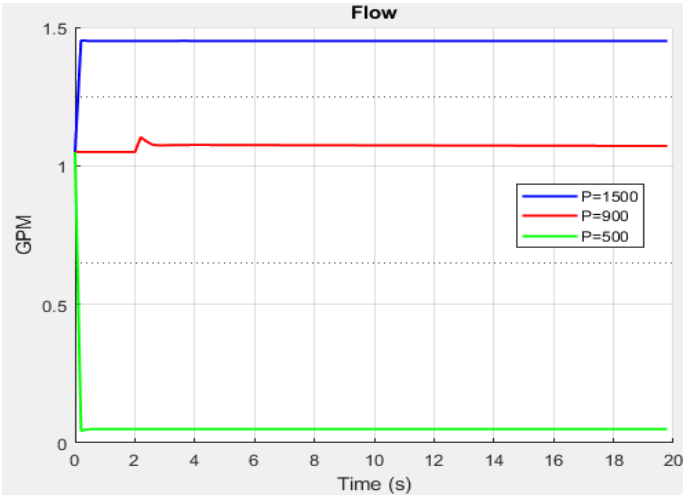

Fig. 3.12 : Permeate flow response for various P_{op} with $pH_{op} = 6.45$

Simulation results highlight critical behaviors depending on the operating pressure P_{op} :

- **Permeate Flow (Figure 5.8)** :
  - At $P_{op} = 1500$ psi : flow reaches **1.5 GPM**, exceeding the upper limit.
  - At $P_{op} = 900$ psi : nominal flow at **1.05 GPM**.
  - At $P_{op} = 500$ psi : flow drops to **0 GPM** due to hydraulic blockage.
- **Conductivity (Figure 5.7)** :
  - At $P_{op} = 500$ psi : **655.8 μS/cm**, above drinkability limits.
  - At $P_{op} = 900$ psi : **425 μS/cm**, within specifications.
  - At $P_{op} = 1500$ psi : **333 μS/cm**, possibly due to model limitations.
- **MPC Controller Behavior** :
  - At $P_{op} = 1500$ psi : constraint violation and saturation due to model limitations.
  - At $P_{op} = 900$ psi : robust tracking with overshoot $< 2\%$.

3.5.5 Conclusion

The multivariable control strategy offers superior global performance, but it requires significantly more computational resources.
Its use is justified in critical applications that demand joint optimization of coupled constraints, provided a reliable model and adequate hardware are available.

3.6 Performance Comparison Between Decoupled and Multivariable MPC

3.6.1 Prediction and Control Horizon Selection

In this study, we selected a prediction horizon of $N_p = 10$ and a control horizon of $N_c = 3$ for both control configurations (decoupled and multivariable). This choice is based on the analysis of the dynamic characteristics of each output :

- The **conductivity**, influenced by pH and pressure, exhibits a fast dynamic response with a short time constant ($T_{\text{cond}} \approx 0.0217$ min).
- The **permeate flow**, primarily influenced by pressure, evolves more slowly, with a significantly longer time constant ($T_{\text{flow}} \approx 0.5717$ min).

The chosen prediction horizon is sufficient to capture the essential system dynamics while ensuring computational efficiency. The shorter control horizon ($N_c = 3$) helps limit the complexity of the optimization problem while maintaining good controller responsiveness.

3.6.2 Simulation Results : Performance Comparison

This section presents the simulation results of the two MPC strategies :

- **Decoupled MPC**, using separate SISO transfer functions (G_{11} and G_{22}),
- **Multivariable MPC**, using the full 2×2 MIMO model accounting for cross-interactions.

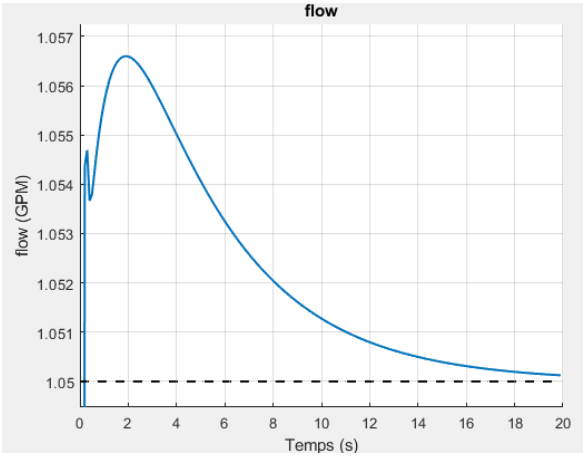

Fig. 3.13 : Flow response under decoupled MPC

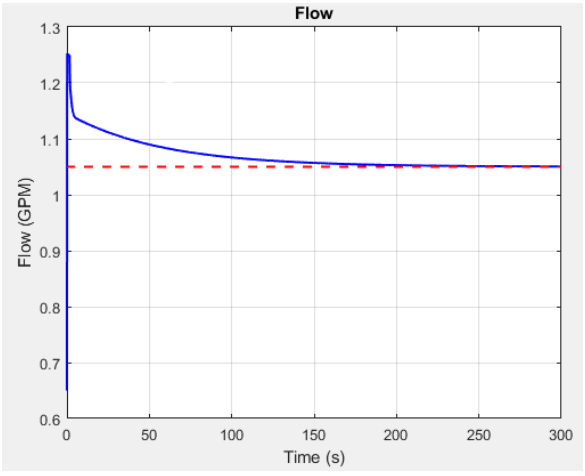

Fig. 3.14 : Flow response under multivariable MPC

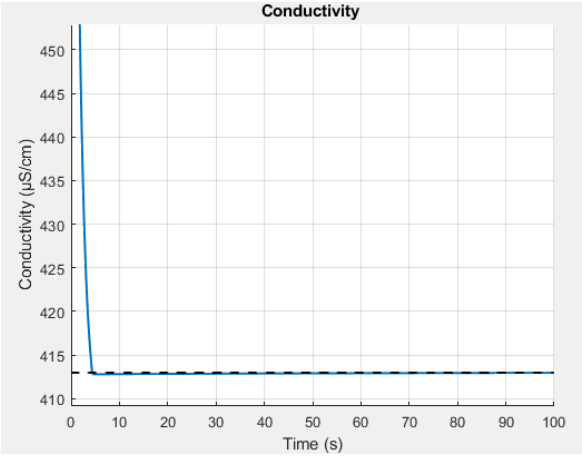

Fig. 3.15 : Conductivity response under decoupled MPC

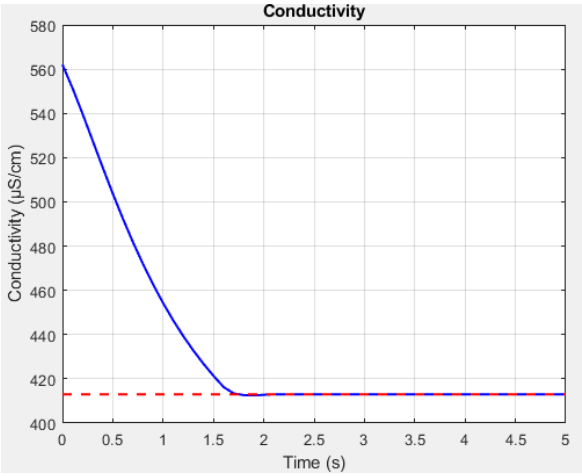

Fig. 3.16 : Conductivity response under multivariable MPC

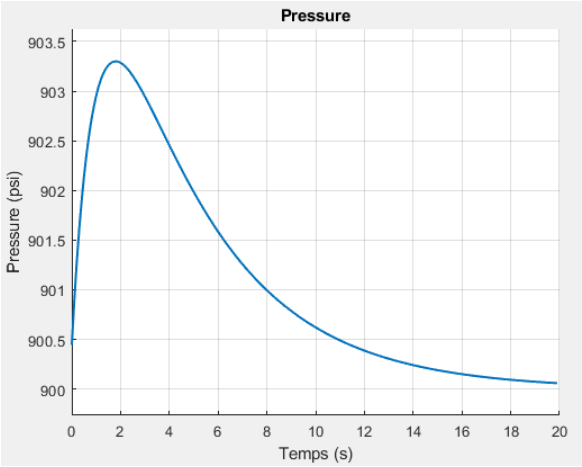

Fig. 3.17 : Pressure evolution under decoupled MPC

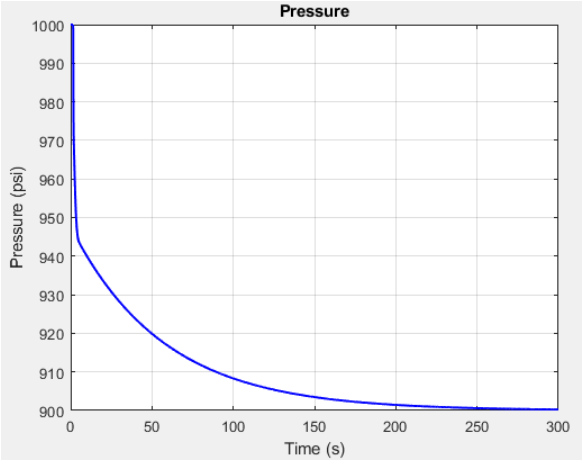

Fig. 3.18 : Pressure evolution under multivariable MPC

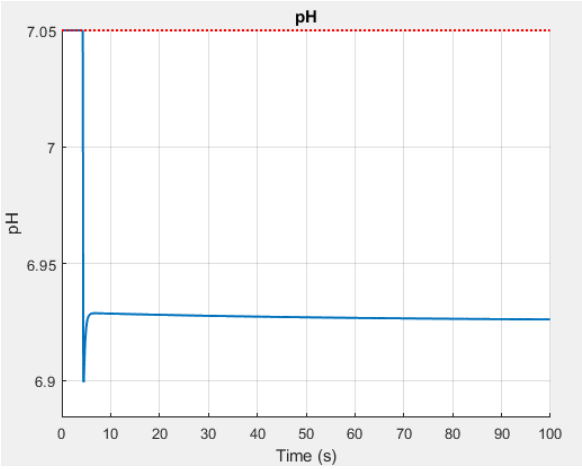

Fig. 3.19 : pH evolution under decoupled MPC

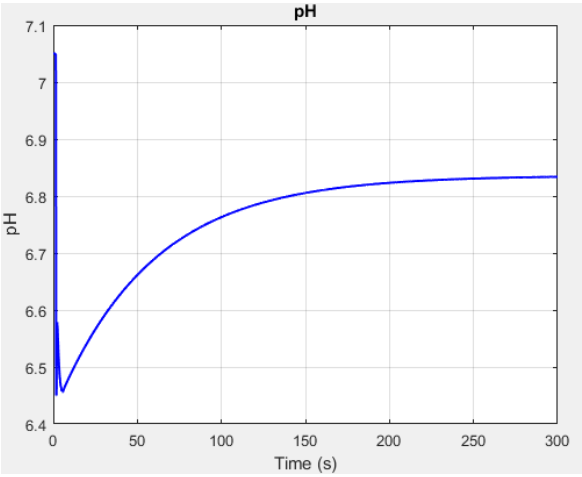

Fig. 3.20 : pH evolution under multivariable MPC

3.6.3 Performance Analysis

This section presents the results obtained from simulations of systems controlled by Model Predictive Control (MPC). The performance evaluation relies on four classical indicators : the Integral of Absolute Error (IAE), steady-state error (ess), overshoot, and the 5% settling time. These indicators quantify the tracking accuracy, response speed, and transient behavior of the system.

3.6.3.0.1 Permeate Flow Control System The flow regulation system exhibited highly satisfactory dynamic behavior. The numerical results are as follows :

- **IAE** = 0.0877;
- **Steady-state error (ess)** = -0.0001 GPM ;
- **Overshoot** = 0.0066 GPM ;
- **Settling time to ±5%** = 0.10 s.

These values indicate excellent reference tracking. The steady-state error is practically zero, meaning the system accurately reaches the reference value in steady-state. The overshoot is very low, demonstrating effective control of the transient phase. Finally, the fast settling time highlights the system's responsiveness.

3.6.3.0.2 Conductivity Control System The simulation of the conductivity regulation system yielded the following results :

- **IAE** = 207.3150;
- **Steady-state error (ess)** = $-0.0380\ \mu S/cm$;
- **Overshoot** = $149.0000\ \mu S/cm$;
- **Settling time to ±5%** = 2.60 s.

Although the system manages to reach the setpoint in steady-state with a moderate steady-state error, the initial overshoot is significant. This is also reflected in a high IAE value. The settling time remains reasonable but is slower than in the previous case, indicating slower dynamics or a more complex control effort required by this system.

The multivariable system studied involves two inputs (pressure and pH) and two main outputs : the permeate flow and conductivity. Performance analysis for each output is carried out individually, using the standard indicators : IAE, steady-state error, overshoot, and 5% settling time.

3.6.3.0.3 Output 1 – Flow Performance related to flow regulation is summarized below :

- **IAE** = 5.3352;
- **Steady-state error (ess)** = $0.0070\,\text{GPM}$;
- **Overshoot** = $0.2030\,\text{GPM}$;
- **Settling time to ±5%** = $34.30\,\text{s}$.

The system successfully reaches the reference with a low steady-state error, but the settling time is relatively long. The overshoot is more pronounced than in previous cases, indicating a less damped transient response, probably due to variable interactions or the complexity of coupled dynamics.

3.6.3.0.4 Output 2 – Conductivity The results obtained for the conductivity output are as follows :

- **IAE** = 112.6690;
- **Steady-state error (ess)** = $0.0000\,\mu\text{S/cm}$;
- **Overshoot** = $149.0000\,\mu\text{S/cm}$;
- **Settling time to ±5%** = $1.30\,\text{s}$.

The conductivity control exhibits excellent steady-state accuracy, with a final error of zero. However, the overshoot remains significant, indicating an abrupt transient phase. The relatively fast settling time demonstrates good responsiveness of the controller for this output.

3.6.4 Comparison Between Decoupled and Multivariable Systems

This section compares the performance of the two tested control configurations : on one hand, MPC controllers applied in a decoupled manner to each loop (independently on G_{11} and G_{22}), and on the other hand, a multivariable MPC (MIMO) acting simultaneously on both inputs (pressure and pH).

3.6.4.0.1 Permeate Flow For the flow output, the decoupled system demonstrated very good performance : a very low IAE (0.0877), a nearly zero steady-state error, negligible overshoot ($0.0066\,\text{GPM}$), and a very short settling time ($0.10\,\text{s}$). In contrast, performance significantly deteriorated in the multivariable system. The IAE increased substantially (5.3352), the overshoot became noticeable ($0.2030\,\text{GPM}$), and the settling time rose significantly to $34.30\,\text{s}$.

This can be explained by the dynamic interactions introduced in the MIMO system, which make flow control more difficult when both inputs are manipulated simultaneously.

3.6.4.0.2 Conductivity Regarding the conductivity output, the situation is reversed. The multivariable system enabled more efficient regulation than the decoupled one : the IAE decreased significantly (from 207.3150 to 112.6690), and the steady-state error was completely eliminated. The overshoot remained the same in both cases (149.0000 µS/cm), but the settling time was twice as fast in the multivariable configuration (1.30 s vs. 2.60 s).

This shows that taking interactions into account in the multivariable model improves conductivity control, likely due to better coordination between the actions on pressure and pH.

3.7 Conclusion

The results obtained show that :

- The **multivariable MPC** provides better regulation of **conductivity**, with a significant reduction in IAE, zero steady-state error, and a shorter settling time. This reflects the controller's ability to exploit the interactions between pressure and pH.
- The **decoupled MPC** shows very good performance for **permeate flow**, with a very short settling time, negligible overshoot, and nearly zero steady-state error. However, it shows limitations in conductivity control due to the lack of coordination between pressure and pH actions.

This comparison highlights the value of using a multivariable (MIMO) model when the variables are strongly coupled. While decoupling simplifies implementation and provides excellent results for outputs with weak cross-interactions, multivariable MPC remains the preferred choice for robust and coordinated regulation of complex outputs.

Chapitre 4

PID and IMC-Based Control of Permeate Flow and Conductivity

4.1 Classical PID Control Design

4.2 Introduction

PID control (Proportional-Integral-Derivative) is a robust and widely used solution for regulating dynamic systems, particularly after a decoupling step. In this chapter, we apply this method to the independent subsystems obtained through the decoupling strategy previously presented. The two resulting SISO (Single Input Single Output) loops—one for controlling the permeate flow via pressure, and the other for regulating conductivity via pH—are well suited to a PID controller approach.

The main objective is to determine the optimal parameters (proportional gain K_p, integral time T_i, and derivative time T_d) for each controller, based on the dynamic characteristics of the decoupled transfer functions $G_{11}(s)$ and $G_{22}(s)$.

This study aims to validate the effectiveness of PID control in a decoupled system context, while also identifying its potential limitations, particularly in the presence of residual disturbances or parametric variations. The results will serve as a foundation for further improvements, such as incorporating adaptive strategies or combining with other advanced control methods.

4.3 PID from Reference Literature

The reference article proposes specific PID parameter values for the decoupled transfer functions $G_{11}(s)$ (permeate flow) and $G_{22}(s)$ (permeate conductivity). These settings, determined using classical tuning methods, serve as a starting point for our analysis. Table (**??**) below presents a structured comparison of the various control configurations :

- **Basic actions :** Proportional (P), Proportional-Integral (PI)
- **Advanced configuration :** Proportional-Integral-Derivative (PID) with their respective parameters K_c, τ_i, τ_d

Loop	**Type**	K_c	τ_i	τ_d
$G_{11}(s)$	P	596	–	–
	PI	536	0.23	–
	PID	715	0.14	0.03
$G_{22}(s)$	P	-0.06	–	–
	PI	-0.05	1.81	–
	PID	-0.07	1.09	0.27

Tab. 4.1 : PID controller parameters for the decoupled loops

This summary enables a systematic evaluation of the impact of each control action (P, I, D) on system performance, while facilitating the reproducibility of the results. The provided values will guide our Simulink implementation and serve as a reference for the comparative analysis of time-domain responses and robustness.

4.4 Closed-Loop Simulation

4.4.1 Response of $G_{11}(s)$ (Flow)

As part of this final-year project (PFE), a PID controller was implemented to regulate the **permeate flow** in a reverse osmosis (RO) system. A **multi-step reference signal** for the flow was designed with smooth transitions using an exponential function, in order to test the controller's performance under progressive yet significant changes in the setpoint.

The applied PID controller corresponds to the one derived from the G_{11} **model in the reference article**. This choice is based on prior system identification and optimized tuning to ensure both stability and fast response. The closed-loop system response was simulated using Simulink and compared against the reference setpoint.

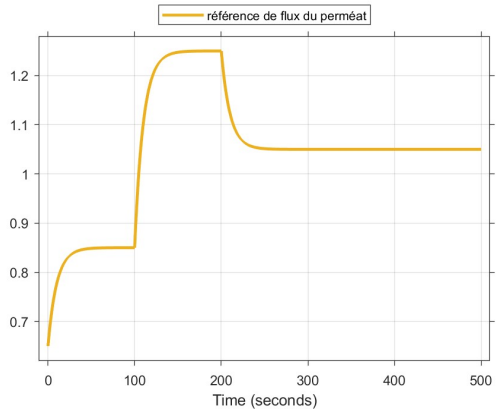

Fig. 4.1 : Evolution of the permeate flow reference over time

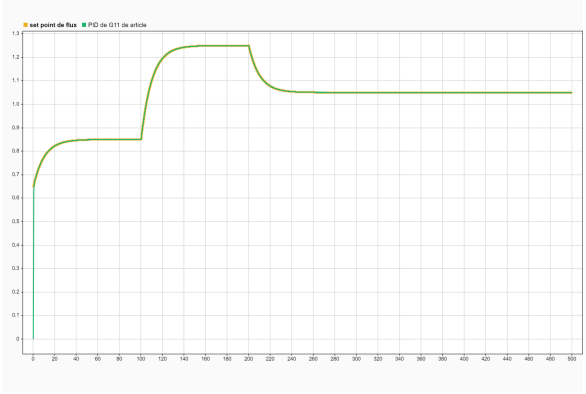

Fig. 4.2 : Response of the article's PID controller for $G_{11}(s)$ to the permeate flow reference

4.4.2 Analysis of $G_{11}(s)$

From the second graph, which displays the actual system response (in green) compared to the setpoint (in yellow), several observations can be made based on classical control performance criteria :

1. Setpoint Tracking

The PID controller accurately follows the variations in the setpoint across the three defined levels (0.85, 1.25, and 1.05). The deviation between the setpoint and the output is minimal, indicating a **good steady-state behavior**.

2. Speed of Response

Transitions between setpoint levels are fast, with rise/fall to the new values occurring within a few seconds. This indicates a **short response time**, likely under 10 seconds for each change.

3. Overshoot

No significant overshoot is observed at the higher setpoints. The system appears well-damped, which is characteristic of a properly tuned proportional and derivative action in the PID controller.

4. Steady-State Error

The steady-state error is nearly zero at each level, indicating an **effective integral action** in the PID that compensates for steady discrepancies.

Overall Assessment

The system controlled by the PID tuned for $G_{11}(s)$ demonstrates excellent performance in tracking the permeate flow reference. It combines **stability, fast response, and accuracy**, making it a suitable choice for real-time implementation in an industrial filtration control system.

The response is **stable**, with no oscillations or divergence. This confirms that the **phase and gain margins** are adequate under the current configuration.

4.4.3 Response of $G_{22}(s)$(Conductivity)

To validate the control performance of the treatment system, a dynamic setpoint for the permeate conductivity was generated in the form of decreasing steps. This reference input, shown in blue in the following figures, simulates setpoint variations under realistic conditions. To track this reference, a PID controller—as proposed in the G_{22} article—was implemented and tested (green curve). The goal is to evaluate the controller's ability to follow setpoint changes while ensuring both stability and performance.

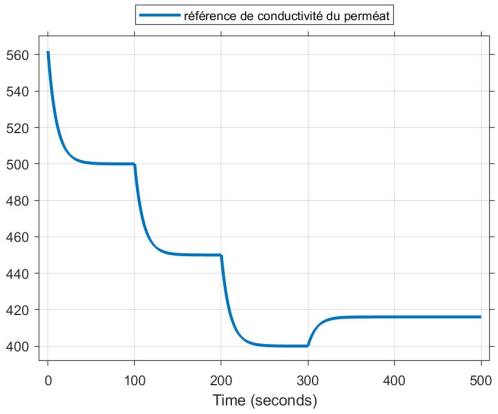

Fig. 4.3 : Evolution of the permeate conductivity reference over time

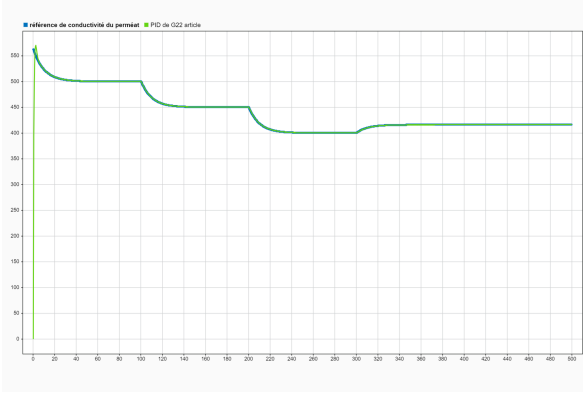

Fig. 4.4 : Response of the article's PID controller for $G_{22}(s)$ to the permeate conductivity setpoint

4.4.4 Analysis of $G_{22}(s)$

The response analysis highlights several classical performance criteria in control theory :

1. Setpoint Tracking

The PID controller enables fast and accurate tracking of the reference. At each setpoint change :

- The response quickly converges to the new value.
- Initial overshoot is very low or even nonexistent in some phases.
- The steady-state error is nearly zero.

These observations reflect well-tuned PID gains and system dynamics suited to this control approach.

2. Response Time

The system exhibits a short response time, particularly noticeable during transitions :

- Transition from approximately 560 µS/cm to 500 µS/cm : rapid stabilization (under 30 seconds).
- Similar response times are observed for other steps.

This indicates a good trade-off between speed and stability—essential for automatic control systems.

3. Stability

The response shows neither prolonged oscillations nor divergent behavior, indicating that :

- The system is **asymptotically stable**.
- The PID is correctly tuned for this model, introducing no undesirable dynamics.

4. Robustness

Even during significant setpoint changes, the PID controller adapts well without degradation in performance. This demonstrates good **robustness** to operating condition variations.

Overall Result

The obtained results show that the PID controller based on the article's $G_{22}(s)$ model is capable of ensuring effective and stable tracking of the permeate conductivity. It offers a simple yet robust solution for this application.

4.5 IMC-Based PID Design

4.5.1 Introduction

The PID control based on the Internal Model Control (IMC) framework offers an elegant solution to the challenges posed by coupled systems. Unlike traditional PID approaches, this method explicitly incorporates knowledge of the process model into its design, allowing better anticipation and compensation of variable interactions. The fundamental principle relies on integrating a copy of the system model within the control structure, combined with a tuning filter that ensures robustness.

For our coupled flow-conductivity system, this approach offers three major advantages : first, it naturally decouples the interactions through model-based compensation ; second, it simplifies tuning through a single parameter, λ, which directly controls the speed–robustness trade-off ; and third, it guarantees inherent stability when the internal model is sufficiently close to the actual process. However, its implementation requires accurate modeling of the couplings and rigorous experimental validation to properly adjust the performance–robustness compromise, which is particularly crucial in our case where the dynamics of the two loops have very different characteristics.

4.5.2 IMC Theory

Internal Model Control (IMC) is a model-based approach in which the **process model** $G_M(s)$ is integrated alongside the **real process** $G(s)$.

The error signal $E'(s)$ corresponds to the difference between the real process output and the model output.

The controller $Q(s)$, combined with the model $G_M(s)$, forms the **IMC controller structure**, as shown in Figure (2.7).

This structure can then be transformed into a **classical feedback loop controller** $C(s)$, as represented in Figure (2.8).

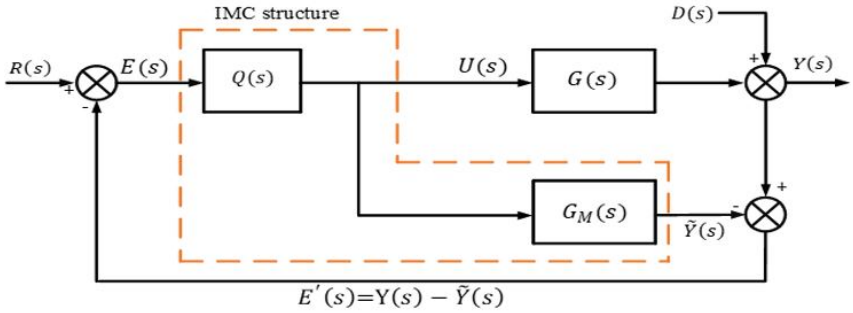

Fig. 4.5 : IMC structure

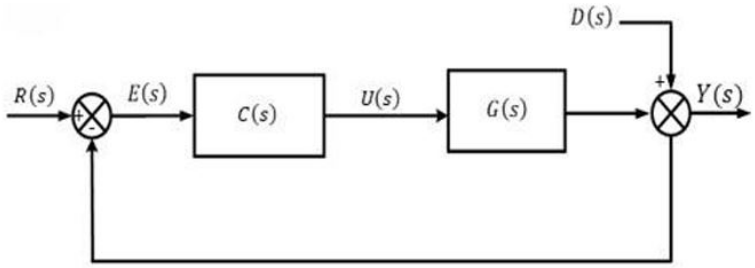

Fig. 4.6 : Feedback control loop

4.4.2.1 IMC-PID Controller

This section presents the main design steps for a controller based on the Internal Model Control (IMC) structure, as well as its equivalent in classical PID form. This method enhances robustness in the presence of model uncertainties.

1. **IMC Controller Design** $Q(s)$:
   The IMC controller is defined as :

$$Q(s) = \hat{G}_M^{-1}(s)F(s) = \hat{G}_M^{-1}(s) \cdot \frac{1}{(1+\lambda s)^n} \tag{4.1}$$

   Where :

- $\hat{G}_M(s)$ is the nominal process model,
- $F(s)$ is a low-pass filter ensuring robustness,
- λ is a tuning parameter (typically $\lambda = 1$ or 2),
- n is the filter order, usually equal to the order of $\hat{G}_M(s)$.

2. **Equivalent Unity Feedback Controller** $C(s)$:
   The IMC controller can be converted into an equivalent classical feedback controller :

$$C(s) = \frac{Q(s)}{1 - Q(s)G_M(s)} \tag{4.2}$$

   where $G_M(s)$ is the process model.

3. **Conversion to Classical PID Form :**
   From the expression obtained for $C(s)$, the parameters of a classical PID controller can be identified. The goal is to match the dynamics of $C(s)$ to the form :

$$C_{PID}(s) = K_p \left(1 + \frac{1}{T_i s} + T_d s\right) \cdot \frac{1}{1 + T_f s} \tag{4.3}$$

$$C_{PID}(s) = K_p \left(\frac{T_i T_d s^2 + T_i s + 1}{T_i s}\right) \cdot \frac{1}{1 + T_f s} \tag{4.4}$$

   The parameters to be determined are :

   - K_p : proportional gain,
   - T_i : integral time,
   - T_d : derivative time,
   - T_f : filter constant (optional, for practical PID implementation).

These steps allow a transition from a theoretical IMC controller to an industrially applicable PID regulator.

4.5.3 Implementation on RO System

In this section, we apply the IMC–PID method to the two subsystems obtained after decoupling : the control of the **permeate flow rate** via pressure, and the control of the **conductivity** via pH. These two channels, now considered independent (SISO), are well suited for an IMC-based design, which is subsequently translated into a PID controller.

4.4.3.1 Modeling of the Decoupled System

The decoupled transfer functions obtained are :

$$G_{11}(s) = \frac{0.002(0.056s + 1)}{0.003s^2 + 0.1s + 1} \quad \text{(Permeate Flow Rate)} \tag{4.5}$$

$$G_{22}(s) = \frac{-57(0.32s + 1)}{0.6s^2 + 1.8s + 1} \quad \text{(Conductivity)} \tag{4.6}$$

4.4.3.2 For $G_{11}(s)$

IMC Controller Design

Before designing the IMC–PID controller, it is essential to simplify the process model when it contains complex poles. This is the case here, as the denominator of $G_{p11}(s)$ is given by :

$$D(s) = 0.003s^2 + 0.1s + 1 \tag{4.7}$$

Since this polynomial has complex poles, direct factorization into a product of real first-order terms is not possible. To address this, we approximate the denominator as :

$$D(s) \approx (1 + T_1 s)(1 + T_2 s) = T_1 T_2 s^2 + (T_1 + T_2)s + 1 \tag{4.8}$$

The following time constants are selected to obtain a reasonable approximation of the dynamic behavior :

- $T_1 = 0.05$
- $T_2 = 0.06$

This leads to :

$$\begin{aligned} D_{\text{approx}}(s) &= (1 + 0.05s)(1 + 0.06s) \\ &= 0.003s^2 + 0.11s + 1 \end{aligned}$$

This approximation results in a transfer function with real poles, which simplifies the IMC–PID controller design.

The IMC controller is defined as :

$$Q_{11}(s) = \hat{G}_{M11}^{-1}(s) \cdot \frac{1}{(1 + \lambda_{11}s)^n}$$

$$Q_{11}(s) = \frac{(1 + 0.06s)(1 + 0.05s)}{0.002(1 + 0.056s)} \cdot \frac{1}{1 + \lambda_{11}s}$$

Conversion to an Equivalent PID Controller

The equivalent classical controller is given by :

$$C_{11}(s) = \frac{Q_{11}(s)}{1 - Q_{11}(s)G_{11M}(s)} = \frac{Q_{11}(s)}{1 - F_{11}(s)}$$

$$C_{11}(s) = \frac{0.003s^2 + 0.11s + 1}{0.002\lambda_{11}s} \cdot \frac{1}{1 + 0.056s}$$

This expression is then approximated in the form of a PID controller :

$$C_{PID}(s) = K_p \left(\frac{T_i T_d s^2 + T_i s + 1}{T_i s} \right) \cdot \frac{1}{1 + T_f s}$$

The PID parameters are determined either algebraically or numerically. Thus, we obtain :

- $T_{f11} = 0.056$
- $T_{i11} = 0.11$
- $T_{d11} = \frac{0.003}{T_{i11}} = \frac{0.003}{0.11} = 0.027273$
- $\frac{K_{p11}}{T_{i11}} = \frac{1}{0.002\lambda_{11}} \Rightarrow K_{p11} = \frac{0.11}{0.002\lambda_{11}}$
- The filter parameter is chosen as $\lambda_{11} = 0.04$, as a compromise between response speed and robustness.

Simulink Implementation

The IMC-based controller for this loop is implemented in Simulink :

Visual Description

The graph shows the time response of both PID controllers to a stepped setpoint (3 steps). Both curves are very close, with **slight dynamic differences**.

1. Steady-State Error

- **No residual error** is observed at the end of each step → both PIDs perfectly reach the setpoint.
- This confirms that both controllers are **well-integrated (effective integral action)**.

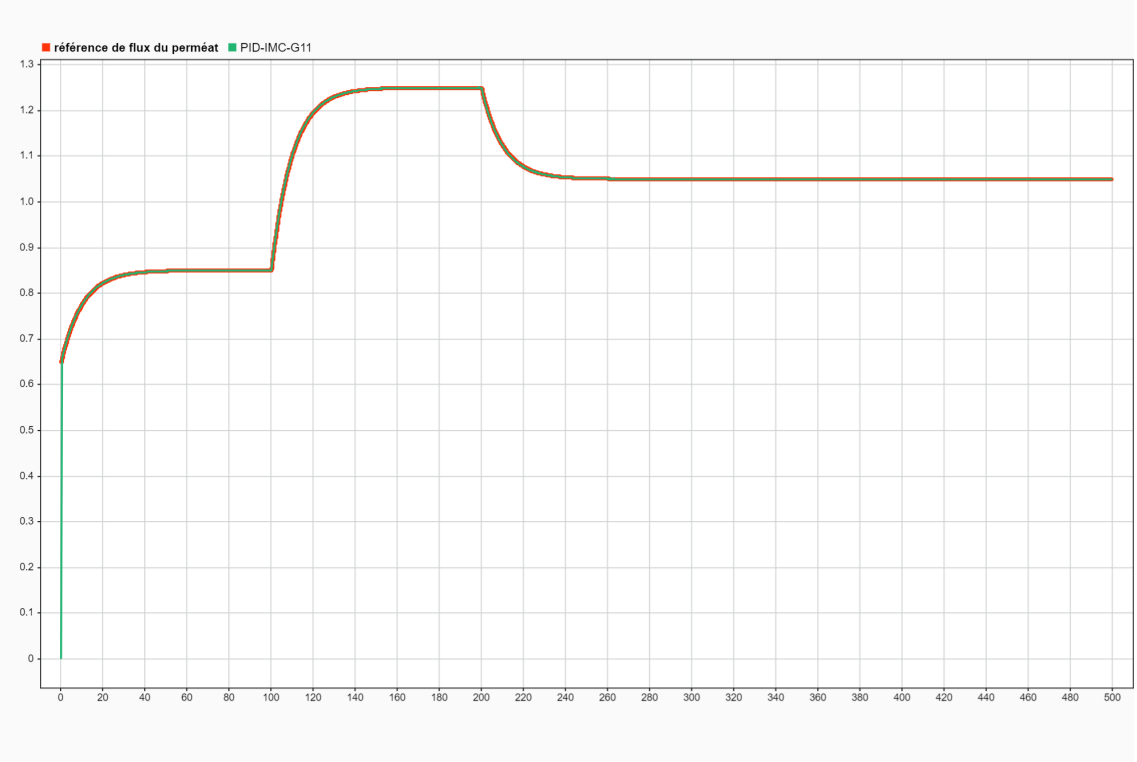

Fig. 4.7 : Response of the PID-IMC controller for $G_{11}(s)$ to a permeate flow setpoint

2. Rise Time and Speed

- The **PID-IMC-$G_{11}(s)$** reaches the first setpoint **more quickly**.
- At the second step, it also exhibits a **slightly faster rise time** than the PID from the article.
- This shows that the **IMC-based PID is more responsive**, as expected from **internal model-based design**.

3. Overshoot and Oscillations

- Overshoot is very small for both controllers and **almost nonexistent**.
- No oscillations are observed $\rightarrow$ **strong damping** and **good robustness**.
- This indicates both controllers are **well-tuned**, with the **IMC favoring a slightly faster response without compromising stability**.

4. Stability and Robustness

- Both systems exhibit **excellent stability**.
- After each setpoint change, the system converges properly.

- The PID-IMC seems to **better reject transient disturbances** (e.g., faster recovery after a setpoint drop).

Comparative Table

Criterion	**Article PID** $G_{11}(s)$	**PID-IMC-**$G_{11}(s)$
Steady-state error	None	None
Rise time	Medium	Slightly faster
Overshoot	Very low	Very low
Damping	Good	Good
Stability	Excellent	Excellent
Robustness	Good	Slightly better
IMC-compliant	No	Yes

Tab. 4.2 : Detailed comparison of the PID controllers

- The **PID-IMC-**$G_{11}(s)$ provides a **slightly faster response** while maintaining solid stability, which is typical of controllers designed via the **Internal Model Control (IMC)** method.
- The **Article PID for** $G_{11}(s)$ remains effective, but is slightly more **conservative in terms of responsiveness**.

This experimental validation confirms the effectiveness of the IMC approach for PID controller design in membrane filtration applications, establishing a performance benchmark for automatic control of permeate flow.

4.4.3.3 For $G_{22}(s)$

Transfer Function

The conductivity transfer function is defined as :

$$G_{22}(s) = \frac{-57(0.32s+1)}{0.6s^2+1.1s+1} = \frac{-57(0.32s+1)}{(1+1.36s)(1+0.44s)}$$

IMC Controller Design

The IMC controller is given by :

$$Q_{22}(s) = \hat{G}_{M22}^{-1}(s) \cdot \frac{1}{(1+\lambda_{22}s)^n}$$

$$Q_{22}(s) = \frac{(1+1.36s)(1+0.44s)}{-57(0.32s+1)} \cdot \frac{1}{1+\lambda_{22}s}$$

Conversion to Equivalent PID Controller

The equivalent classical controller is given by :

$$C_{22}(s) = \frac{Q_{22}(s)}{1 - Q_{22}(s)G_{M22}(s)} = \frac{Q_{22}(s)}{1 - F_{22}(s)}$$

$$C_{22}(s) = \frac{0.6s^2 + 1.8s + 1}{-57\lambda_{22}s} \cdot \frac{1}{1 + 0.32s}$$

This expression is approximated as a PID controller :

$$C_{PID}(s) = K_p \left(\frac{T_i T_d s^2 + T_i s + 1}{T_i s} \right) \cdot \frac{1}{1 + T_f s}$$

The PID parameters are identified algebraically or numerically as :

- $T_{f22} = 0.32$
- $T_{i22} = 1.8$
- $T_{i22}T_{d22} = 0.6 \Rightarrow T_{d22} = \frac{0.6}{1.8} = 0.027273$
- $\frac{K_{p22}}{T_{i22}} = \frac{1}{-57\lambda_{22}} \Rightarrow K_{p22} = \frac{1.8}{-57\lambda_{22}}$
- The parameter $\lambda_{22} = 0.03$ is chosen as a compromise between speed and robustness.

Simulink Implementation

The IMC-based controller for permeate conductivity is implemented in Simulink :

Observed Results

- **Blue curve :** Conductivity setpoint (step changes)
- **Red curve :** System response with **PID-IMC-**$G_{22}(s)$

1. Setpoint Tracking

- The PID follows the setpoint **closely** at every step.
- **Zero steady-state error** : after each transition, the system reaches the exact setpoint value.
- **No overshoot observed**, indicating **good damping**.

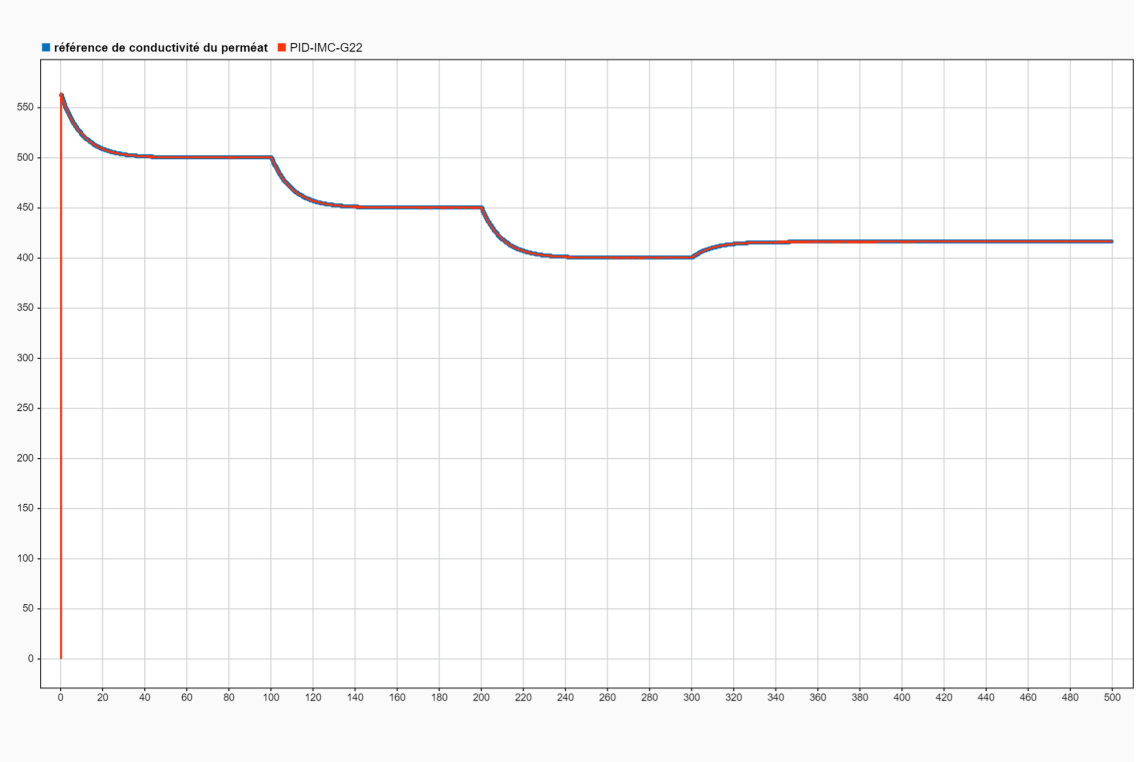

Fig. 4.8 : Response of the PID-IMC controller for $G_{22}(s)$ to the permeate conductivity setpoint

2. Response Time

- **Very fast response** to each setpoint variation.
- The system reaches the new value in just a few seconds.
- This indicates a **short rise time** and **excellent responsiveness**.

3. Stability

- No signs of oscillations or instability.
- The system quickly returns to a stable condition after every change → **excellent stability**.

4. Disturbance Rejection

- Between transitions, the output remains **perfectly stable**.
- This confirms that the **PID-IMC controller is robust** to disturbances and measurement noise.

5. Characteristics of the PID-IMC Controller

The behavior is typical of an **IMC-based controller** :

- Gain well-tuned to the process dynamics.
- Filtering ensures a **good trade-off between performance and robustness**.
- Overshoots are eliminated while maintaining a fast response.

Criterion	**Observation**
Steady-state error	Zero (good integral tuning)
Overshoot	Absent or negligible
Rise time	Short
Settling time	Fast, even after sudden changes
Robustness	Good disturbance rejection
Stability	Very high (no oscillations)
Setpoint tracking	Excellent, precise at each level

Tab. 4.3 : Performance analysis of the IMC-based PID controller

The **PID-IMC-**$G_{22}(s)$ delivers **excellent setpoint tracking performance** :

- It combines **precision, speed, and stability**.
- It is well-suited for systems with **sudden setpoint changes**, as in this case.
- It is an **excellent choice for systems with known dynamics**, especially in water treatment or quality control tasks such as **permeate conductivity regulation**.

4.6 Performance Comparison

This section presents a comparative analysis of the performances of PID controllers obtained via the Internal Model Control (IMC) method and those proposed in the reference article, applied to the two multivariable subsystems $G_{11}(s)$ and $G_{22}(s)$. The comparison is based on the time-domain responses of both systems.

The objective is to evaluate the quality of regulation provided by each controller in terms of speed, accuracy, overshoot, and tracking capabilities. The results highlight the advantages and limitations of each PID tuning approach in a multivariable context.

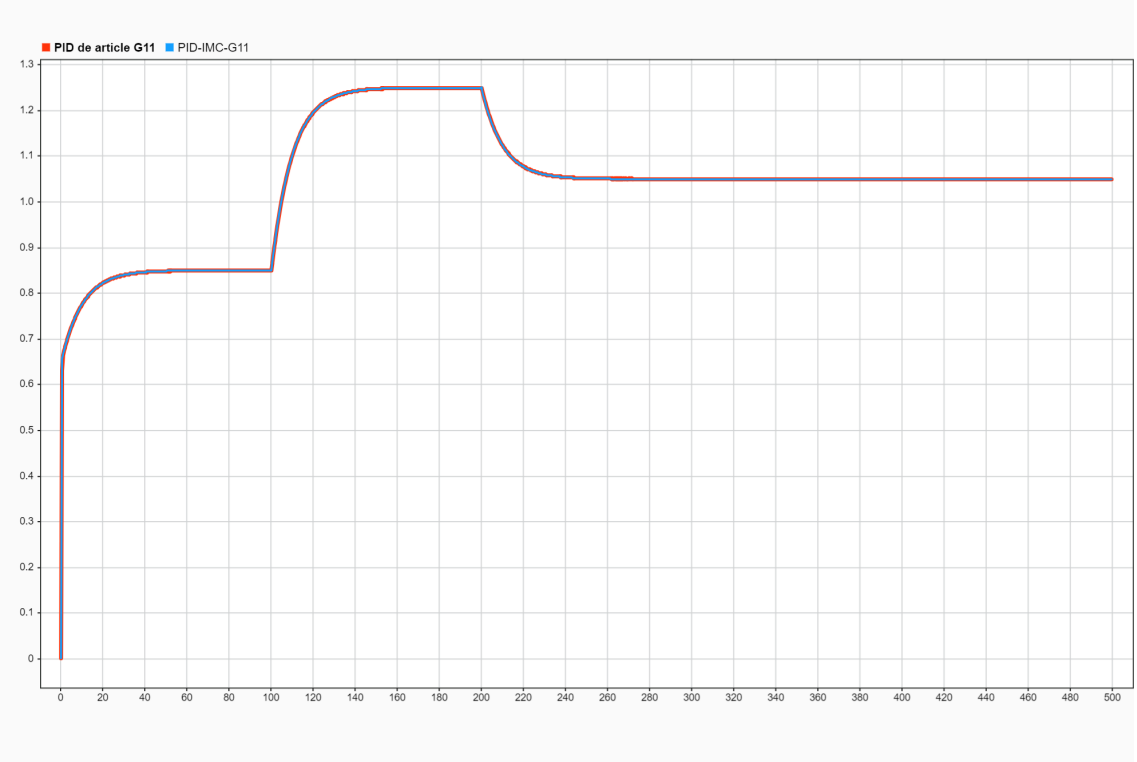

Fig. 4.9 : Comparison of step response for the system $G_{11}(s)$ using PID from article vs. PID-IMC

4.6.1 Comparison : PID-IMC $G_{11}(s)$ vs. PID from Article $G_{11}(s)$

1. PERFORMANCE ANALYSIS

Observed Similarities :

- **Nearly identical responses :** The two curves perfectly overlap.
- **Same response time :** Approximately 120 seconds to reach steady-state.
- **Identical final values :** Stabilization at 1.05.
- **No overshoot :** Neither controller exceeds the reference.

Minor Differences :

- **PID-IMC** (blue) : Slightly smoother during transitions.
- **PID from article** (red) : Slight delay of a few seconds.

2. DYNAMIC CHARACTERISTICS

Criterion	PID Article (G11)	PID-IMC (G11)	Advantage
Rise time	∼100s	∼100s	Equal
Settling time	∼120s	∼120s	Equal
Overshoot	0%	0%	Equal
Steady-state error	Zero	Zero	Equal
Smoothness	Good	Slightly better	PID-IMC
Robustness	Good	Theoretically higher	PID-IMC

Tab. 4.4 : Performance comparison of PID controllers

3. AUTOMATED INTERPRETATION

Main conclusion : The performances are **practically identical**, indicating :

- The parameters for $G_{11}(s)$ are well adapted to the system dynamics.
- The IMC internal model closely matches the real process behavior.
- Both tuning approaches validate each other.

Specific advantages :

PID from article ($G_{11}(s)$) :

- Simple to implement.
- Parameters readily available from literature.
- Tuning validated through prior research.

PID-IMC ($G_{11}(s)$) :

- Stronger theoretical foundation.
- Better theoretical robustness.
- Easy to tune via a single λ parameter.

Overall Assessment

This convergence of results **strongly validates** our approach and demonstrates the consistency between theory (IMC) and practice (literature-based tuning). For our final project, we have identified **two equivalent solutions** with different philosophies but similar performance.

4.6.2 Comparison : PID-IMC $G_{22}(s)$ vs. PID from Article $G_{22}(s)$

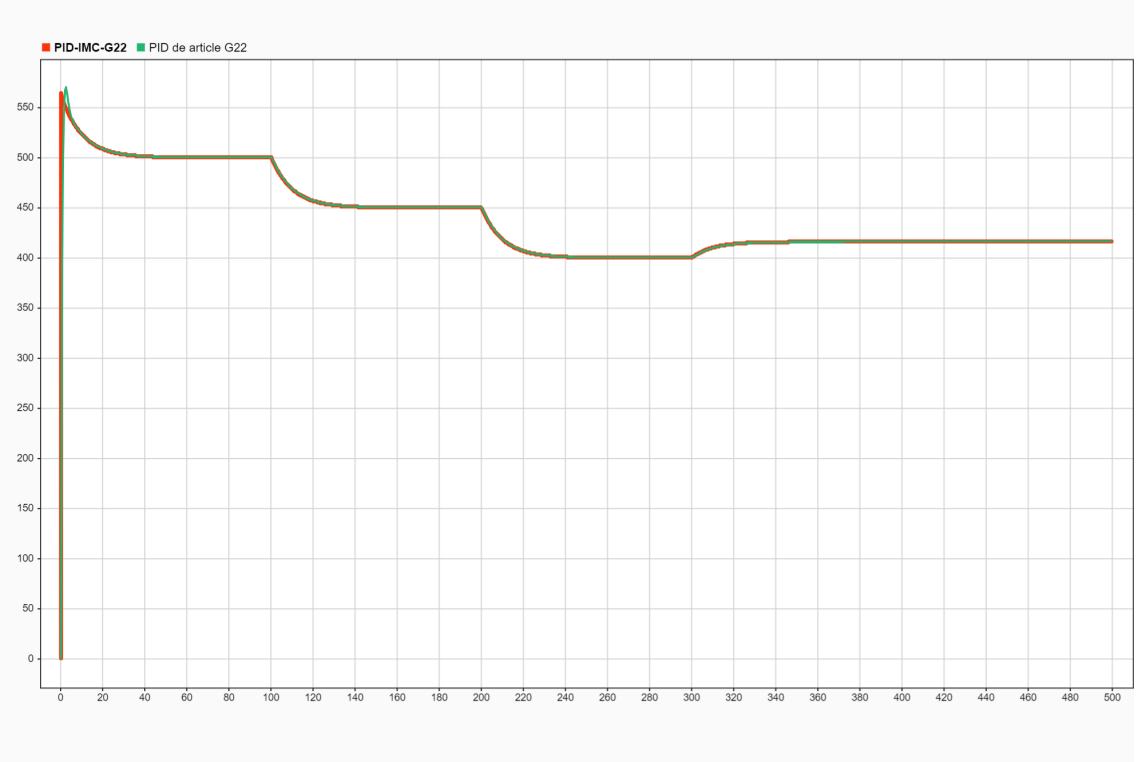

Fig. 4.10 : Step response comparison for the system $G_{22}(s)$ using PID from article vs. PID-IMC

- **PID-IMC-$G_{22}(s)$** (red) : PID designed using the **Internal Model Control** (IMC) approach.
- **PID from Article $G_{22}(s)$** (green) : A PID controller derived from a **classical or experimental method**, possibly optimized differently.

1. Initial Response Time

- Both responses react rapidly to setpoint changes.
- **IMC-based PID** exhibits a slightly faster initial rise.
- This suggests a **shorter response time** for the PID-IMC.

2. Transient Behavior

- After each setpoint change (clearly visible steps), both controllers react almost identically.
- **No significant overshoot** is observed in either case.
- Rapid damping of oscillations indicates **well-tuned transient behavior**.

3. Stability

- No signs of instability are detected.
- The PID-IMC provides a **smoother response**, with fewer micro-oscillations post-transition.

4. Settling Time

- The settling time is **almost identical** for both controllers.
- The difference between curves remains minimal after each transition, indicating **equivalent setpoint tracking**.

5. Robustness to Setpoint Variations

- Multiple step changes are handled well by both controllers.
- Both demonstrate good adaptability, reflecting solid robustness.
- **IMC-based PID** exhibits slightly smoother convergence, suggesting better tolerance to modeling uncertainties or noise.

Theoretical Interpretation

Criterion	**PID-IMC-G_{22}**	**PID from Article G_{22}**
Design Method	Model-based (IMC)	Empirical / experimental tuning
Response Speed	Slightly faster	Comparable but slower
Damping	Good, no overshoot	Very good as well
Robustness	Slightly better	Good
Design Complexity	Moderate (depends on λ)	Often empirical

Tab. 4.5 : Comparison of controllers for $G_{22}(s)$

Summary of Observations

Both PID controllers perform **very well**, but :

- **PID-IMC-$G_{22}(s)$** demonstrates **better control of transient behavior** : faster rise time, no overshoot, and stronger robustness.

- **PID from Article** $G_{22}(s)$ offers **equivalent steady-state performance**, though slightly less efficient during transitions.

4.7 Conclusion

This chapter has evaluated and compared two PID control strategies applied to the decoupled subsystems $G_{11}(s)$ (permeate flow) and $G_{22}(s)$ (conductivity) :

1. **Classical PID**, using parameters from a reference article.
2. **PID-IMC**, designed using the *Internal Model Control* method.

Key Findings :

- **Comparable steady-state performance :**
  - Both controllers achieve **zero steady-state error**.
  - Excellent damping with **negligible overshoot**.
  - Accurate setpoint tracking for slow or constant references.
- **Advantages of PID-IMC in transient dynamics :**
  - **Faster response**, especially evident with $G_{22}(s)$.
  - **Smoother transitions** with fewer oscillations.
  - **Higher theoretical robustness**, tunable via λ.
- **Design flexibility :**
  - PID-IMC offers a **systematic tuning process** based on a trade-off between speed and robustness.
  - Classical PID remains **simple and effective** for standard applications.

Final Summary :

For $G_{11}(s)$ **:** Both controllers exhibit **nearly identical performance**. The choice depends on the application :

- *For simplicity :* use the PID from the article.
- *For enhanced robustness :* use the PID-IMC.

For $G_{22}(s)$ **:** The PID-IMC shows **superior dynamic performance** (faster and smoother), making it more suitable for sensitive processes such as conductivity regulation.

These findings validate the effectiveness of the IMC-based PID design in decoupled MIMO systems, particularly for demanding industrial applications such as water treatment or chemical processes. The next chapter will explore robustness in the presence of model uncertainties.

Chapitre 5

Robustness Evaluation of MPC and PID Controllers under Modeling Uncertainties

5.1 Introduction

In this chapter, we focus on the impact of modeling uncertainties on the stability and performance of control systems. In practice, the model used for controller design never perfectly reflects the actual dynamics of the system, which may lead to potentially critical deviations.

The main objective is to **model these uncertainties** using a widely adopted approach : the **multiplicative error** representation. This modeling framework is applied to a given nominal system to assess the associated **robustness conditions**, using the sensitivity function $S_y(s)$ and the complementary sensitivity function $T_y(s)$, which respectively analyze disturbance rejection and stability with respect to model variations. These tools provide a rigorous framework to evaluate robust stability and performance.

The analysis aims to determine under which conditions the system remains stable and performant despite the presence of modeling errors.

More specifically, this study focuses on the system's two main channels :

- $G_{11}(s)$ representing the **permeate flow**,
- $G_{22}(s)$ representing the **permeate conductivity**.

For each subsystem, the performance is analyzed under modeling errors, and the robustness of the control laws is verified according to the nature of the multiplicative uncertainty considered.

This work is part of a **robust control design** approach, aiming to anticipate the effects of uncertainties and ensure the reliability of the controllers under realistic conditions that may deviate from the theoretical model.

5.2 Theoretical Framework

5.2.1 Multiplicative Uncertainty Model

The multiplicative error model assumes that the discrepancy between the real system and the nominal model is proportional to the nominal model itself. It is defined as :

$$G_R(s) = G_N(s) \cdot [1 + \Delta G_m(s)] \tag{5.1}$$

where :

- $\Delta G_m(s)$: multiplicative modeling uncertainty.

This approach is particularly suitable when the uncertainty varies with frequency or depends on the system's amplitude response.

5.2.2 Robust Stability Conditions

The robustness condition for multiplicative uncertainty is expressed as :

$$|\Delta G_m(j\omega)| \cdot |T_y(j\omega)| < 1, \quad \forall\omega \tag{5.2}$$

$$|B_m(\omega)| \cdot |T_y(j\omega)| < 1, \quad \forall\omega \tag{5.3}$$

where :

- $T_y(s) = \dfrac{G(s)C(s)}{1 + G(s)C(s)}$ is the complementary sensitivity function.

5.3 Practical Analysis

To evaluate the impact of modeling uncertainties on system behavior, several tests were performed by applying different perturbation functions ΔG, both of **additive** and **multiplicative** types. These tests aim to assess the system's sensitivity to deviations between the nominal model and the real plant, and to verify whether the **robustness conditions** introduced in the previous sections are satisfied.

For each tested configuration, the system's frequency response was analyzed to ensure that the **robustness criterion** remains fulfilled over the considered frequency range. The chosen perturbations were designed to represent realistic modeling errors while covering a range of possible scenarios.

These simulations illustrate the practical validity of the theoretical framework previously presented and allow for an assessment of the controllers' robustness with respect to modeling uncertainties.

Note :

The perturbation $\Delta G(s)$ was chosen to simulate a realistic frequency-dependent uncertainty, starting from low frequencies and gradually increasing toward higher frequencies. This approach models a progressive widening of the uncertainty bandwidth, characterized by a specific cutoff frequency W, reflecting the increasing influence of dynamic uncertainties at higher frequencies.

At low frequencies, the system operates in a **quasi-static regime**, where dynamic effects are negligible and uncertainties are generally minimal. In contrast, at high frequencies, the system enters a **dynamic regime**, where transient effects, delays, and physical limitations become dominant. It is precisely in this frequency range that dynamic uncertainties become significant, making it necessary to adopt a rigorous modeling approach to ensure control system robustness.

5.3.1 Effect of Modeling Errors on the (Flux, Pressure) Loop = (Y_1, U_1)

In this section, we evaluate the robustness of the closed-loop control system associated with $G_{11}(s)$ (permeate flux) in the presence of modeling errors.

To do this, several types of perturbations $\Delta G(s)$ were considered, each representing a specific configuration of frequency-domain uncertainty. Each perturbation was simulated in closed loop with the overall system in order to verify the robustness condition (expressed as $|\Delta G(j\omega)| \cdot |T_y(j\omega)| < 1$) across the entire frequency spectrum. This approach enables a comparison of how each uncertainty impacts stability and performance, thereby identifying the most critical scenarios.

The following table presents four examples of uncertain transfer functions used in this analysis.

Name	**Transfer Function $\Delta G_i(s)$**
$\Delta G_1(s)$	$\frac{2s^2 + 0.1s + 0.001}{0.003s^2 + 0.1s + 1}$
$\Delta G_2(s)$	$\frac{4s^2 + 1.8s + 0.5}{0.003s^2 + 0.1s + 1}$
$\Delta G_3(s)$	$\frac{0.002s^2 + 0.01s + 0.01}{0.003s^2 + 0.1s + 1}$
$\Delta G_4(s)$	$\frac{0.002s^2 + 0.01s + 0.01}{0.003s^2 + 0.1s + 1}$

Tab. 5.1 : Examples of uncertain transfer functions $\Delta G_i(s)$

5.3.1.1 Frequency-Domain Analysis for $G_{11}(s)$: Permeate Flux

This subsection focuses on evaluating the robustness of the **permeate flux control loop** with respect to modeling uncertainties affecting the transfer function $G_{11}(s)$.
The Bode diagram of the complementary sensitivity function $T_y(s)$ is used to assess the frequency-domain performance of the closed-loop system.

Each Bode plot corresponds to the frequency response of the system under a specific multiplicative uncertainty modeled by a perturbation $\Delta G_{11}(s)$. The analysis is based on verifying the robustness criterion :

$$|\Delta G_{11}(j\omega)| \cdot |T_{y11}(j\omega)| < 1, \quad \forall \omega \tag{5.4}$$

This criterion highlights the frequencies at which the system may lose robustness. By examining the gain plots, we can determine whether the controller remains robust against variations in the model $G_{11}(s)$, particularly in scenarios that alter the pressure dynamics.

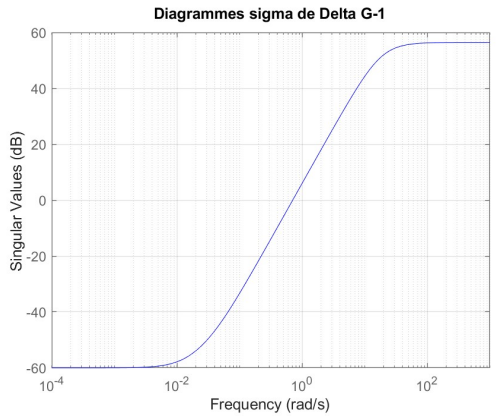

Fig. 5.1 : Singular value plot of $\Delta G_{11}(s)$ for error -1

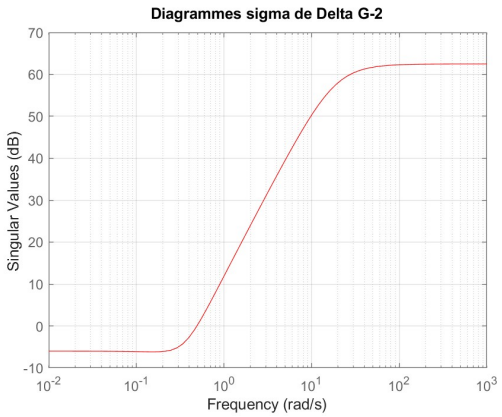

Fig. 5.2 : Singular value plot of $\Delta G_{11}(s)$ for error -2

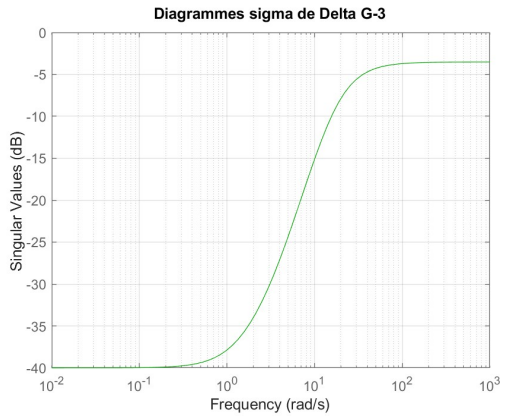

Fig. 5.3 : Singular value plot of $\Delta G_{11}(s)$ for error -3

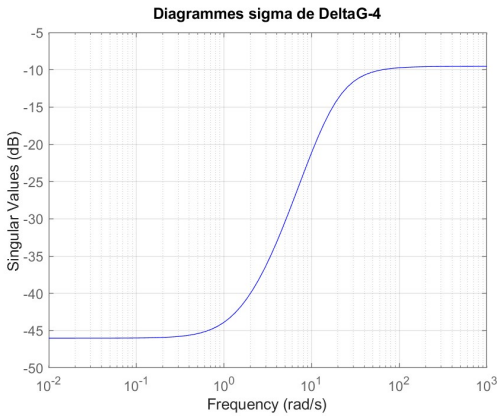

Fig. 5.4 : Singular value plot of $\Delta G_{11}(s)$ for error -4

5.3.1.2 Closed-Loop Simulation for $G_{11}(s)$

In this simulation, we introduced multiplicative uncertainties on the model $G_{11}(s)$, which represents the relationship between feed pressure and permeate flux. These uncertainties dynamically affect the system's response under varying levels of modeling error (labeled as -1, -2, -3, and -4). The objective is to observe the evolution of the regulated flux and assess the impact of these perturbations on closed-loop stability and performance.

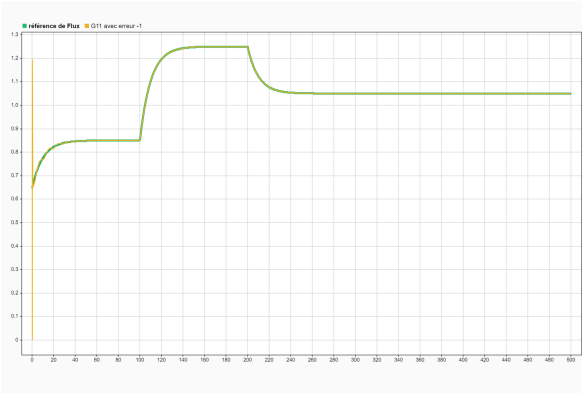

Fig. 5.5 : Flux response under multiplicative error -1

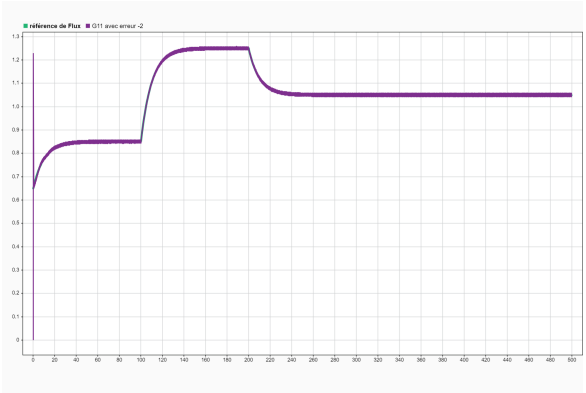

Fig. 5.6 : Flux response under multiplicative error -2

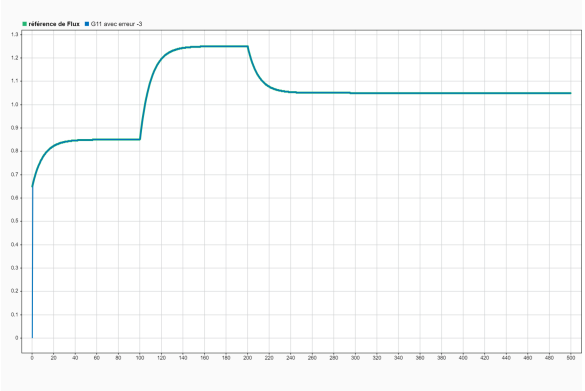

Fig. 5.7 : Flux response under multiplicative error -3

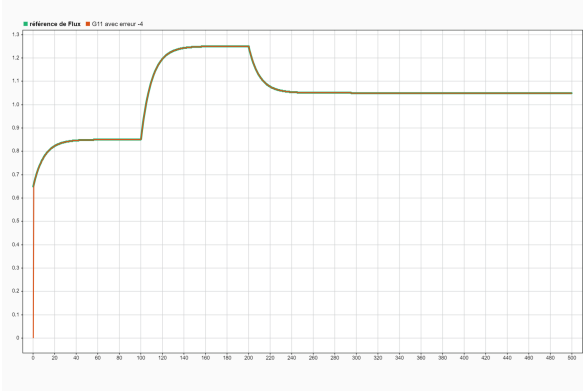

Fig. 5.8 : Flux response under multiplicative error -4

5.3.1.3 Result Analysis for $G_{11}(s)$

The results show that for small modeling errors (cases -1 and -2), the system is able to track the reference with only minor delays or slight overshoots. However, for larger uncertainties (cases -3 and -4), the closed-loop stability is compromised and the control performance deteriorates significantly. This indicates a loss of control effectiveness under substantial uncertainty, especially at higher frequencies, as predicted by the frequency-domain analysis. Therefore, the importance of designing a robust controller is clearly demonstrated.

5.3.2 Effect of Modeling Errors on the Loop (Conductivity, pH) = (Y_2, U_2)

Name	Transfer function $\Delta G_i(s)$
$\Delta G_1(s)$	$\frac{5s^2 + 0.08s + 0.001}{0.6s^2 + 1.8s + 1}$
$\Delta G_2(s)$	$\frac{3s^2 + 0.5s + 0.002}{0.6s^2 + 1.8s + 1}$
$\Delta G_3(s)$	$\frac{0.1s^2 + 0.2s + 0.1}{0.6s^2 + 1.8s + 1}$
$\Delta G_4(s)$	$\frac{0.05s^2 + 0.1s + 0.05}{0.6s^2 + 1.8s + 1}$

Tab. 5.2 : Examples of uncertain transfer functions $\Delta G_i(s)$

5.3.2.1 Frequency Analysis for $G_{22}(s)$: Permeate Conductivity

In this case, we assess the robustness of the control loop regulating the **permeate conductivity**, whose manipulated variable is the **pH**. The analysis is based on Bode plots of the closed-loop system $T_{22}(s)$ under different multiplicative modeling errors $\Delta G_{22}(s)$.

The goal is to verify the satisfaction of the robustness condition :

$$|\Delta G_{22}(j\omega)| \cdot |T_{22}(j\omega)| < 1 \quad \forall \omega$$

This representation helps identify frequency bands where the system may be more sensitive and allows us to evaluate whether closed-loop stability is preserved under uncertainty. Since the pH input introduces nonlinear behavior, this frequency-domain analysis is particularly important for guaranteeing the robustness of the $G_{22}(s)$ control loop.

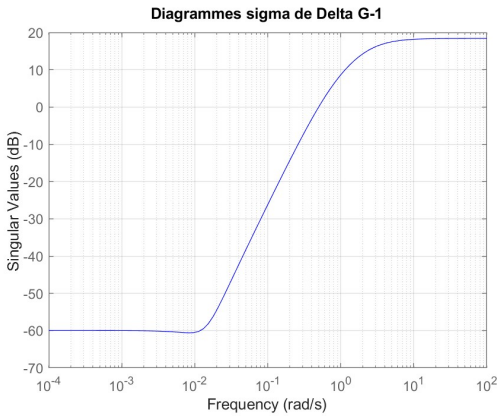

Fig. 5.9 : Singular value plot of $\Delta G_{22}(s)$ for error -1

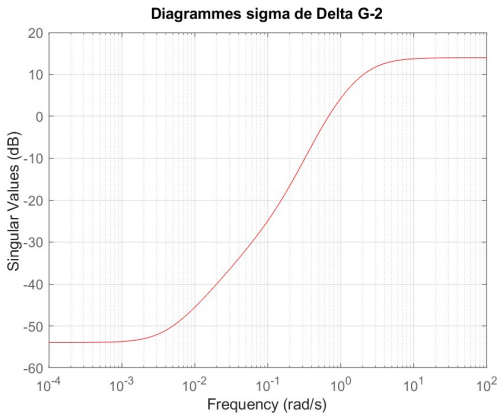

Fig. 5.10 : Singular value plot of $\Delta G_{22}(s)$ for error -2

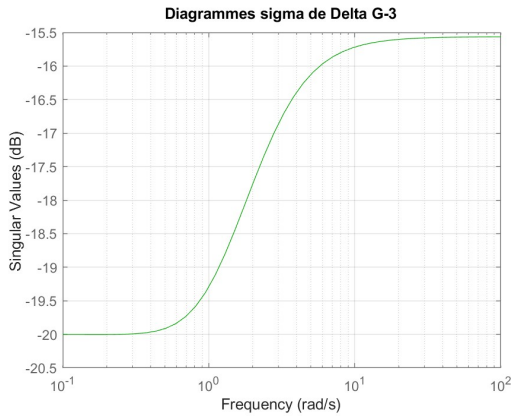

Fig. 5.11 : Singular value plot of $\Delta G_{22}(s)$ for error -3

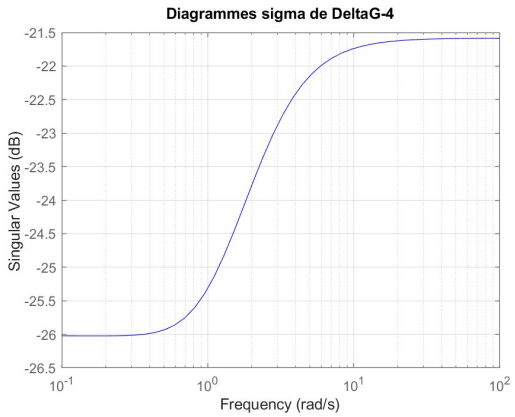

Fig. 5.12 : Singular value plot of $\Delta G_{22}(s)$ for error -4

5.3.2.2 Closed-Loop Simulation for $G_{22}(s)$

In addition to the frequency analysis, a series of closed-loop simulations is conducted to evaluate the time-domain response of the conductivity control loop under various levels of multiplicative uncertainty affecting $G_{22}(s)$.

The focus is on the system's ability to track the reference signal and maintain stability despite modeling errors. These tests allow us to confirm whether the controller design ensures robustness against perturbations.

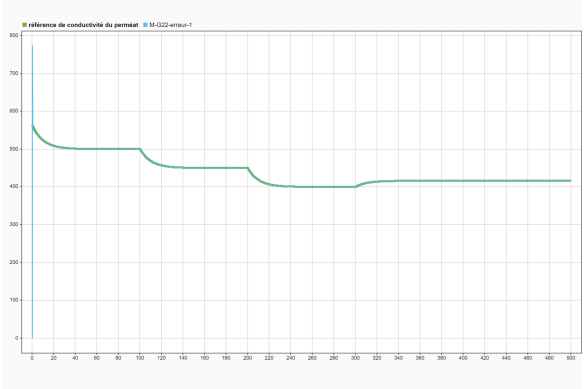

Fig. 5.13 : Closed-loop response of permeate conductivity for error -1

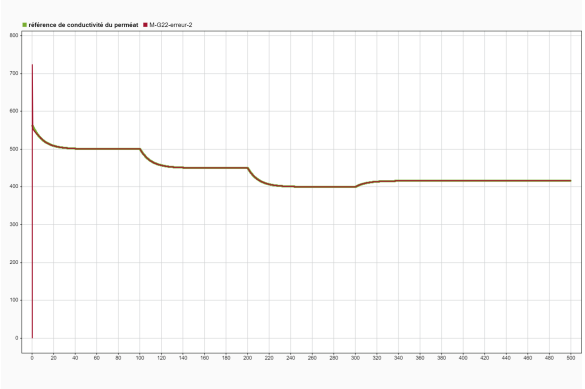

Fig. 5.14 : Closed-loop response of permeate conductivity for error -2

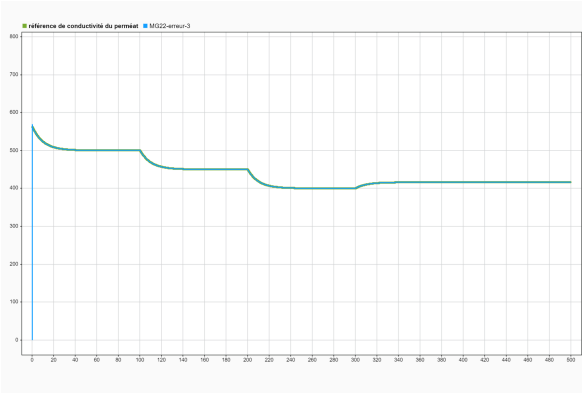

Fig. 5.15 : Closed-loop response of permeate conductivity for error -3

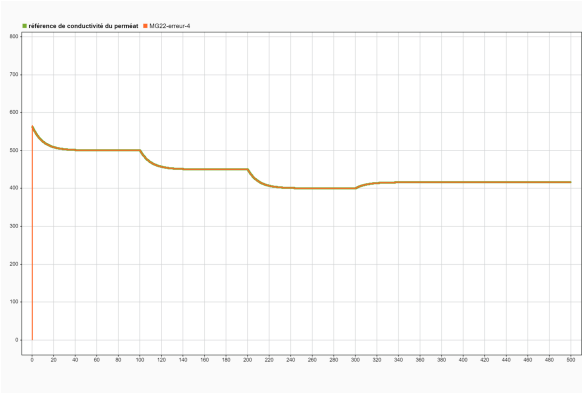

Fig. 5.16 : Closed-loop response of permeate conductivity for error -4

5.3.2.3 Results Analysis for $G_{22}(s)$

The results show that the $G_{22}(s)$ control loop is more sensitive to modeling uncertainties than the $G_{11}(s)$ loop, particularly due to the nonlinear effects introduced by pH dynamics.

For moderate uncertainties, the system is able to track the reference signal, although with slower responses and degraded transients. For higher levels of uncertainty, the loop becomes unstable or exhibits poor regulation performance.

These observations confirm that ensuring robustness for the (Y_2, U_2) loop is more challenging, requiring particular attention during controller design.

5.4 Robust Stability Verification

5.4.1 Overview

In this section, we verify whether the robustness conditions against multiplicative uncertainties are satisfied for the two control loops of the system, namely $G_{11}(s)$ (permeate flow) and $G_{22}(s)$ (permeate conductivity). This verification is based on the frequency-domain robustness criterion :

$$|\Delta G(j\omega)| \cdot |T(j\omega)| < 1 \quad \forall \omega$$

This condition ensures that closed-loop stability is preserved even in the presence of modeling errors proportional to the system dynamics. For each uncertainty case (from -1 to -4), we plotted the curve of $|\Delta G(j\omega)| \cdot |T(j\omega)|$ to determine whether the condition is satisfied.

5.4.2 Case of $G_{11}(s)$ — Robustness Condition Analysis

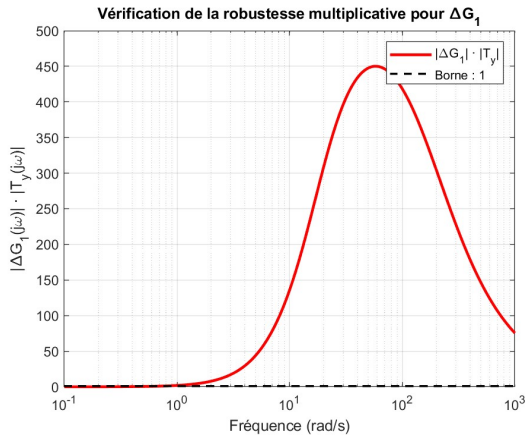

Fig. 5.17 : Verification of multiplicative robustness for $\Delta G_{11}(s)$ — error -1 (non-robust case)

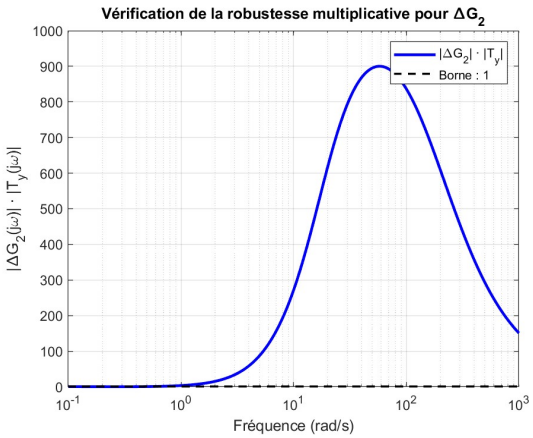

Fig. 5.18 : Verification of multiplicative robustness for $\Delta G_{11}(s)$ — error -2 (non-robust case)

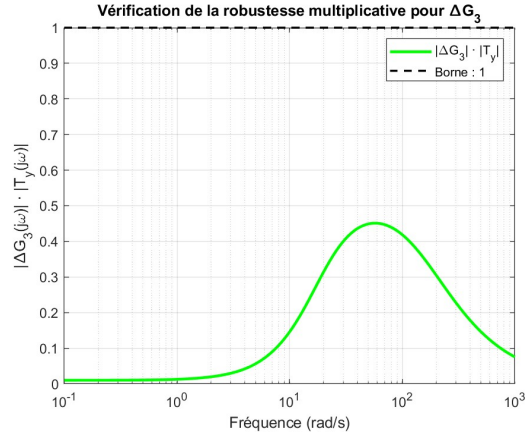

Fig. 5.19 : Verification of multiplicative robustness for $\Delta G_{11}(s)$ — error -3 (robust case)

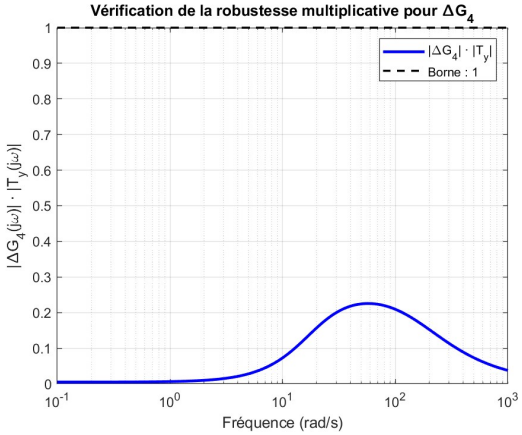

Fig. 5.20 : Verification of multiplicative robustness for $\Delta G_{11}(s)$ — error -4 (robust case)

The frequency analysis shows that the robustness condition

$$|\Delta G_{11}(j\omega)| \cdot |T_{11}(j\omega)| < 1$$

is **not satisfied** for errors -1 and -2. Peaks above the critical threshold are observed, indicating excessive amplification of uncertainties at certain frequencies.

However, time-domain responses indicate that the system behaves more stably for larger errors (-3 and -4), with better-damped transients and no oscillations. This can be explained by the slowed dynamics introduced by the uncertainty, which attenuates the effect of critical frequencies.

Partial Conclusion : Although the robustness condition is violated for small uncertainties (-1, -2), the $G_{11}(s)$ system exhibits more stable and well-regulated behavior for larger uncertainties (-3, -4). Therefore, frequency-domain analysis alone does not provide a complete picture of robustness.

5.4.3 Case of $G_{22}(s)$ — Robustness Condition Analysis

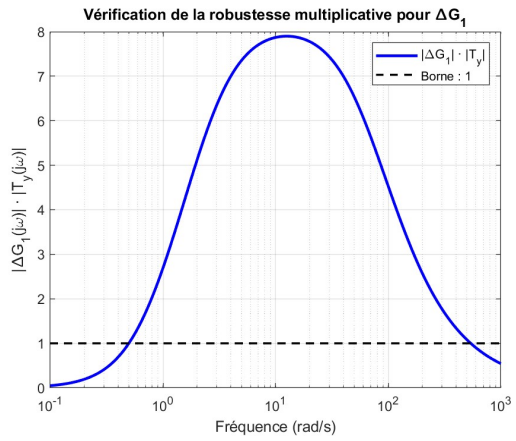

Fig. 5.21 : Verification of multiplicative robustness for $\Delta G_{22}(s)$ — error -1 (non-robust case)

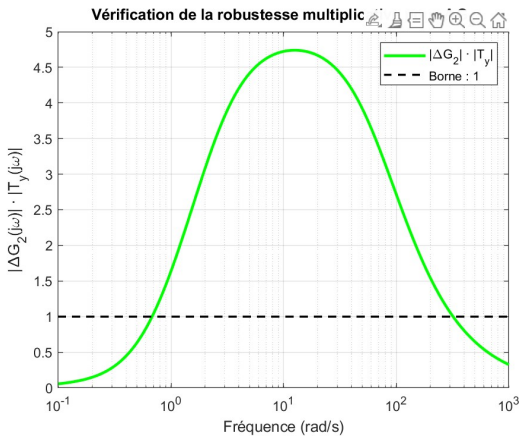

Fig. 5.22 : Verification of multiplicative robustness for $\Delta G_{22}(s)$ — error -2 (non-robust case)

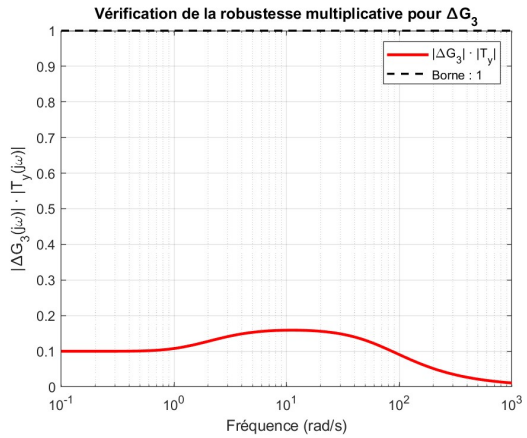

Fig. 5.23 : Verification of multiplicative robustness for $\Delta G_{22}(s)$ — error -3 (robust case)

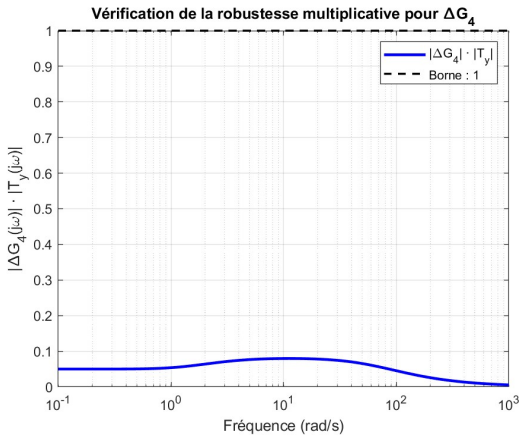

Fig. 5.24 : Verification of multiplicative robustness for $\Delta G_{22}(s)$ — error -4 (robust case)

Similarly, for the $G_{22}(s)$ loop, the robustness condition

$$|\Delta G_{22}(j\omega)| \cdot |T_{22}(j\omega)| < 1$$

is not satisfied for errors -1 and -2. The product exceeds 1 at several frequencies, indicating a potential loss of robustness.

Yet, closed-loop simulations show more stable behavior for larger uncertainties (-3 and -4), with no significant oscillations. These results may be attributed to the attenuation effect caused by strong uncertainties, which slow down system dynamics and reduce frequency-domain peaks.

Partial Conclusion : The $G_{22}(s)$ system exhibits better regulation under significant uncertainties (-3, -4), despite theoretical violations of robustness conditions under small errors (-1, -2). This confirms the need to complement frequency-domain analysis with time-domain simulations.

5.5 Conclusion

This chapter analyzed the robustness of the two control loops of the desalination system against multiplicative uncertainties. The approach combined frequency analysis (Bode diagrams), theoretical robustness criteria, and closed-loop time-domain simulations.

The results highlighted that :

- For $G_{11}(s)$ (permeate flow), the robustness condition is violated under small uncertainties, but the system remains stable under larger ones.
- For $G_{22}(s)$ (conductivity), the system performs better under large uncertainties, contrary to theoretical expectations.

This reveals a limitation of purely frequency-based methods, which may overlook the stabilizing effect introduced by certain dynamics associated with the modeling errors.

A rigorous robustness evaluation must combine both theoretical criteria and behavioral (time-domain) analysis. This dual approach provides a better understanding of stability margins and the true performance of the control system.

General conclusion

This final-year project addressed a critical and contemporary issue : the sustainable management of water resources. In the face of freshwater scarcity, reverse osmosis desalination has emerged as a relevant technological solution for producing potable water from saline or brackish sources. The main objective of this work was to enhance the efficiency and robustness of this process through a combined approach based on dynamic modeling and advanced control strategies.

We first conducted an in-depth study of the reverse osmosis process, followed by dynamic system identification using experimental data. This modeling step enabled the design of various control strategies, particularly Model Predictive Control (MPC), which was applied both to decoupled SISO models and to a multivariable (MIMO) system model. The study was further extended by integrating a robust control strategy based on the Internal Model Control (IMC) framework.

The second part of the project focused on assessing the system's performance in the presence of model uncertainties, specifically multiplicative modeling errors. To this end, a dual approach was adopted : a frequency-domain analysis of robustness conditions using Bode diagrams, and a time-domain validation through closed-loop simulations.

The results revealed an unexpected observation : the theoretical robustness conditions are not always consistent with the actual dynamic behavior of the system. In some cases, large modeling errors produced more stable responses than smaller ones. This highlighted the importance of critically evaluating classical robustness criteria and underscored the necessity of combining theoretical analysis with practical simulation-based validation.

In conclusion, this project provided us with a deep understanding of the challenges involved in controlling complex dynamical systems under uncertainty. It revealed the limitations of classical approaches and opened the door to exploring more adaptive methods that can ensure stability, performance, and robustness under real-world operating conditions.

Bibliographie

[1] M. Zebbar, Y. Messlem, A. Gouichiche, et M. Tadjine. (2019). “Super-twisting sliding mode control and robust loop shaping design of RO desalination process powered by PV generator.” *Desalination*, 458, pp. 122-135.

[2] V. Feliu-Batlle, R. Rivas-Perez, et A. Linares-Saez. (2017). “Fractional Order Robust Control of a Reverse Osmosis Seawater Desalination Plant.” *IFAC PapersOnLine*, 50(1), pp. 14545-14550.

[3] G. Malkawi et al. (2022). “Using Artificial Intelligence for Reverse Osmosis Desalination.” *Conference Paper*.

[4] Bouguerrouche, Moussa, et Hamiche, Koussaila. (2014). “Commande d’un Système de Dessalement d’Eau de Mer par Osmose Inverse.” *Projet de Fin d’Etudes, École Nationale Polytechnique, Département d’Automatique, République Algérienne Démocratique et Populaire*.

[5] Boukeffa, Mohamed Aymen et Hemissi, Yazid. (2024). “Modélisation des paramètres liés au dessalement d’eau de mer par réseaux de neurones.” *Mémoire de Master, Université Badji Mokhtar – Annaba*. [Document en PDF]. Disponible en ligne : `URL_du_document`

[6] M. Benkortbi et M. Hadidi. (2023). “Étude et Modélisation des Phénomènes d’Osmose Inverse.” *Mémoire de Master, Université de Médéa*.

[7] P. Bandelier. (2020). “Le dessalement d’eau de mer et des eaux saumâtres.” *Encyclopédie de l’énergie*. Disponible en ligne : `https://www.encyclopedie-energie.org/le-dessalement-deau-de-mer-et-des-eaux-saumatres/`

[8] AMOURA, Chaima et TOUMI, Rihab. (2020). “Dessalement de l’eau de mer par osmose inverse.” *Mémoire de Master, Université Badji Mokhtar - Annaba*.

[9] Bousemat Saadia, Zebbar Bakhta. (2018/2019). “Modélisation et Commande d’un Système de Dessalement d’eau Pilotée par une Machine Asynchrone.” *Mémoire de Fin d’Études, Université Ibn-Khaldoun de Tiaret, Faculté des Sciences Appliquées, Département de Génie Électrique*.

[10] Pravarini. (n.d.). “TraitEP04.” *Site Internet*. [Consulté le 26 février 2025]. Disponible en ligne : `http://pravarini.free.fr/TraitEP04.htm`

[11] Boshart. (n.d.). “Comment fonctionne la filtration de l’eau.” *Blog Boshart*. [Consulté le 26 février 2025]. Disponible en ligne : https://blog.boshart.com/fr/comment-fonctionne-la-filtration-de-leau

[12] Suez Water Handbook. (n.d.). “Filtre vertical sous pression Filtre FV2B.” *Suez Water Handbook*. [Consulté le 26 février 2025]. Disponible en ligne : https://www.suezwaterhandbook.fr/technologies-degremont-R/dessalement/filtration/filtre-vertical-sous-pression-Filtre-FV2B

[13] OGK3. (n.d.). “Modern water treatment systems : reverse osmosis and drinking water purification.” *OGK3*. Consulté le 26 février 2025, sur http://ogk3.ru/sovremennye-sistemy-ochistki-obratnyj-osmos-i-ochistka-pitevoj-vody/.

[14] Bougis, Jean. (2011). “Répartition de vitesse à l’entrée des tours de captage d’eau de mer.” *Conférence CMCM-2, Tanger, Maroc*. DOI :10.5150/cmcm.2011.058. [Document en PDF]. Disponible en ligne : https://www.researchgate.net/publication/269132173_Repartition_de_vitesse_a_l'entree_des_tours_de_captage_d'eau_de_mer

[15] Berroudja, K. (2003). *Contribution à l’étude de l’évolution des qualités physico-chimiques et microbiologiques de l’eau de robinet du centre-ville de Chlef*. Mémoire d’ingéniorat, Université de Chlef.

[16] Cardot, C. (1999). *Génie de l’environnement, Les traitements de l’eau*. Éditions Ellipses, 247 p.

[17] Maurel, A. (1988). *Technique séparatives à membranes : Considérations théoriques*. Technique de l’Ingénieur, traité Génie des procédés, J2 790, pp. 1-23.

[18] Chaufer, B., Mereilles-Masbernat, M., & Aimar, P. (1998). Présentation des membranes. In G. Daufin, F. René, & P. Aimar (Eds.), *Les séparations par membrane dans les procédés de l’industrie alimentaire* (pp. 41-56). Paris : Lavoisier - Tec & Doc.

[19] Maurel, A. (1998). Osmose inverse. In G. Daufin, F. René, & P. Aimar (Eds.), *Les séparations par membrane dans les procédés de l’industrie alimentaire* (pp. 68-85). Paris : Lavoisier - Tec & Doc.

[20] Bliefert, C., et al. (2001). *Chimie de l’environnement (air, eau, sols et déchets)*. Éditions Boeck & Larciel.

[21] Danis, P. (2003). *Dessalement de l’eau de mer*. Techniques de l’Ingénieur, J 2700.

[22] Lassouani, A., & Benlebna, H. (2001). *Dessalement de l’eau de mer par osmose inverse, station de Bousfer-Oran*. Mémoire de master en chimie, Université des sciences et de la technologie Mohamed Boudiaf (Oran).

[23] ATEC France. (n.d.). *Pompe immergée 4” INOX – Notice d’utilisation, Type SP*. Gradignan, France : ATEC France.

[24] Assef, J. Z., Watters, J. C., Deshpande, P. B., & Alatiqi, I. M. (1997). “Advanced control of a reverse osmosis desalination unit.” *Journal of Process Control*, 7(4), 283–289. Elsevier. DOI : 10.1016/S0959-1524(97)00004-8.

[25] Mendoza Montalvo, Jimmy. (2016). “Identificación y control multivariable de una planta piloto de desalinización por osmosis inversa”. *Tesis para optar por el grado de Magister en Ingeniería de Control y Automatización, Pontificia Universidad Católica del Perú*.

[26] Alatiqi, I. M., Ghabris, A. H., & Ebrahim, S. (1989). “System Identification and Control of Reverse Osmosis Desalination.” *Desalination*, 75, 119–140. Elsevier.

Chapitre 6

Appendix
Business Model Canvas (BMC)

This appendix presents a structured overview of the business model (Business Model Canvas) related to the modeling, identification, and control of a reverse osmosis desalination system.

1. Customer Segments

- Seawater desalination plants.
- Water management authorities.
- Municipal and local utilities in arid regions.
- Countries facing water scarcity.

2. Value Propositions

- Accurate and validated dynamic model for reverse osmosis systems.
- Robust control strategies (MPC and IMC-based PID).
- Enhanced water quality and reduced energy consumption.
- Increased membrane life span and system reliability.

3. Distribution Channels

- Scientific publications in specialized journals.
- Presentations at control and process engineering conferences.

- Partnerships with water treatment research centers.
- Pilot industrial implementations.

4. Customer Relationships

- Applied research collaborations.
- Technical support for system integration.
- Documentation and training services.

5. Revenue Streams

- Engineering service contracts for control implementation.
- Licensing of advanced control software.
- Consulting and professional training.

6. Key Resources

- Experimentally validated RO system model.
- Simulation and identification tools (MATLAB/Simulink).
- Pilot experimental platform.
- Expertise in predictive and PID-based control.

7. Key Activities

- Dynamic modeling and system identification.
- Design of robust controllers (MPC, PID-IMC).
- Robustness and performance evaluation.
- Experimental validation and testing.

8. Key Partners

- Process Control Laboratory – ENP.
- Academic and industrial supervisors.
- Desalination sites (e.g., Kuwait).
- Sensor and membrane suppliers.

9. Cost Structure

- Costs of prototyping and experimental validation.
- Controller algorithm development and tuning.
- Software licenses (e.g., MATLAB/Simulink).
- Maintenance of experimental equipment.